National Library of Canada
Acquisitions and Bibliographic Services Branch
395 Wellington Street
Ottawa, Ontario
K1A 0N4

Bibliothèque nationale du Canada
Direction des acquisitions et des services bibliographiques
395, rue Wellington
Ottawa (Ontario)
K1A 0N4

NOTICE

The quality of this microform is heavily dependent upon the quality of the original thesis submitted for microfilming. Every effort has been made to ensure the highest quality of reproduction possible.

If pages are missing, contact the university which granted the degree.

Some pages may have indistinct print especially if the original pages were typed with a poor typewriter ribbon or if the university sent us an inferior photocopy.

AVIS

La qualité de cette microforme dépend grandement de la qualité de la thèse soumise au microfilmage. Nous avons tout fait pour assurer une qualité supérieure de reproduction.

S'il manque des pages, veuillez communiquer avec l'université qui a conféré le grade.

La qualité d'impression de certaines pages peut laisser à désirer, surtout si les pages originales ont été dactylographiées à l'aide d'un ruban usé ou si l'université nous a fait parvenir une photocopie de qualité inférieure.

Canada

FLOW AND DRYING CHARACTERISTICS OF A ROTATING JET SPOUTED BED

by

Rami Yousef Jumah

Department of Chemical Engineering
McGill University, Montreal

July 1995

A thesis submitted to the Faculty of Graduate Studies and Research in partial fulfillment of the requirements for the degree of Doctor of Philosophy

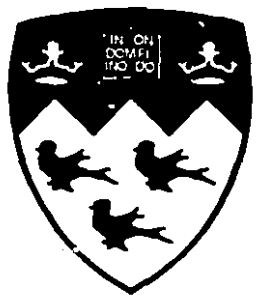

ISBN 0-612-08118-4

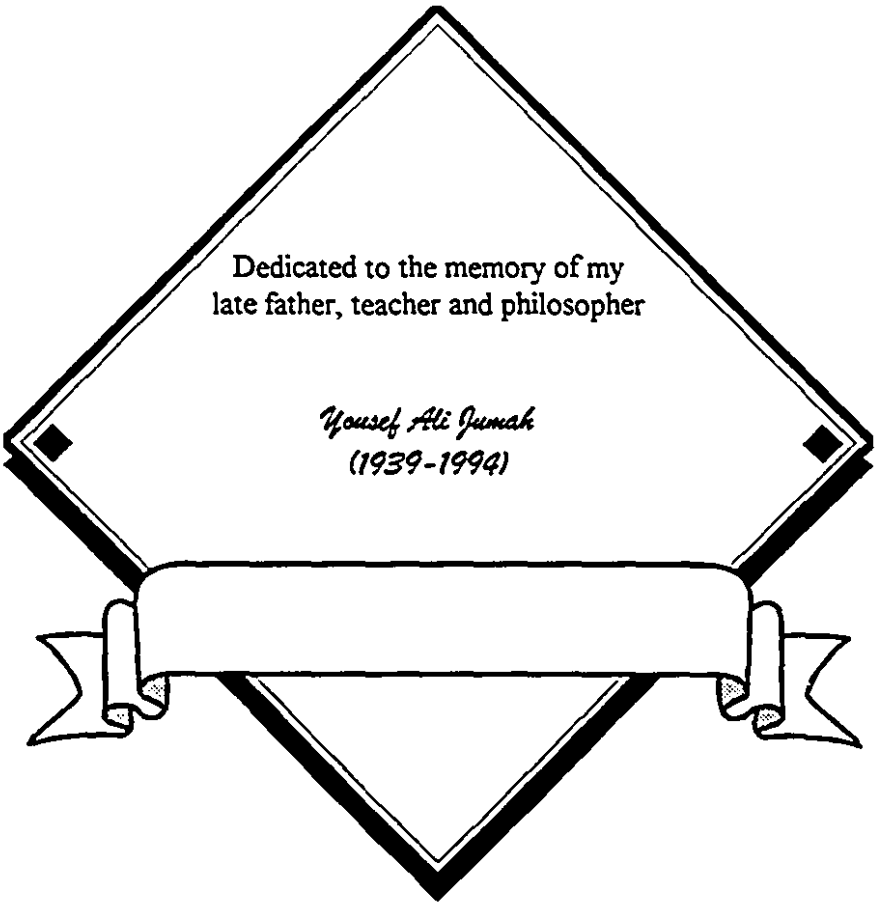
Dedicated to the memory of my
late father, teacher and philosopher
Yousef Ali Jumah
(1939-1994)

ABSTRACT

A novel rotating jet spouted bed (RJSB) is developed and tested. It consists of a rotating air distributor with two radially located spouting air nozzles. The effects of bed height, distributor rotational speed, nozzle diameter and particle properties on the flow characteristics were examined. Various flow regimes were mapped as functions of distributor rotational speed and superficial air velocity for different materials and column dimensions. Empirical correlations were developed for the minimum spouting velocity, peak pressure drop and steady spouting pressure drop.

Drying kinetics of corn as a test material was investigated using both continuous and intermittent (on/off) spouting/heating schemes. The parameters investigated include inlet air temperature, bed height, superficial air velocity, nozzle diameter, distributor rotational speed and intermittency of spouting and heat input. The results indicate that the drying kinetics are comparable with conventional spouted and fluidized beds for slow drying materials and that intermittent drying can save up to 40 % of the thermal energy consumption.

A fully predictive diffusion-based mathematical model was developed and validated for both continuous and intermittent drying in the RJSB. Several other time-dependent spouting/heating schemes were evaluated numerically in the light of their potential practical applications.

RÉSUMÉ

Un nouveau système de séchage à jet d'air rotatif et soufflant en dessous du matériau à sécher a été développé et testé. Il consiste en un distributeur d'air rotatif avec deux orifices de soufflage placés radialement. Les effets de la hauteur du matériau, de la vitesse de rotation du distributeur, du diamètre des orifices ainsi que des propriétés des particules, sur les caractéristiques d'écoulement ont été examinés. Divers régimes d'écoulement ont été dessinés en fonction de la vitesse de rotation du distributeur et de al vitesse superficiel de l'air pour différents matériaux et pour différentes dimensions de colonne. Des relations empiriques ont été dévelppées pour la vitesse minimale de soufflage; la chute de la pression de pointe et la chute de la pression de soufflage en régime permanent.

La cinétique de séchage du maïs, matériel utilisé pour les tests, a été étudiée en utilisant un régime de soufflage et de chauffage en continu d'une part et un régime intermittent d'autre part. Les paramètres étudiée sont: la température de l'air à l'entrée, la hauteur du matériau à sécher, la vitesse superficiel de l'air, le diamètres de l'orifice, la vitesse de rotation du distributeur et l'intermittence du soufflage et du chauffage. Les résultats indiquent que la cinétique de séchage du maïs est comparable avec le soufflage conventionnel et au séchage où le maïs est fluidisé dans le cas de séchage lente. De même, les résultats montrent que le séchage intermittent peut réduitre de 40% la consommation énergétique.

Un modèle mathématique basé sur la diffusion a été développé pour le séchage continu ainsi que pour le séchage intermittent. Plusieurs autres scénarios de soufflage/chauffage ont été évalués numériquement en tenant compte de leurs applications potentielles.

ACKNOWLEDGMENTS

I wish to record my sincere thanks to my academic advisor, Professor A.S. Mujumdar. As my advisor, he gave me the liberty to pursue this project, yet was always available for guidance and direction when it was needed. He also provided constant inspiration through his creative influence on my professional activities during my time spent at McGill University. I would also like to thank Professor G.S.V. Raghavan for his support and encouragement and for providing me with every facility during my experimental work.

My heartfelt appreciation to my friends S. Sotocinal and B. Ranganna for their help in the design and fabrication of the equipment. They spent countless hours and days in suggesting changes and improvements. Their friendship and company in the drying laboratory made life more bearable. Thanks also to. Mr. R. Cassidy, Mr. R. Nattress, Mr. I. Ansari, Mr. Y. Gariépy, Miss V. Orsat, Mr. D. Nsengiyumva, Mr. N. Prasad and other friends for their assistance during my studies at McGill.

I would like to express my thanks to the members of the Chemical Engineering machine shop particularly Mr. Walter Greenland for their help in the fabrication of the preliminary equipment, to Mr. J. Dumont and Mr. L. Cusmich for their kind assistance.

The financial support from the Ministry of Education, Quebec in the form of "Formation de Chercheurs et L'Aide à la Recherche" (FCAR) grant, Natural Sciences and Engineering Research Council (NSERC) of Canada, and McGill University is gratefully acknowledged.

Last, and certainly not least, I am vastly indebted to my late father for his love, sacrifices, support and encouragement throughout his life and to my mother, brothers and sisters for their moral support, love and patient.

TABLE OF CONTENTS

LIST OF FIGURES

LIST OF TABLES

Chapter 1
Introduction

1.1 General Introduction

Development of more efficient solid-fluid contactors for heat/mass transfer processes as well as chemical reactions is important to the process industries. Efficient gas-particle contactors can be used for drying applications. The objective of the present research project was to develop a novel gas-particle contactor for more efficient and cost-effective drying of particulate solids than the conventional spouted bed or fluid bed dryers.

It is nearly four decades since the advent of the spouted bed as a fluid-solid contacting device. Its beginning can be traced back to 1954 when Mathur and Gishler [1,2] unsuccessfully tried to fluidize wheat grains. They discovered that a new recirculatory gas-solid contact regime could be achieved by blocking most of the grid area and introducing the air as a jet from a small nozzle at the center of the chamber.

The first application of spouted beds was for drying of wheat [3]. Since then the use of spouted beds has been extended to many other thermal, mechanical and chemical processing applications such as drying of a large variety of other coarse particles, suspensions or solutions, particle coating and granulation, blending, heating, cooling, grinding, combustion, gasification, heterogeneous reactions, etc.

1.2 Spouting Principle

Conventional spouted beds (CSBs) consist essentially of a cylindrical or conical-cylindrical vessel fitted at the base with a centrally located gas inlet (Figure 1.1). If the gas velocity is high enough (above the particle terminal velocity), the resulting gas jet penetrates the bed of particles creating a central high voidage spout zone and a low voidage annulus region surrounding the spout. After attaining a certain height above the bed surface, the particles decelerate to their terminal velocity, separate from the carrying gas stream and rain back as a fountain into the annulus. In this way a systematic cyclic movement of the solid particles is established. A dilute phase pneumatic transport of particles by the spouting jet in the central region and dense phase downward motion of particles along the annulus with countercurrent percolation of gas phase characterize the spouted bed device.

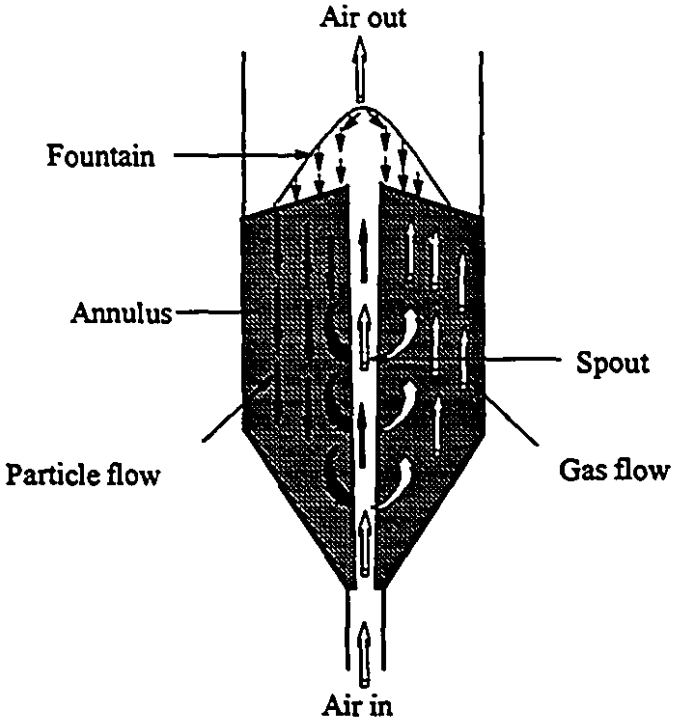

Figure 1.1 Schematic representation of a conventional spouted bed

1.3 Advantages and Limitation of CSBs

The conventional spouted bed has some desirable and several undesirable characteristics with respect to aerodynamics, air and energy requirements and scale-up. Table 1.1 lists some of the advantages and limitations of CSBs. Such limitations have been responsible for the limited commercial use of the spouted bed system as compared to fluidized beds although its potential is increasing with the several successful modifications proposed recently. Chapter 2 presents several spouted bed configurations, showing their characteristics and applications. Several reviews dealing with the fluid-solid mechanics of the spouted beds and their applications have been published [4-11]. The interested reader is referred to these reviews and cited literature for details.

Table 1.1 Advantages and Limitation of Conventional Spouted Beds

Advantages	Limitations
• Can handle coarse particles (D_p > 1 mm)	• Gas flow rate governed by the requirements of spouting rather than heat/mass transfer or chemical kinetics
• Predictable and reproducible solids and gas flow patterns	• Low bed-to-wall or bed-to-surface heat transfer rates
• Regular cyclic movement of solids	• High pressure drop prior to onset of spouting
• Intensive particle circulation	• Low annulus aeration
• Minimal back-mixing	• Limitations on vessel size and maximum spoutable bed height
• Lower pressure drop compared to fluid beds	• Stability problems under certain geometric conditions
• Reduced particle segregation	• Difficulty of scale-up
• Low gas residence time	• Slow solids turnover
• Simple construction and maintenance with no mechanical moving parts	
• Low investment cost	
• Small space requirements	

1.4 Objectives

In the light of the above introductory remarks, the intent of this research was to develop and investigate a novel gas-solid contacting system. The proposed contactor, the Rotating Jet Spouted Bed (RJSB), consists of a rotating inlet air distributor with multiple nozzles for air injection. The major objectives of this research were:

1. To design and construct a new spouted bed with a rotating inlet air distributor.
2. To study the flow characteristics of the system using different solid materials.
3. To investigate the drying kinetics of corn in the RJSB using both continuous and intermittent spouting/heating schemes.
4. To develop empirical and theoretical models for the flow and drying processes.
5. To explore using simulation the possibility of using different time-dependent spouting and heating schemes for more efficient drying.

1.5 Hypotheses

The main hypotheses tested in this study are as follows:

1. Multiple rotating spouting improves particle mixing and circulation and reduces limitations on the vessel diameter.
2. Particles with different size and physical properties can be processed in the RJSB.
3. RJSB can be used for drying large particles (e.g. grains, seeds).
4. Intermittent drying can reduce the net drying time and energy consumption compared with the continuous drying process.
5. Application of time-dependent spouting and heating schemes enhances product quality and results in thermal energy savings.

1.6 Thesis Layout

This thesis is divided into seven chapters of which this introduction is the first. Chapter 2 includes the background for spouted beds design variations and modifications, drying models, and intermittent drying. Chapter 3 describes the experimental set-up, materials, procedures, and the uncertainty analysis. The flow and aerodynamic characteristics of the RJSB are presented and discussed in Chapter 4. Chapter 5 discusses the drying kinetics of corn in the system. A diffusion-based mathematical model for drying in the RJSB is developed in Chapter 6. Finally, Chapter 7 reports the concluding remarks, contributions to knowledge, and recommendations for further work.

References

1. Gishler and K.B. Mathur, "Method of contacting solids particles with fluid", *US Patent No. 2, 786, 280 to N.R.C. of Canada*, (1957) (filled 1954).
2. K.B. Mathur and P.E. Gishler, "A technique for contacting gases with coarse particles", *AIChE J.*, 1, 157-164 (1955).
3. K.B. Mathur and P.E. Gishler, "A study of the application of the spouted bed technique to wheat drying", *J. Appl. Chem.*, 5, 624-636 (1955).
4. K.B. Mathur, Spouted Beds, Chapter 17 in *Fluidization*, J.F. Davidson and D. Harrison, Academic Press, London (1972).
5. K.B. Mathur and N. Epstein, *Spouted Beds*, Academic Press, New York (1974).
6. K.B. Mathur and N. Epstein, "Development in spouted bed technology", *Can. J. Chem. Eng.*, 52, 129-144 (1974).
7. N. Epstein and K.B. Mathur, Applications of Spouted Beds, Section 8.5.6 in *Handbook of Multiphase Systems*, G. Hetsroni (Ed.), McGraw-Hill, New York (1982).
8. N. Epstein and J.R. Grace, Spouting of Particulate Solids, Chapter 11 in *Handbook of Powder Science and Technology*, M.E. Fayed and L. Otten (Eds.), Van Nostrand Co., New York (1984).
9. A.S. Mujumdar "Spouted bed technology - a brief review", in *Drying'84*, A.S. Mujumdar (Ed.), Hemisphere McGraw-Hill, New York, 151-157 (1984).
10. J. Bridgwater, Spouted Beds, in *Fluidization*, J.F. Davidson, R. Clift and D. Harrison (Eds.), 2nd Ed., 201-224, Academic Press, London (1985).
11. M.L. Passos, A.S. Mujumdar and V.G.S. Raghavan, Spouted Beds for Drying: Principles and Design Considerations", in *Advances in Drying*, Vol. 4, A.S. Mujumdar (Ed.), Hemisphere Publishing Corp., New York, 359-398 (1987).

Chapter 2
Background

2.1 Introduction

This chapter presents a brief review of the literature relevant to the research subject. The diverse spouted bed designs that have been developed along with their advantages, disadvantages, and applications are surveyed in section 2.2. Mathematical models for drying of particles, their theoretical basis and limitations are summarized in section 2.3. Section 2.4 is devoted to previous work on time-dependent drying.

2.2 Modified Spouted Beds

Numerous modified spouted bed designs have been developed to overcome some of the limitations of the conventional spouted beds (CSBs), to accommodate the diverse properties of the materials handled, and to enhance the operability, heat and mass transfer characteristics and solid-fluid contacting efficiency [1-5]. These modifications are concerned with changes in the vessel geometry, spouting operation and mechanism, air supply, etc. Table 2.1 updates and extends the classification schemes for spouted bed modifications originally developed by Mujumdar in 1984 [4]. Schematics of some of the spouted bed modified designs along with their characteristics and applications are shown in Figure 2.1 and summarized in Table 2.2. Table 2.2 can also be used as a preliminary selection guide for the spouted bed system to handle specific process requirements. The selection depends mainly on the type of material handled (particles, suspensions, solutions,

etc.), the process to be carried out (drying, coating, granulation, reaction, etc.), and the product specification (quality, yield, etc.) among others.

Table 2.1 Classification of Spouted Beds

CLASSIFICATION CRITERIA	CONFIGURATION
I. *Mechanism of spouting*	• Pneumatic (e.g., CSB,draft tube SB) • Mechanical (e.g., screw conveyor SB) • Vibratory (e.g., vibro-spouted bed)
II. *Vessel geometry*	• Cylindrical-conical (CSB) • Conical • Flat bottom
III. *Cross-section of bed*	• Axisymmetric (CSB, conical) • Two dimensional (large aspect ratio) • Three dimensional (small aspect ratio,half or sector columns,triangular)
IV. Air entry	• Single nozzle at bottom • Central nozzle with auxiliary flow along the annulus • Tangential or swirling air entry along the periphery • No air (vibro-spouted bed) • Multiple nozzles • Rotating nozzles
V. Spouting air flow	• Continuous • Pulsed or intermittent
VI. *Internals*	• With draft tube or divider plates • Active internals (screw conveyor SB) • No internals (CSB)
VII.*Operational mode*	• Batch • Continuous • Multi-stage
VII. *Bed particles*	• Active • Inert (e.g., drying of pastes or slurries)
VIII. *Combined modes*	• Spout-fluid bed • Fluid-spout bed • Jet spouted bed • Rotating jet spouted bed
IX. Spouting fluid phase	• Two-phase spouting (gas-solid,liquid-solid, liquid-liquid) • Three-phase spouting (gas-liquid-solid)

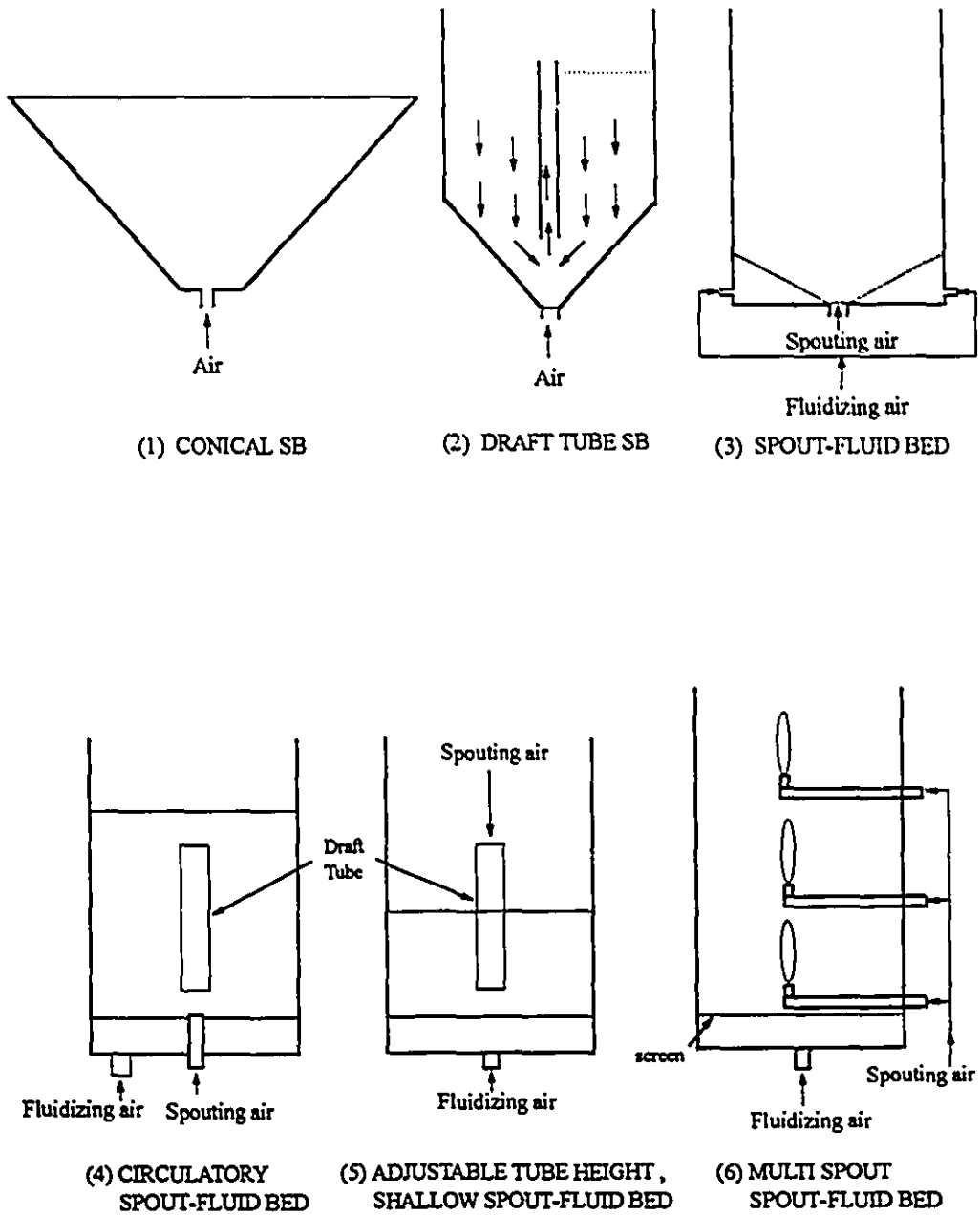

Figure 2.1 Schematics of modified spouted bed configurations

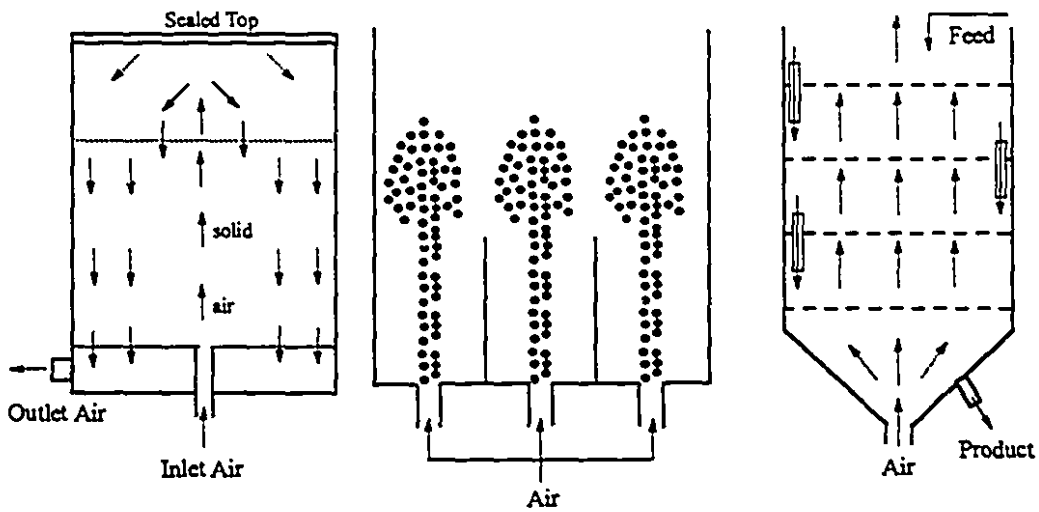

(7) TOP-SEALED SB (8) RECTANGULAR OR CIRCULAR TRIPLE SB (9) MULTISTAGE SB

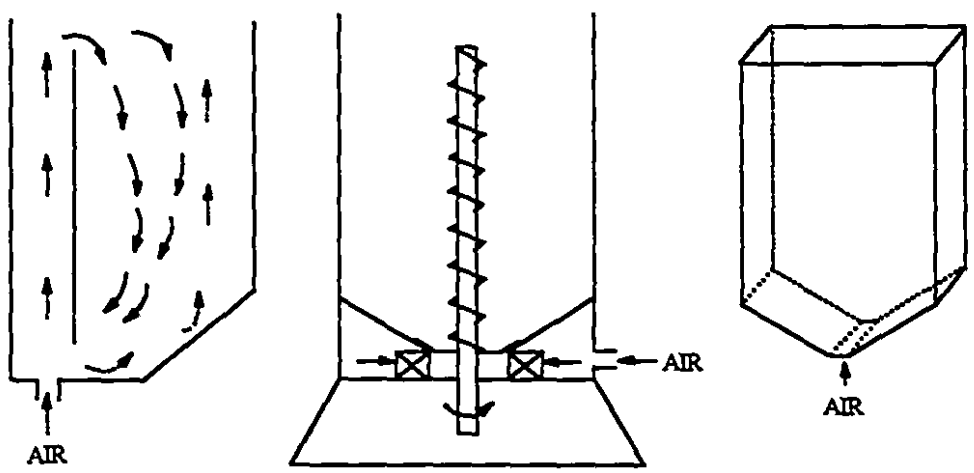

(10) 1/2 SPOUTED BED (11) SCREW CONVEYOR SB (12) 2D SPOUTED BED

Figure 2.1 Schematics of modified spouted bed configurations (*continued*)

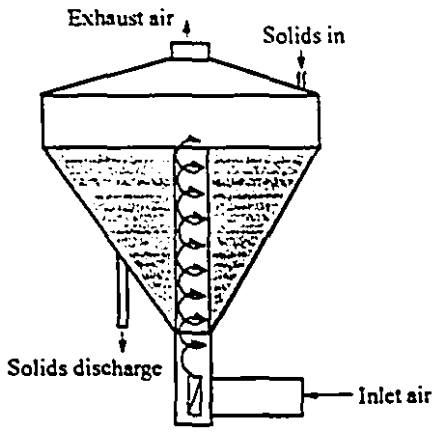

(13) SWIRLED SPOUTED BED

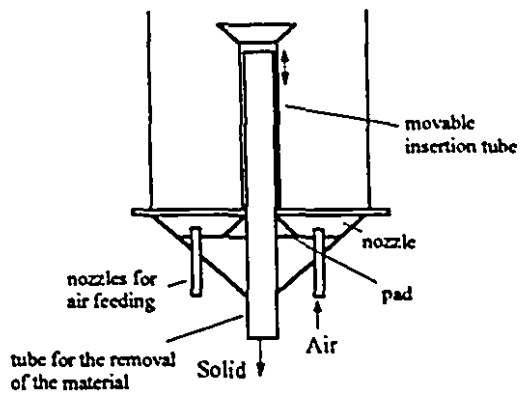

(14) SPOUTED BED WITH FOUR NOZZLES

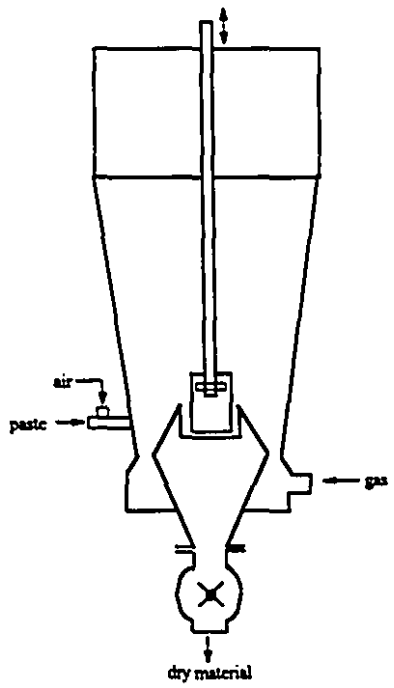

(15) RING SPOUTED BED

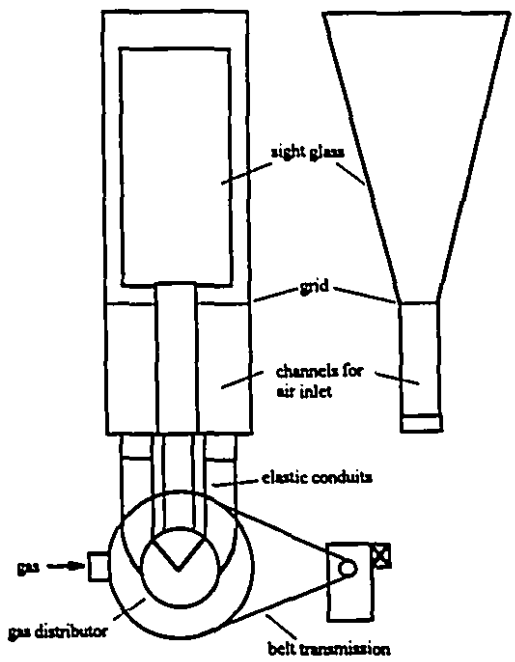

(16) CYCLICALLY SHIFTED SPOUTED BED

Figure 2.1 Schematics of modified spouted bed configurations (*continued*)

Table 2.2 Characteristics and Applications of Modified Spouted Beds

DESIGN	MAIN CHARACTERISTICS	APPLICATIONS
1. *Slot or Two Dimensional Spouted Bed* [4,6-8] (Fig. 2.1 (12))	• more spouting flexibility • lower pressure drop • improved volumetric capacity • simpler design and construction • lower pressure drop • higher air flow rate	• grain drying • drying of wet or sticky material • grain popping • dehydration of gypsum • granulation of solids
2. *Spout-fluid Bed* [9-14] (Figs 2.1 (3)-(6))	• overcomes limitations of CSB (height,stability,poor mixing) and fluidized beds (slugging,stratification) • higher air flow rates • more complex grid design	• granulation • coal gasification • particle coating • incineration of tarry waste
3. *Conical Spouted Bed* [16-19] (Fig. 2.1 (1))	• no limitation of bed height • lower pressure drop • lower annular flow rate • more intensive circulation • high attrition rate	• grain drying • drying of pastes and slurries • particle coating • drying of animal blood
4. *Draft Tube Spouted Bed* [20-24] (Fig. 2.1 (2))	• no limitations of bed height • more control of solid circulation • low minimum spouting pressure drop and air flow rate • lower annular air flow rate • reduced mixing and heat/mass transfer • tendency to clog or choke during startup and shutdown	• drying of grains and chemicals • thermal disinfestation • solids blending
5. *Multistage Spouted Bed* [25,26] (Fig. 2.1 (9))	• higher throughput rates • higher heat utilization efficiency • longer gas contact time with solids • narrow solids RTD • higher pressure drop	• heating of solids
6. *Rectangular or Circular Triple Spouted Bed* [27] (Fig. 2.1 (8))	• larger capacity • more mixing • rapid turnover • higher air flow rates • problems in spouting stability	• drying of heat sensitive materials • cooling of fertilizers

Table 2.2 Characteristics and Applications of Modified Spouted Beds (*continued*)

DESIGN	MAIN CHARACTERISTICS	APPLICATIONS
7. Screw Conveyor Spouted Bed [28-31] (Fig. 2.1 (11))	• air flow rate governed by the process • lower pressure drop • controlled particle circulation rate • no starting up problems • more complex design	• drying of agricultural products • drying of pastes and slurries • drying of chemicals & pharmaceuticals
8. Top-sealed Spouted Bed [32] (Fig. 2.1 (7))	• more uniform gas RTD	• catalytic processes
9. Half Spouted Bed [33] (Fig. 2.1 (10))	• easier scale-up • more stable spouting • lower pressure drop and higher bed height than full column	• grain drying • coating of particles • granulation • drying of sludges
10. Ring Spouted Bed [34,35] (Fig. 2.1 (15))	• increased capacity	• continuous drying of pastes and solutions
11. Cyclically Shifted Spouted Bed [36] (Fig. 2.1 (16))	• reduction of air flow rate • small reduction in ΔP_M • improved mixing	• grain drying • agglomeration of food products
12. Swirled Spouted Bed [37-40] (Fig. 2.1 (13))	• lower pressure drop and air flow rate • higher heat and mass transfer rates • reduced intrainment of treated products • higher energy consumption	• thermal treatment of particles • thermal granulation • drying of adhesive materials
13. Spouted Bed with Four Nozzles [2,3] (Fig. 2.1 (14))	• increased capacity • increased drying efficiency	• drying of solids
14. Vibro-spouted Bed [41]	• residence time of particles could be controlled by adjusting vibration frequency and amplitude • pressure drop peaks are damped	• drying of sticky materials • vacuum drying
15. Jet Spouted Bed [42-45]	• high particle velocity and bed voidage • shallow bed height	• coal gasification • benzyl alcohol polymerization • drying of bio-products • drying of slurries

2.3 Drying Models

Drying can be defined as the removal of moisture (either water or other liquids) by thermal and diffusional process to produce a solid product. It is a unit operation of widespread importance in many process industries e.g. chemical, food, agricultural, paper, textiles, mineral, polymer etc. Drying is usually performed to minimize packaging, handling and transportation costs, to attain a desired moisture content for safe storage or subsequent processing of the product etc.

Drying is often called as much an art as a science. It is a complex operation, involving interactions between heat and mass transfer as well as the flow field of the drying medium in the case of convective drying. Moisture flow occurs within the product to the surface and away from the surface to the surroundings, while heat is transferred from the surface into the product. In addition the presence of solids affects heat, liquid and vapor movement, retarding both transfer processes.

In the drying process a considerable influence is exerted both by external conditions (temperature, humidity and air flowrate) and by the internal structure of the wet solid. Two drying periods are commonly encountered: the constant drying rate period where the external conditions control the process and the falling rate period where the controlling factor becomes the transport resistance inside the material. Development of mathematical models to describe the drying of solids under different conditions has attracted a great deal of attention for several decades. The purpose of modeling is to allow reliable process design and scale-up as well as selection of appropriate method of drying and suitable operating conditions in order to minimize the capital and energy costs.

Generally, a drying model consists of the following main parts:

1. Material model: constitutive heat and mass transfer equations.
2. Equipment model: overall energy and mass balances.
3. Thermodynamic and transport properties models: empirical equations describing the effect of various factors (temperature, moisture content, air humidity etc.) on thermophysical properties.

The most important difficulty in modeling drying is concerned with identification of the mechanism by which the moisture is transferred from within the material (during the falling rate period), depending on the solid/moisture characteristics. Although, no unified theory exists presently to describe the total process involved in a variety of solids, a number of mechanisms have been proposed for moisture transfer; these include: diffusion, capillary flow, evaporation-condensation etc. [46-49]. These mechanisms and the corresponding driving forces are summarized in Table 2.3. The mass transfer deriving forces include gravity and gradients in concentration, partial pressure, total pressure and temperature.

Most of the previous work on drying models has assumed one or more of these moisture transport mechanisms to exist or applied the concepts of irreversible thermodynamics to analyze the coupled heat and mass transfer phenomena [50-56]. Use of a simple mathematical model to describe drying began in the 1920's with Lewis [57], Newman [58], and Sherwood [59]. These early studies assumed moisture transfer to occur by liquid diffusion. This was followed by Hougen et al. [60,61] and Miller and Miller [62,63] who based their work on capillarity theory [64]. Unlike the previous studies, Henry [65] considered simultaneous heat and mass transfer and proposed that the moisture transfer is entirely in the vapor phase based on the vaporization-condensation theory. Krischer [66], Berger and Pei [67], and Philip and De Vries [68] derived drying

models based on the mechanistic approach using different variants of the transfer mechanisms.

Irreversible thermodynamics principles have been used to develop drying models that account for cross-effects between different driving forces. For example, according to Luikov's analysis [69,70], temperature gradients can cause mass diffusion (Soret effect) and concentration gradients can cause heat conduction (Dufour effect) resulting in a coupled set of nonlinear partial differential equations. Fortes and Okos [71,73] have developed a set of heat and mass transfer equations by combining both the mechanistic and irreversible thermodynamic approaches. Based on the local equilibrium principle, it was shown that the driving force for both liquid and vapor transfer in a porous medium is the gradient of equilibrium moisture content.

Whitaker [74-75] attempted to establish a more fundamental theoretical approach to drying of porous media. Based on the assumption of local thermal equilibrium, volume averaged equations for mass, energy and momentum were derived for the gas, liquid and solid phases. In these equations, the relative permeability and capillary pressure have to be extracted from experimental data. However, this theory assumes nonhygroscopic granular porous media (rigid solid phase contains no moisture) and thus it can not be directly applied to the drying of foodstuffs.

It is worthwhile to point out that none of the above models is fully predictive. Transport and coupling coefficients must be determined from experimental drying data and all are strong functions of temperature and moisture content and thus they become adjustable parameters to force the theory to fit a given set of experimental data. Results from these models indicated that the cross-effects are negligible compared to the effects caused by classical equilibrium thermodynamic considerations. As far as grain drying is concerned, temperature and total pressure gradients, surface diffusion, and liquid flow due to gravity are generally neglected under normal grain drying conditions (low or moderate

temperature and atmospheric pressure) typically used in spouted and fluidized bed dryers. Table 2.4 presents a summary of the well-known drying models.

Table 2.3 Moisture Transfer Mechanisms

Mechanism	Driving force
Liquid diffusion	Concentration gradients
Vapor diffusion	Partial pressure gradients (due to temperature gradients)
Capillary movement of liquid	Capillary forces (surface tension)
Liquid/vapor bulk flow	Total pressure gradients (caused by external pressure, shrinkage, high temperatures etc.)
Surface diffusion (on adsorbed liquid layers on the pore surfaces)	Surface concentration gradients
Liquid flow (mainly in coarse-pored solids)	Gravity forces
Liquid-vapor diffusion in partially air-filled pores or vaporization-condensation in capillaries	Difference in partial pressures
Liquid and vapor diffusion	Concentration and temperature (thermodiffusion) gradients

Table 2.4 Selected Drying Models

Model and Mechanism	Transfer Equations	Heat/Mass Balances
Lewis [57], Newman [58], Sherwood [59] {Isothermal liquid diffusion}	$n_l = -\rho_s D_l \nabla X$	$\frac{\partial X}{\partial t} = \nabla.(D_l \nabla X)$
Hougen et al. [60,61] {Capillary flow}	$n_l = -\rho_s k_H \nabla X$	$\frac{\partial X}{\partial t} = \nabla.(k_H \nabla X)$
Henry [65] {Evaporation condensation}	$n_v = -D_v \nabla X_v$ $q = -k_s \nabla T$	$\frac{1-a}{a}\rho_s \frac{\partial X}{\partial t} = \varepsilon \nabla.(D_v \nabla X_v) - \frac{\partial X_v}{\partial t}$ $\rho_s c_{ps} \frac{\partial T}{\partial t} = -\nabla.(k_s \nabla T) - \varepsilon \frac{\partial X}{\partial t}$
Krischer's [66], Berger and Pei [67] {Capillary-vapor diffusion}	$n_l = -\rho_l D_l \nabla X$ $n_v = -D_v (a-u) \nabla \rho_v$ $q = -k_s \nabla T$	$(\rho_l - \rho_v)\frac{\partial u}{\partial t} + (a-u)\frac{\partial \rho_v}{\partial t} = \rho_l D_l \nabla^2 u + [(a-u)\nabla^2 u \rho_v - \nabla u \nabla \rho_v]$ $\frac{\partial T}{\partial t} = \alpha_T \nabla^2 T + \frac{\Delta H_v}{\rho_s c_{ps}}\left[D_v\{(a-u)\nabla^2 \rho_v - \nabla u \rho_v\} - (a-u)\frac{\partial \rho_v}{\partial t} + \rho_v \frac{\partial u}{\partial t}\right]$
Philip and De Vries [68] {Capillary-vapor diffusion under T and X gradients }	$n_v = -D_v \nabla X - D_{vT} \nabla T$ $n_l = -D_l \nabla X - D_{lT} \nabla T - K_l$ $q = -k_s \nabla T$	$\frac{\partial X}{\partial t} = \nabla.((D_{lT} + D_{vT})\nabla T) + \nabla.((D_l + D_v)\nabla X) + \frac{\partial K_l}{\partial Z}$ $\rho_s c_{ps} \frac{\partial T}{\partial t} = -\nabla.(k_s \nabla T) + \Delta H_v \nabla.(D_v \nabla X)$
Luikov [69,70] "Irreversible thermodynamics" {vapor: diffusion + effusion} {liquid: diffusion + capillary}	$n_w = -\rho_s D(\nabla X + \delta \nabla T)$ $q = -k_s \nabla T$	$\frac{\partial X}{\partial t} = \nabla.[D(\nabla X + \delta \nabla T)]$ $\rho_s c_{ps} \frac{\partial T}{\partial t} = \nabla.(k_s \nabla T) + \rho_s \varepsilon \Delta H_v \frac{\partial X}{\partial t}$
Fortes and Okos [71-73] "Irreversible thermodynamics" (deriving force: equilibrium moisture content gradient) {no specific mechanism is required}	$n_l = -\rho_l k_l R \ln(RH\ \nabla T) - \rho_l k_l \frac{RT}{RH}\frac{\partial RH}{\partial X}\nabla X$ $n_v = -k_v\left(\rho_w \frac{\partial RH}{\partial T} + RH \frac{d\rho_w}{dT}\right)\nabla T - k_v \frac{RT}{RH}\frac{\partial RH}{\partial X}\nabla X$ $q = -k_s \nabla T - \left[\rho_l k_l R \ln RH + k_v\left(\rho_w \frac{\partial RH}{\partial T} + RH \frac{d\rho_w}{dT}\right)\right] \times \frac{RT^2}{RH}\frac{\partial RH}{\partial X}\nabla X$	$\rho_s \frac{\partial X}{\partial t} = -\nabla.(n_l + n_v)$ $\rho_s c_{ps} \frac{\partial T}{\partial t} - \rho_s \Delta H_v \frac{\partial X}{\partial t} = -\nabla.q - \Delta H_v \nabla n_v$

2.4 Time-dependent Drying

The aim of any drying process is to produce a solid product of desired quality at minimum cost and maximum throughput, and to maintain these consistently. Good quality implies that the product corresponds to a number of technical, chemical, and/or biological parameters, each within specified limits. Thermal drying is an energy-intensive operation that accounts for up to 15 % of all industrial energy usage, with low thermal efficiency, typically between 25 % and 50 %. Among the methods for enhancement heat and mass transfer during drying, reducing energy consumption and preserving quality, the following should be considered [76,77]: development of heat recovery methods, use of nonconventional energy sources (microwaves, radiofrequency, etc.), reduction of heat losses, development of new drying techniques, optimum choice of drying conditions, implementation of automatic control algorithms, and application of time-dependent drying schemes.

Time-dependent drying processes can be classified into the following categories:

1. Intermittent drying: supplying heat only intermittently rather than continuously. This can be done by interrupting the air flow to provide the material a "rest" period, by a continuous air flow periodically heated, or by periodic reduction of air flow.
2. Dryaeration: which is a grain drying process involving a combination of high temperature short drying period, tempering, and slow cooling concluded by final drying.
3. Airflow reversal: applying the drying airflow in one direction for some time and then reversing the direction of the flow for the next period.
4. Inherent time-dependent drying: this can found in certain dryers such as rotary, plug-flow and vibrated fluid beds, recirculating grain dryers, deep conventional and draft

tube spouted beds (very short tempering period during particle passage through the annulus), etc.

Several experimental studies have been carried out to investigate different schemes for time-dependent drying of grains and granular materials in different dryers [78-89]. These studies (summarized in Table 2.5) lead to the establishment of the following features of time-dependent drying:

1. Thermal energy savings.
2. Shorter effective drying time.
3. Higher moisture removal rates (while energy is supplied).
4. Lower solid surface temperature.
5. Higher product quality: reduced shrinkage, cracking, and brittleness, germinability, and protein denaturation.
6. Moisture gradients at the surface of the solid are flattener than during drying with constant temperature.

Numerical and simulation investigations have been conducted to study the thermal, mass, and mechanical effects of time-dependent drying. Hällstrom [79] presented an approximate method to describe the flight-and-soaking movement of granules in a rotary dryer. It is assumed that the periodicity can be characterized by a mass transfer coefficient, proportional to $\sqrt{t_d}/(t_d + t_r)$, where t_d and t_r are the durations of the drying and resting periods, respectively. Davidson [90] set out an approximate theory to describe the diffusion of moisture within a granule subjected to alternating boundary conditions during its passage through a rotary dryer. Assuming that the granule is surrounded by a fictitious permeable membrane layer, the drying time could be predicted within 10 % as compared with the classical diffusion equation.

The Fortes and Okos drying model [72,73] has been used by Fortes et al. [91] and Litchfield and Okos [92] to model the dryaeration of corn. Their analysis predicted the development and relaxation of temperature and concentration gradients inside the kernel as well as stress and breakage during drying, tempering, and cooling. Using the finite element method and Luikov's model, Zhang and Mujumdar [93] analyzed temperature, moisture and stress distributions at different instances during intermittent thermal drying using volumetric heating.

Garside et al. [82], Yebo and Chongwen [94] and Brook and Bakker-Arkema [95] solved the mass diffusion equations to predict the intermittent drying phenomena in a rotary dryer, a recirculating grain dryer, and a commercial concurrentflow grain dryer, respectively. Toyoda [96] proposed a simple "two-tank model" to predict the intermittent drying of rough rice in a crossflow recirculating dryer. The effects of air temperature, air and grain flowrates on the dryer performance were studied.

Glowacka and Malczewki [87] solved Luikov's equations to predict the fluidized bed drying of granular materials using time-varying inlet air temperature. The effect of intermittency on energy saving was also proved. A mechanistic heat and mass transfer model has been developed by Hemati et al. [89] to validate their experimental intermittent drying data in a flotation fluidized bed. The model assumes zero transfer rates at the surface of the particle during the rest period and the results of the simulation are in good agreement with the experimental results.

Ratti and Mujumdar [97] presented a simulation study for batch drying of shrinking hygroscopic materials in a fixed bed using time-varying inlet air flowrate. It is shown that the total air consumption for drying is reduced with minor or no increase in drying times. In a later study, Ratti and Mujumdar [98] extended their analysis to investigate the case of airflow reversal. The results showed that both moisture and

temperature profiles in the bed were flatter when airflow reversal was applied to the drying process while the average drying curves were practically unchanged.

The limited studies on intermittent drying of materials in a batch dryer confirm the potential advantages of time-dependent supply of energy for drying viz. reduced energy consumption, reduced air consumption and enhanced product quality of heat sensitive products.

Table 2.5 Summary of Experimental Time-dependent Drying Studies

STUDY	MATERIAL & DRYER TYPE	DRYING SCHEME
Edhom [78]	wheat (thin layer)	intermittent drying: drying periods: 2-60 min rest periods: 15 min-3 h
Thomson and Foster [80]	maize (thin layer)	dryaeration: 8 h tempering
Woodforde and Lawton [81]	Brussels sprouts, carrot, cocksfoot, sugar beet (thin layer)	drying periods: 7 h rest periods: 17 h
Garside et al. [82]	granular fertilizer (rotary dryer simulator)	intermittent drying: flight period: 0.8 sec soaking periods: 3.5-60 sec
Sabbah et al. [83]	corn (thin layer)	dryaeration: tempering periods: 0-4 h
Troeger and Butler [84]	peanuts (bin dryer)	intermittent drying: airflow interrupted at 15-45 min/h or 1 in 4 h.
Harnoy and Radajewski [85]	maize (bin dryer)	intermittent drying: aeration periods: 1-6 min rest periods: 3-90 min

Table 2.5 Summary of Experimental Time-dependent Drying Studies (continued)

STUDY	MATERIAL & DRYER TYPE	DRYING SCHEME
Phinheiro Filho et al. [86]	soybeans (cylindrical container with shaft valve)	intermittent heating: heating periods: 5,10 min cooling fraction: 0.4, 0.8
Glowacka and Malczewski [87]	wheat (fluidized bed)	Sinusoidal heating
Hallstrom [79]	compound fertilizer (fluid bed)	intermittent drying: drying periods: 2.5-6 s rest periods: 4.5-6 s
Zhang and Litchfield [88]	corn (thin layer)	intermittent drying: drying period: 20 min rest periods: 0-120 min
Hemati et al. [89]	corn (flotation fluid bed)	intermittent drying: drying period: 20 min rest periods: 0-60 min

Nomenclature

Symbols

a	volume fraction of air in pores
c_p	specific heat
D	Diffusion coefficient
ΔH_v	latent heat of vaporization
ΔH_w	differential heat of wetting
k	hydraulic, thermal, liquid, or vapor conductivity
K_i	gravitational flux
n	moisture flux
ΔP	pressure drop
q	heat flux
R	universal gas constant
RH	relative humidity
t	time
T	absolute temperature
u	volumetric moisture content (volume of water/volume of dry solid)
X	moisture content (kg moisture/kg dry solid)
Z	vertical ordinate

Greek Letters

α_T	thermal diffusivity
δ	thermodiffusion coefficient
ε	tortuosity factor for the diffusion of vapor or phase conversion factor
ρ	density

Subscripts and Superscripts

d	drying
H	hydraulic
l	liquid phase
m	mass transfer characteristics
M	maximum
o	saturated state
p	particle
r	rest
s	solid
T	thermal, heat transfer characteristics
v	vapor phase
w	total moisture (liquid + vapor)

References

1. K.B. Mathur and N. Epstein, *Spouted Beds*, Academic Press, New York (1974).
2. J. Nemeth and E. Pallai, "Scale-up examination of spouted bed dryers", *Can. J. Chem. Eng.*, 61, 419-425 (1983).
3. E. Pallai, J. Nemeth, and E. Aradi, "Developement of spouted bed dryer", in *Drying'84*, A.S. Mujumdar (Ed.), Hemisphere McGraw-Hill, New York, 158-165 (1984).
4. A.S. Mujumdar "Spouted bed technology - a brief review", in *Drying'84*, A.S. Mujumdar (Ed.), Hemisphere McGraw-Hill, New York, 151-157 (1984).
5. M.L. Passos, A.S. Mujumdar and V.G.S. Raghavan, Spouted Beds for Drying: Principles and Design Considerations, Chapter 7 in *Advances in Drying*, Vol. 4, A.S. Mujumdar (Ed.), Hemisphere Publishing Corp., New York, 359-398 (1987).

6. W.C. Rockwell, E. Lowe, H.G. Walker and A.I. Morgan, "Hot air grain popping", *Feedlot*, November (1986).
7. M.L. Passos, A.S. Mujumdar and V.G.S. Raghavan, "Design parameters for a two dimensional spouted bed", *Paper Presented in Third International Symposium on Spouted Beds*, Vancouver, BC (1991).
8. M.L. Passos, A.S. Mujumdar and V.G.S. Raghavan, "Spouting and spout-fluidization of dry/wet particles in a two-dimensional bed", in *Drying of Solids*, A.S. Mujumdar (Ed.), Sarita Prakashan Publishers, New Delhi, 211-220 (1990).
9. A. Chatterjee, "Spout-fluid bed technique", *Ind. Eng. Chem. Process Des. Develop.*, 9, 340-341 (1970).
10. A.A. Pomortseva and A.P. Baskakov, "Hydrodynamics and heat transfer in fluidized beds of fine grained materials with local spouting zones", *Khim. Technol.* Masel., 15, 34 (1970). Quoted by Mathur and Epstein [1].
11. A. Chatterjee, S.R. Patwardhan and D.D. Chinchmalatpure, "Spout-fluid bed technique for inceneration of tarry wasts", *33rd Annual Session Proc., Indian Inst. of Chem. Engineers*, New Delhi, Dec., 17-20 (1980).
12. A. Chatterjee, R.S.S. Adusumilli, and A.V. Deshmuk, "Wall-to-bed heat transfer characteristics of spout-fluid beds", *Can. J. Chem. Eng.*, 61, 390-397 (1983).
13. B. Ye, C.J. Lim, and J.R. Grace, "Hydrodynamics of spouted and spout-fluidized beds at high temperature", *Can. J. Chem. Eng.*, 70, 840-847 (1992).
14. M.L. Passos, *Flow Characteristics of Two-dimensional Spouted and Spout-fluidized Beds of Particles*, Ph.D. Thesis, McGill University, Montreal, PQ (1991).
15. Passos, A.S. Mujumdar and V.G.S. Raghavan, "Spouted and spout-fluidized beds for grain drying", *Drying Technology*, 7, 663-696 (1989).
16. D.S. Povrenovic, D.E. Hadzismajlovic, Z.B. Grbavcic, V. Vukovic and H. Littman, "Minimum fluid flowrate, pressure drop and stability of a conical spouted bed", *Proc. 9th Int. Cong. of Chem. Eng. (CHISA '87)*, E9.27 (1987).
17. A. Kmiec, "The minimum spouting velocity in conical beds", *Can. J. Chem. Eng.*, 61, 274-280 (1983).

18. J. Kucharski and A. Kmiec, "Hydrodynamics, heat and mass transfer during coating of tablets in a spouted bed", *Can. J. Chem. Eng.*, 61, 435-439 (1983).
19. Pham, "Behaviour of a conical spouted-bed dryer for animal blood", *Can. J. Chem. Eng.*, 61, 426-434 (1983).
20. R.H. Buchanan and B. Wilson, "The fluid-lift solids recirculator", *Mech. Chem. Eng. Trans.*, 1, 117-124 (1965).
21. J.K. Claflin and A.G. Fane, "Gas distributor and heat transfer in a draft-tube spouted bed", *AIChE Symp. Ser.*, 241, 80, 17-23 (1984).
22. J.K. Claflin and A.G. Fane, "Fluid mechanics, heat transfer and drying in spouted beds with draft-tubes", in *Drying'84*, A.S. Mujumdar (Ed.), Hemisphere McGraw-Hill, New York, 137-141 (1984).
23. M.I. Kalwar, *Aerodynamics and Drying Characteristics of Grains in Two-dimensional spouted Beds*, Ph.D. Thesis, McGill University, Montreal, PQ (1991).
24. M.I. Kalwar, G.S.V. Raghavan, and A.S. Mujumdar, "Spouting of two-dimensional beds with draft plates", *Can. J. Chem. Eng.*, 70, 887-894 (1992).
25. L.A. Madonna, R.F. Lama and W.L. Brisson, "Solids-air jets", Brit. Chem. Eng., 6, 524 (1961).
26. M.A. Malek and T.H. Walsh, "The treatment of coal for coking by the spouted bed process", *Rep. No. FMP 66/54-SP. Dept. Mines and Tech. Surveys*, Ottawa, Can., (1966).
27. W.S. Peterson, "Multiple spouted bed", *Can. Patent No. 739,660 to Nat. Res. Council of Can.* (1966).
28. J. Nemeth, E. Pallai, M. Peter, and R. Toros, "Heat transfer in a novel type spouted bed", *Can. J. Chem. Eng.*, 61, 406-410 (1983).
29. T. Szentmarjay, E. Pallai, and A. Szalay, "Drying process on inert particles in mechanically spouted bed dryer", *Drying'94*, V. Rudolph, R.B. Keey, and A.S. Mujumdar (Eds.), University of Queensland, Brisbane, Australia, 471-478 (1994).
30. T. Szentmarjay, A. Szalay, and E. Pallai, "Scale-up aspects of the mechanically spouted bed dryer with inert particles", *Drying Technology*, 12, 341-350 (1994).

31. E. Pallai, T. Szentmarjay, and A.S. Mujumdar, "Spouted bed drying", Chapter 13 in *Handbook of Industrial Drying*, 2nd ed., A.S. Mujumdar (Ed.), vol. 1, 453-488 (1995).
32. F.G. Ageyev, V.E. Soroko, and I.P. Mukhlenov, "Contact apparatus with a jet circulative bed of granular material", *Khim. Prom.* (Mosko), 46, 465 (1970). Quoted by Mathur and Epstein [1].
33. C. Brereton and C.J. Lim, "Spouted bed drying of sludge from metal finishing industries wastewater treatment plants", *Drying Technology*, 11, 389-399 (1993).
34. P.G. Romankov, Drying. in *Fluidization*, J.F. Davidson and D. Harrison (Eds.), Chapter 12, Academic Press, New York (1971).
35. P.G. Romankov and N.B. Rashkovskaya, *Drying in a Suspended State*, 2nd ed., in Russian, Chem. Publ. House, Leningrad Branch (1968). Quoted by Mathur and Epstein [1].
36. A. Jezowska, "Kinetics of drying in cyclically shifted spouted bed", *Drying Technology*, 11, 319-337 (1993).
37. E. Arradi, E. Pallai, T. Blickle, E. Monostori, J. Nemeth and J. Varga, "Contacting and drying of material in a spouted bed system", *Hung. Pattent Off. No. 176.030* (1976).
38. A.F. Dolidovich and V.S. Efremtsev, "Hydrodynamics and Heat transfer of spouted beds with two-component (gas-solid) dispersing medium", *Can. J. Chem. J.*, 61, 398-405 (1983).
39. A.F. Dolidovich and V.S. Efremtsev, "Experimental study of thermal granulation process in a spouted bed", *Can. J. Chem. Eng.*, 61, 454-459 (1983).
40. A.F. Dolidovich, "Hydrodynamics and interphase heat transfer in a swirled spouted bed", *Can. J. Chem. Eng.*, 70, 930-937 (1992).
41. J.R. Finzer and T.G. Kieckbusch, "Performance of an expereimental vibro-spouted bed dryer", *Drying'92*, A.S. Mujumdar (Ed.), Elsevier, Amsterdam, 762-772 (1994).
42. A. Markowski and W. Kaminski, "Hydrodynamics characteristics of jet-spouted beds", *Can. J. Chem. Eng.*, 61, 377-381 (1983).

43. O. Uemaki and T. Tsuji, "Particle velocity and solids circulation rate in a jet-spouted bed", *Can. J. Chem. Eng.*, 70, 925-929 (1992).

44. A. Markowski, "Drying characteristics in a jet-spouted bed dryer", Can. J. Chem. Eng., 70, 938-944 (1992).

45. Grabowski, A.S. Mujumdar, H.S. Ramaswamy, and C. Strumillo, "Particle size distribution of L-lysine dried in jet-spouted bed", *Drying'92*, A.S. Mujumdar (Ed.), Elsevier, Amsterdam, 1940-1946 (1994).

46. W.B. Van Arsdel, *Food Dehydration - Principles*, Vol. 1, Avi, Westport (1963).

47. M. Fortos and M.R. Okos, Drying Theories: Their Bases and Limitations as Applied to Foods and Grains, Chapter 5 in *Advances in Drying*, Vol. 1, A.S. Mujumdar (Ed.), Hemisphere Publishing Corp., New York, 119-154 (1980).

48. S. Bruin and K. Ch. Luyben, Drying of Food Materials, Chapter 6 in *Advances in Drying*, Vol. 1, A.S. Mujumdar (Ed.), Hemisphere Publishing Corp., New York, 155-215 (1980).

49. A.S. Mujumdar, "Heat transfer problems in drying", Special Keynote Lecture, *10th Int. Heat Transfer Conf.*, Brighton, UK, vol. 1, 105-116, Taylor & Francis, N.Y. (1994).

50. K.M. Waananen, J.B. Litchfield, and M.R. Okos, "Classification of drying models for porous solids", *Drying Technology*, 11, 1-40 (1993).

51. K.N. Shukla, *Diffusion Processes During Drying of Solids*, World Scientific, Singapore (1990).

52. J.L. Parry, "Mathematical modelling and computer simulation of heat and mass transfer in Agricultural grain drying: a review", *J. Agric. Engng Res.*, 32, 1-29 (1985).

53. D.S. Jayas, S. Cenkowski, S. Pabis, and W.E. Muir, "Review of thin-layer drying and wetting equations", *Drying Technology*, 9, 551-588 (1991).

54. M. Abid, R. Gibert, and C. Laguerie, "An experimental and theoritical analysis of the mechanisms of heat and mass transfer during the drying of corn grains in a fluidized bed", *Int. Chem. Eng.*, 30, 632-642 (1990).

55. S. Sokhansanj, "Improved heat and mass transfer models to predict grain quality", *Drying Technology*, 5, 511-525 (1987).

56. J. Irudayaraj, K. Haghighi, and R.L. Stroshine, "Finite element analysis of drying with application to cereal grains", *J. agric. Engng Res.*, 53, 209-229 (1992).

57. W.K Lewis, "The rate of drying of solid materials", *J. Ind. Eng. Chem.*, 13, 427-432 (1921).

58. A.B. Newman, "Diffusion and surface emission equation", *Trans. AIChE*, 27, 203-220 (1931).

59. T.K Sherwood, "Application of the theoritical diffusion equations to the drying of solids", *Trans. AIChE*, 27, 190-202 (1931).

60. O.A. Hougen, H.J. McCauley, and W.R. Marshall, "Limitation of diffusion equations in drying", *Trans. AIChE*, 35, 193-206 (1940).

61. N.H. Ceaglske and O.A. Hougen, "The drying of granular solids", *Trans. A.I.C.E.*, 33, 283-312 (1937).

62. E.E. Miller and R.D. Miller, "Theory of capillary flow: I. practical applications", *Proc. Soil Sci. Soc. Am.*, 19, 267-271 (1955).

63. E.E. Miller and R.D. Miller, "Theory of capillary flow: II. experimental information", *Proc. Soil Sci. Soc. Am.*, 19, 271-275 (1955).

64. E.A. Buckingham, "Studies on the movement of soil moisture", *U.S. Dept. Agr. Bull.* 38 (1907).

65. P.S.H. Henry, "Diffusion in absorbing media", *Proc. R. Soc. London*, 171A, 215-241 (1939).

66. O. Krischer, *Die wissenschaftlichen Grundlagen der Trocknungstechnik*, 2nd ed., Springer-Verlag, Berlin (1963).

67. D. Berger and D.C.T. Pei, "Drying of Hygroscopic capillary porous solids, a theoritical approach", *Int. J. Heat Mass Transfer*, 16, 293-302 (1973).

68. J.R. Philip and D.A. De Vries, "Moisture movement in porous materials under temperature gradients", *Trans. Am. Geophys. Union*, 38, 222-232 (1957).

69. A.V. Luikov, *Heat and Mass Transfer in Capillary-Porous Bodies*, Pergamon Press, Oxford (1966).

70. A.V. Luikov, "Systems of differential equations of heat and mass transfer in capillary-porous bodies (review)", *Int. J. Heat Mass Transfer*, 18, 1-14 (1975).

71. M. Fortes and M.R. Okos, "A non-equilibrium thermodynamics approach to transport phenomena in capillary porous media", *Trans. ASAE*, 24, 756-760 (1981).

72. M. Fortes and M.R. Okos, "Non-equilibrium thermodynamics approach to heat and mass transfer in corn Kernels", *Trans. ASAE*, 24, 761-769 (1981).

73. M. Fortes and M.R. Okos, "Heat and mass transfer in Hygroscopic capillary extruded products", *AIChE J.*, 27, 255-261 (1981).

74. S. Wataker, Simultaneous, Heat, Mass and Momentum transfer in Porous Media, in *Advances in Heat Transfer*, Vol. 13, 119-203, Academic Press, New York (1977).

75. S. Wataker, Heat and Mass transfer in Granular Porous Media, Chapter 2 `in *Advances in Drying*, A.S. Mujumdar (Ed.), Vol. 1, 23-61, Hemisphere, Washington, D.C. (1980).

76. C. Stumillo, P.L. Jones, and R. Zylla, Energy Aspects in Drying, Chapter 40 in *Handbook of Industrial Drying*, 2nd ed., A.S. Mujumdar (Ed.), Marcel Dekker, New York, 1241-1275 (1995).

77. R.Y. Jumah, A.S. Mujumdar, and V.G.S. Raghavan, Control of Industrial Dryers, Chapter 43 in *Handbook of Industrial Drying*, 2nd ed., A.S. Mujumdar (Ed.), Marcel Dekker, New York, 1343-1368 (1995).

78. H. Edholm, "Undersokningar angaende torkning av spannmal", Medd. Nr 31. Jordbrukstekniska Foreningen, Uppsala, Sweden (1932). Quoted by A. Hällstrom [79].

79. A. Hällstrom, "Alternative boundary conditions in drying", *Chem. Eng. Sci.*, 41, 2225-2234 (1986).

80. R.A. Thomson and G.H. Foster, "Dryeration-high speed drying with delayed aeration cooling", *ASAE Paper No. 67-843* (1967).

81. J. Woodforde and P.J. Lawton, "The drying of seeds", *J. agric. Engng Res.*, 10, 283-297 (1965).

82. J. Garside, L.W. Lord, and R. Reagan, "The drying of fertilizers", *Chem. Eng. Sci.*, 25, 1133-1148 (1970).

83. M.A. Sabbah, G.H. Foster, C.G. Hauge, and R.M. Peart, "Effect of tempering after drying on cooling shelled corn", *Trans. ASAE*, 15, 763-765 (1972).

84. J.M. Troeger and J.L. Butler, "Drying peanuts with intermittent airflow", *Trans. ASAE*, 23, 197-199 (1980).

85. A. Harnoy and W. Radajewski, "Optimization of grain drying - with rest periods", *J. agric. Engng Res.*, 27, 291-307 (1982).

86. J.B. Pinheiro Filho, M. Fortes, V.E. Sweat, and M.R. Okos, "Intermittent drying of soybeans", in *Drying'82*, A.S. Mujumdar (Ed.), Hemisphere, New York, 220-226 (1982).

87. M. Glowacka and J. Malczewski, "Oscillating temperature drying", in *Drying of Solids*, A.S. Mujumdar (Ed.), 77-83 (1986).

88. Q. Zhang and Litchfield, "An optimization of intermittent corn drying in a laboratory scale thin layer dryer", *Drying Technology*, 9, 383-395 (1991).

89. M. Hemati, M. Mourad, D. Steinmetz, and C. Laguerie, "Continuous and intermittent drying of maize in a flotation fluidized bed", *Fluidization VII*, Engineering Foundation for International Fluidization Conference, Australia (1992).

90. J.F. Davidson, M.W. Robson, and F.C. Roesler, "Drying of granular solids subjected to alternating boundary conditions", *Chem. Eng. Sci.*, 24, 815-828 (1969).

91. M. Fortes, M.R. Okos, and J.B. Pinheiro Filho, "Modeling of dryaeration processes", *Drying'82*, A.S. Mujumdar (Ed.), Hemisphere, Washington, 12-18 (1982).

92. J.B. Litchfield and M.R. Okos, "Prediction of corn kernel stress and breakage induced by drying, tempering, and cooling", *Trans. ASAE*, 31, 585-594 (1988).

93. D. Zhang and A.S. Mujumdar, "Deformation and stress analysis of poroud capillary bodies during intermittent volumetric thermal drying", *Drying Technology*, 10, 421-443 (1992).

94. Yebo and C. Chongwen, "Simulation and experimental study on recirculating grain dryer", *Drying'94*, V. Rudolph, R.B. Keey and A.S. Mujumdar (Eds.), University of Queensland, Australia, 801-808 (1994).

95. R.C. Brook and F.W. Bakker-Arkema, "Simulation for design of commercial concurrentflow grain dryers", *Trans. ASAE*, 21, 978-981 (1978).

96. Toyoda, "Study of intermittent drying of rough rice in a recirculating dryer", in *Drying'89*, A.S. Mujumdar and M. Roques (Eds.), Hemisphere, New York, 289-296 (1989).

97. C. Ratti and A.S. Mujumdar, "Fixed-bed batch drying of shrinking particles with time varying drying air conditions", *Drying Technology*, 11, 1311-1335 (1993).

98. C. Ratti and A.S. Mujumdar, "Simulation of packed bed drying of foodstuffs with airflow reversal", *J. Food Engineering*, in press (1995).

Chapter 3

Experimental Apparatus, Materials and Procedure

3.1 Introduction

This chapter provides details about the experimental set-up, the design of the rotating jet spouted bed (RJSB), the materials used, and the experimental procedures and techniques employed in both the aerodynamic and drying kinetics experiments. Experimental uncertainty and reproducibility results are also presented.

3.2 Experimental Set-up

A schematic diagram of the experimental set-up and the associated instrumentation is shown in Figure 3.1. The rotating jet spouted bed is realized by using a rotating inlet air distributor *(1)* with two radially located nozzles 2 and 3 cm in diameter, under the bed supporting screen *(2)*. The nozzles, covering both the central and annular regions of the bed, are located at 4.5 and 18 cm from the center of the vessel, respectively. The distributor is enclosed within a perfectly sealed aluminum box *(3)*. The supporting screen is made of galvanized steel wire (2×2 mesh) reinforced along its circumference by a circular metal loop. This main support screen is covered at the upper surface with a 20×20 mesh aluminum wire net. The openings of the finer screen were small enough to contain the particles but large enough that flow of air was unrestricted.

The rotating section (see Figure 3.2 for more details) of the main inlet air pipe is provided on its outer surface with two rubber-sealed ball bearing assemblies *(4)*; all are circumfused by another well sealed coaxial pipe. The downstream part of this rotating section is engaged with two belt-driven pulleys *(5),(6)* connected to a 3-hp variable speed AC motor *(7)* (Boston Gear, Quincy, MA) through a gear speed reducer (Boston Gear, Quincy, MA). The motor speed could be controlled using an AC inverter *(8)* (Boston Gear, Quincy, MA) calibrated using a digital tachometer.

The spouted bed *(9)* consists of a flanged cylindrical vessel 45 cm diameter and 90 cm in high, made of borosilicate glass (Q.V.F.). The whole assembly of the vessel, distributor, and drive was carefully leveled and securely mounted on a rigid metallic frame.

The spouting air is supplied by a high pressure blower *(10)* (GAST Regenair, model no. R7100 B-1, GAST Mfg. Corp., Benton Harbor, MI) and maintained at pre-selected temperatures by a set of electric heaters rated at 6 kW *(11)* and fitted with a PID controller *(12)* (TCU temperature controller, Red Lion Controls, York, Pa). The outer wall of the heating compartment is insulated by fiberglass to minimize heat losses. The air flow rate is measured with a precalibrated pitot tube *(13)* (model no. FPT-6120, Omega Engineering) and regulated by means of gate valves *(14)* on the feed and bypass lines. Differential pressure drop across the pitot tube is measured using a manometer filled with manometric fluid (Merium red fluid, Merium Instrument, Cleveland, OH). Alternatively, the pressure drop could be measured on a pressure transducer *(15)*.

Pressure drop across the bed is measured using static pressure taps *(16)* connected to a calibrated differential pressure transducer *(15)* (model no. PX185, Omega Engineering) mounted on a printed circuit board. The pressure taps are in stainless steel with an internal diameter of 3 mm and an external diameter of 6 mm. The transducers are mounted as close as possible to the measurement points to minimize the signal damping.

A regulated power supply (model no. 1080, Brunelle Instruments, St. Elle D'Orford, Que.) with a variable output 30 V d.c. is employed in conjunction with the transducers.

Several copper-constantan type T thermocouples *(17)* were installed to measure inlet and outlet air temperatures as well as bed temperature at different locations. Thermocouples signals are acquired by a 16 channel analog input multiplexer *(18)* (model no. CIO-MUX16, Omega Engineering) with on board amplifiers and cold junction compensation circuitry.

Outlet air humidity was monitored continuously by an IR hygrometer *(19)* (gas analyzer) (ADC 1454/A, The Analytical Development Company, England) and verified with a pre-calibrated dewpoint hygrometer *(20),(21)* (model no. 1200 APS, General Eastern Instruments Corporation, Watertown, MA). A small outlet air stream is branched away at the top of the dryer and pumped to the hygrometers. A copper tubing is used in order to prevent condensation. The inlet air relative humidity is measured by Vaisala HM-32 humidity meter *(22)*. Both the IR hygrometer and the Vaisala RH meter were calibrated periodically using the dew point hygrometer with LiCl (12 % RH) and K_2SO_4 (97 % RH) as reference salt solutions as well as ambient air.

The analog signals for various sensors are acquired by a data acquisition system connected to a personal computer *(23)* for digitized data gathering. The data acquisition system consists of an analog and digital I/O board (model no.CIO-AD16F, Omega Engineering) with 12-bit A/D and D/A converters, a terminal panel *(24)*, a standard 37-pin D connector, and Labtech© Notebook software package for data acquisition, process control and monitoring.

The exit air duct is connected to a multi-bag filter *(25)* (DUST X, Cascade Technologies, Montreal, PQ) for dust removal. A 0.56-kW vacuum cleaner was used to empty the bed material.

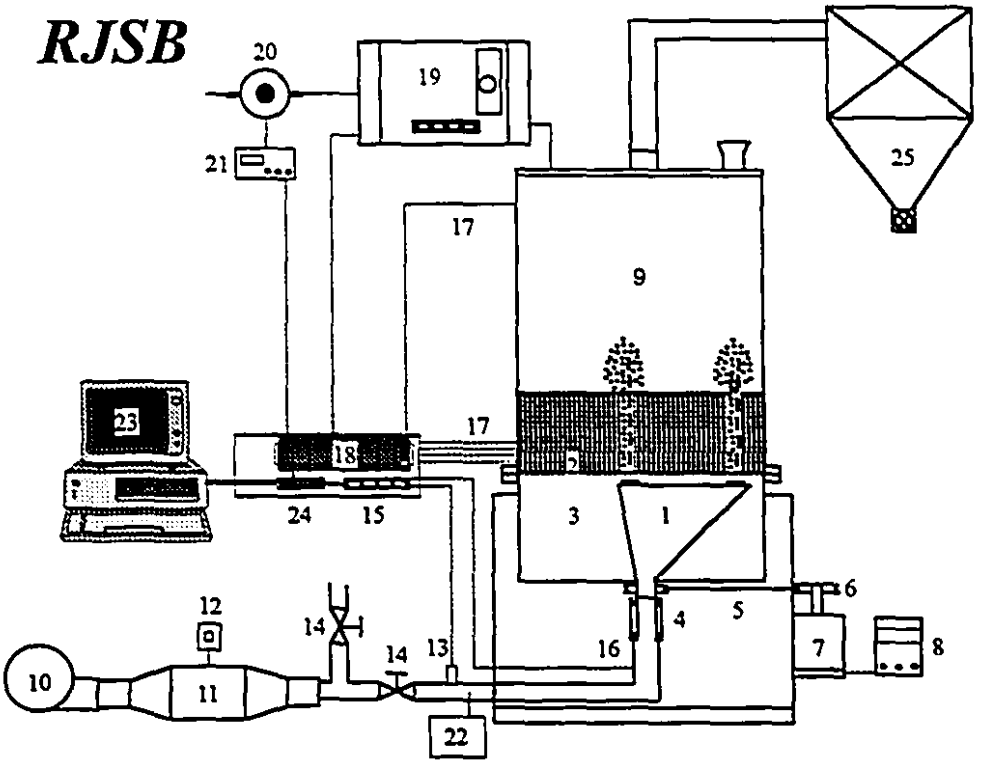

Item #	Description	Item #	Description
1	air distributor	14	gate valve
2	screen	15	pressure transducers
3	distributor cover	16	pressure taps
4	ball bearings	17	thermocouples
5	V-belt	18	multiplexer
6	pulley	19	IR hygrometer
7	motor + gear box	20	dew point sensor
8	motor controller	21	dew point hygrometer
9	glass vessel	22	relative humidity meter
10	air blower	23	personal computer - I/O board
11	electric heaters	24	terminal panel
12	PID controller	25	fabric filter
13	pitot tube		

Figure 3.1: Schematic diagram of the overall experimental set-up.

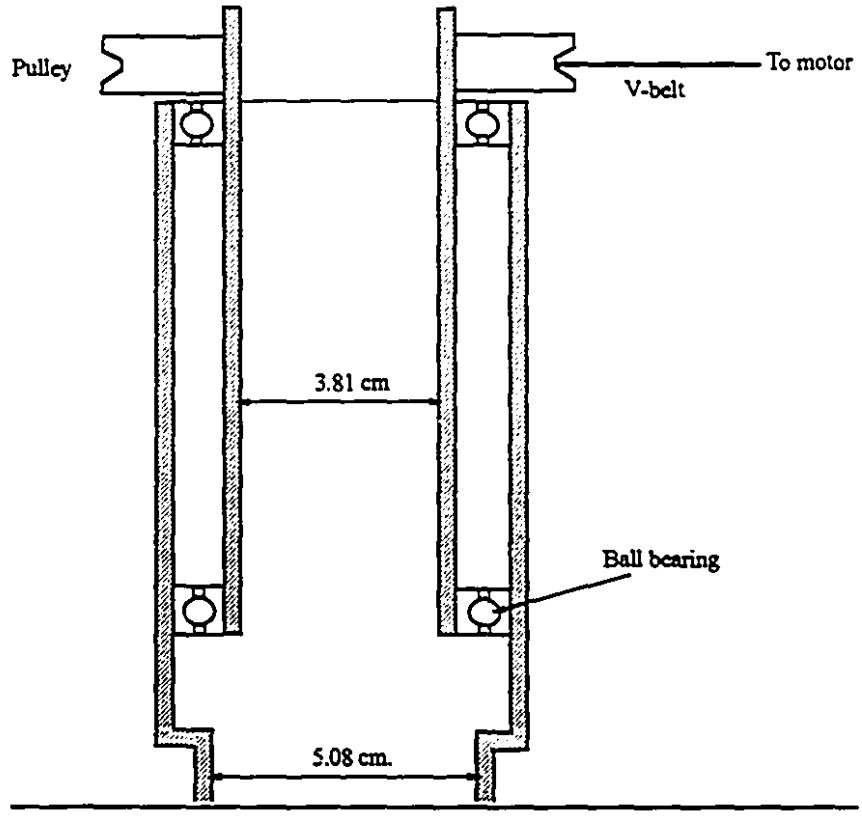

Figure 3.2 Rotation mechanism

3.3 Materials

Seed quality corn, soybean, polyethylene, and polystyrene were used as test materials in the aerodynamic experiments, whilst the drying experiments were performed using rewetted yellow dent corn. Following Geldart's classification [1], all particles used in this study belong to group D, spoutable, large and dense particles. Dimensions and physical properties of the particles along with the particle terminal velocities and the incipient fluidization velocities evaluated from correlations in the literature are given in Tables 3.1-3.3.

The particle dimensions, length (L), breadth (B) and thickness (Z), were measured with a digital calliper (Digimatic Calliper, Mitutoyo Corporation, Japan) having a least count of 0.01 mm. Typically, two hundred particles were measured for each type of material. The bulk density, ρ_b was determined by pouring a weighed amount of sample particles through a funnel into a graduated cylinder, from whence the volume occupied determines the loose bulk density. The particle density, ρ_s was estimated using fluid displacement with toluene and distilled water as measuring fluids. An electronic balance accurate to ± 0.01 g was used in weight determination.

Table 3.1 Dimensions of Particles Used in the Aerodynamics Experiments

Material	L (mm)	B (mm)	Z (mm)	D_{p_e} [1] (mm)	$D_{p_{gm}}$ [2] (mm)	D_p [3] (mm)	ϕ [4] (-)
Polystyrene	3.32	3.00	2.27	3.50	2.82	2.98	0.85
Polyethylene	4.11	3.46	3.28	4.45	3.59	3.90	0.88
Soybean	8.22	6.96	5.97	8.67	6.99	7.37	0.85
Corn	9.05	8.32	6.35	9.67	7.80	8.35	0.86

1 : Equivalent spherical diameter
2 : Geometric particle diameter = $(L \times B \times Z)^{1/3}$ [2]
3 : Effective particle diameter = $D_{p_e} \times \phi$
4 : Sphericity = $D_{p_{gm}} / L$ [2]

Table 3.2 Physical Properties of Bed Particles Used in the Aerodynamics Experiments

Material	ρ_s (kg/m^3)	ρ_b (kg/m^3)	Ar (-)	U_t [1] (m/s)	U_{mf} [1] (m/s)	ε [2] (-)
Polystyrene	1020.0	666.6	8.18×10^5	5.90	0.99	0.35
Polyethylene	914.1	579.9	1.64×10^6	6.75	1.12	0.36
Soybean	1237.9	733.2	1.50×10^7	10.37	1.91	0.41
Corn	1226.4	783.2	2.17×10^7	11.32	2.04	0.36

1 : U_t and U_{mf} are calculated values [3-5]
2 : $\varepsilon = 1-(\rho_b/\rho_s)$

Table 3.3 Physical Properties of Yellow Dent Corn Used in the Drying Experiments

Property	Value	Property	Value
L (mm)	10.67	ρ_s (kg/m^3)	1227.5
B (mm)	8.70	ρ_b (kg/m^3)	764.6
Z (mm)	4.68	Ar (-)	3.07×10^7
$D_{p_{gm}}$ (mm)	7.55	U_t [1] (m/s)	8.58
D_p (mm)	6.66	U_{mf} [1] (m/s)	2.56
D_{p_e} (mm)	9.38	ε [2] (-)	0.38
ϕ (-)	0.71		

1 : U_t and U_{mf} are calculated values [3-5]
2 : $\varepsilon = 1-(\rho_b/\rho_s)$

3.4 Experimental Procedure

3.4.1 Aerodynamics Experiments

The bed was prepared in a standardized manner before starting each experiment in order to prevent any variation in the state of packing which may arise during the filling of the vessel with particles. This was done by allowing a pre-weighed quantity of particles to settle after first spouting the bed for few minutes. The particle motion in the bed, spouting mechanism and flow regimes were studied by visual observation and photography using colored particles in contrast to the main bulk of particles.

The spouting mechanism (i.e., ΔP_{bed} vs. U variations) was established by gradually increasing the air flow rate until the central and annular spouts were formed. After a sufficient steady spouting, the flow was gradually reduced until the spouting ceases. The air flow rate at which the fountain just collapsed was taken as the minimum spouting flow rate (Q_{ms}) for the given bed conditions and rpm. The flow was further reduced in steps to zero. The flow rate and total pressure drop were recorded simultaneously. The bed pressure drop is calculated by subtracting the empty bed pressure drop from the total pressure drop as described by Mathur and Epstein [6]. The superficial minimum spouting velocity is calculated from the total air flow rate, Q_{ms}, just before cessation of spouting, i.e.,

$$U_{ms} = \frac{4Q_{ms}}{\pi D_c^2} \tag{3.1}$$

where D_c denotes the column diameter. It should be noted that the total flow rate is the sum of both nozzles flow rates, i.e. the flow rate in the main inlet pipe.

The flow regimes were identified by first maintaining the air flow rate at a certain value corresponding to full rotating spouting and then gradually increasing the distributor rotational speed until a new flow regime is established.

The ranges of experimental conditions employed are:

1. Distributor rotational speed (N): 0-300 rpm for flow regime identification and 0-10 rpm for spouting mechanism, U_{ms} and ΔP estimation.
2. Bed height (H): 10-20 cm
3. Nozzle diameter (D_n): 2 and 3 cm
4. Particles: polystyrene, polyethylene, corn, and soybeans.
5. Superficial air velocity (U): 0-0.6 m/s

The dependent or observed parameters are:

1. Spouting mechanism (i.e. ΔP_{bed} vs. U)
2. Flow regime diagrams (N vs. U)
3. Minimum spouting velocity (U_{ms})
4. Peak pressure drop (ΔP_M)
5. Steady spouting pressure drop (ΔP_s)

3.4.2 Drying Kinetics Experiments

The drying kinetics were measured in the batch mode using yellow dent corn as a test material. After cleaning and sieving, the corn was rewetted by adding a precalculated amount of tap water to achieve the required initial moisture content and mixing the content thoroughly. The grains were placed in sealed plastic boxes and kept in cold storage with periodic mixing for a minimum of 72 hours to ensure reproducible moisture absorption and uniform moisture distribution.

Before each experiment, the corn was removed from the cold storage and kept at ambient temperature for about 24 hours for thermal equilibrium to be achieved. The experimental procedure was as follows:

a) The data acquisition system, blower, heaters and the motor (fixed rpm) were switched on.
b) Hot air at preestimated flow rate and temperature was passed through the empty bed for thermal stabilization for about 1 hour.
c) When the air passing through the empty bed had attained steady state, the air flow was diverted to the by-pass pipe and the desired weight of wet solids was loaded into the dryer.
d) A relatively high air flow rate was used to initiate spouting; this flow was gradually reduced to the required steady spouting value.
e) Samples weighing 20-30 grams each were periodically taken out for moisture content determination.
f) The time-changes of temperature and humidity of exit air and the bed temperature at different locations were recorded continuously.
g) For intermittent spouting/heating, the hot air was manually diverted to the by-pass pipe for the required "rest" period.

The grain moisture content was determined gravimetrically in an oven maintained at a temperature of 103 °C for 72 hours following the ASAE standards [7]. Throughout the thesis, moisture content values are expressed in dry basis (d.b.).

The ranges of operating parameters are:

1. Inlet air temperature (T_{gi}): 55-90 °C
2. Distributor rotational speed (N): 2-10 rpm
3. Bed height (H): 10-20 cm
4. Air superficial velocity (U): 0.43-0.57 m/s; limited by the aerodynamic requirements
5. Nozzle diameter (D_n): 2 and 3 cm.
6. Intermittency (α) in the intermittent spouting/heating experiments: 1/4 - 1

The dependent or calculated variables are:

1. Sample moisture content (X)
2. Exit air temperature (T_{ge})
3. Exit air absolute humidity (Y_{ge})
4. Bed temperature (T_b) taken as an average value of different locations between the rotating spouts.
5. Drying rate (-dX/dt). This was determined using the gravimetrically estimated X, as well as from the moisture loss monitoring according to the following moisture balance:

$$-m_s \frac{d\bar{X}}{dt} = \dot{m}_g \left[Y_{ge}(t) - Y_{gi} \right] \qquad (3.2)$$

Although equation (3.2) gives a bed-average drying rate, the deviation between the two methods has always been within 10 %. The gravimetric method is adopted in this study.

The digitized temperature, pressure and humidity data were passed through preprocessing steps before presented in the final form. These steps are:

1. Conversion of the digitized data (Volts) to physical units (°C, Pa, and kg/kg) using the relevant calibration equations.
2. Data filtration using fast Fourier transform algorithm.
3. Data smoothing using non-linear regression analysis (if required).

3.5 Experimental Uncertainty and Reproducibility

In this study the measurement uncertainty values due to random errors are the ones supplied by the manufacturers or are estimated from a "single-sample" experiment [8-10]. The rule of thumb in the latter case is that the maximum possible error is equal to plus or minus half the smallest scale division (the least count) of the instrument. The probability of the readings lying between this error bound is 95 %. Based on this method, the propagation of uncertainty in calculating some result, R, from measured values x_1, x_2, ..., x_n is given by

$$u_R = \pm \left[\sum_{i=1}^{n} \left(\frac{x_i}{R} \frac{\partial R}{\partial x_i} u_{xi} \right)^2 \right]^{\frac{1}{2}} \tag{3.3}$$

where u_R and u_{xi} are the relative uncertainties in R and x_i, respectively. Table 3.4 lists the estimated maximum experimental uncertainty values for both measured and calculated variables.

To investigate the reproducibility of the results in the system, two replicates were made for all aerodynamics experiments and 20 % of the drying experiments. From these tests, the reproducibility of U_{ms}, ΔP_s, ΔP_M and the drying curves (Fig. 3.3) were at ± 2 %, ± 3 %, ± 11 % and ± 6 %, respectively. The relatively high nonreproducibility in ΔP_M is related to the fact that the peak pressure drop is a function of the initial structure of the bed. Nevertheless, the results obtained confirmed good reproducibility of the results and reliability of the experimental techniques.

Table 3.4 Maximum experimental uncertainty for measured and calculated variables

Variable	Max. Uncertainty	Variable	Max. Uncertainty
Superficial velocity, U	± 2.77 %	Rotational speed, N	± 0.75 %
Temperature, T	± 0.20 %	Moisture content, X	± 0.10 %
Pressure drop, ΔP	± 0.32 %	dX/dt	± 0.10 %
Particle diameter, D_p	± 0.40 %	Ar	± 2.88 %
Particle density, ρ_s	± 1.35 %	Re_{ms}	± 3.14 %
Bed density, ρ_b	± 1.35 %	H/D_c, D_i/D_c, D_p/D_c	± 1.57 %
Particle sphericity, ϕ	± 0.43 %	$\Delta P/\rho_b gH$	± 1.52 %
Bed voidage, ε	± 2.86 %	V_θ/U_t	± 1.70 %
Particle terminal velocity, U_t	± 1.04 %		

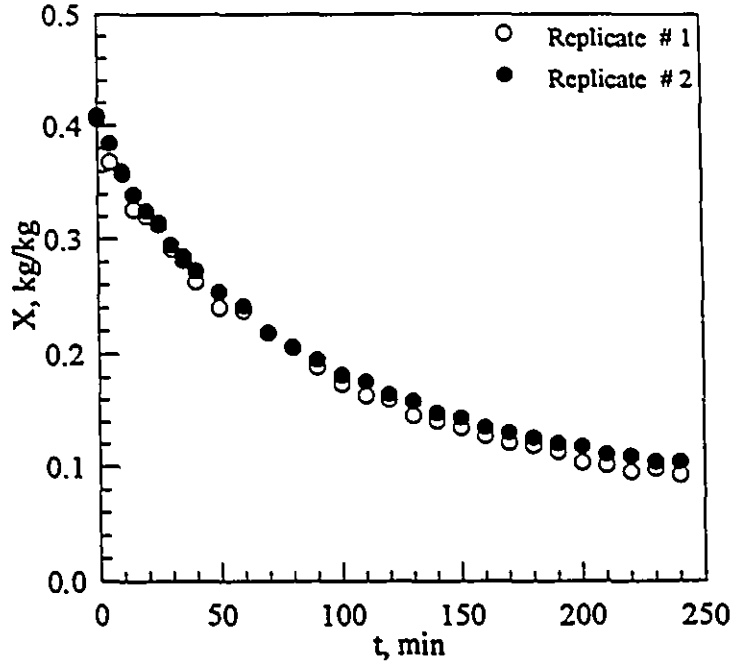

Figure 3.3: Reproducibility of drying curves.
$T_{gi} = 80^{\circ}C$, $D_n = 3$ cm, $N = 2$ rpm, $U = 0.514$ m/s.

Nomenclature

Symbols

Ar	Archimedes number = $\frac{D_p^3 \rho_g (\rho_s - \rho_g) g}{\mu_g^2}$
B	breadth
D_c	column diameter
D_n	nozzle diameter
D_p	effective particle diameter

D_{pc}	equivalent spherical particle diameter
D_{Pgm}	geometric mean particle diameter
g	acceleration of gravity
H	bed height
L	length
$\dot{m}_g$	mass flow rate of dry air
m_s	mass of dry solid in bed
N	distributor rotational speed
ΔP_{bed}	bed pressure drop
ΔP_M	peak pressure drop
ΔP_s	steady spouting pressure drop
Q_{ms}	air flow rate at minimum spouting condition
R	result
Re	particle Reynolds number = $\frac{D_p U \rho_g}{\mu_g}$
RH	relative humidity
t	time
T_b	bed temperature
T_{ge}	exit air temperature
T_{gi}	inlet air temperature
U_{mf}	minimum superficial air velocity for fluidization
U_{ms}	minimum superficial air velocity for spouting
U_t	particle terminal velocity
V_θ	air distributor circumferential velocity
u	relative uncertainty
X	moisture content (dry basis)
$\overline{X}$	bed average moisture content (dry basis)
Y_{ge}	exit air absolute humidity

Y_{gi}	inlet air absolute humidity
Z	thickness

Greek Letters

α	intermittency
ε	voidage
μ_g	viscosity of gas
ρ_b	bulk density
ρ_s	solid density
ϕ	sphericity

Subscripts and Superscripts

b	bed, bulk
c	column
e	exit
g	gas
i	inlet
mf	minimum fluidization
ms	minimum spouting
n	nozzle
p	particle
s	solid

References

1. D. Geldart, "Types of gas fluidization", *Powder Tech.*, 7, 285-292 (1973).
2. N. Mohsenin, *Physical Properties of Plant and Animal Materials*. Vol. 1, Structure, Physical Characteristics and Mechanical Properties, Gordon and Breach Science Publishers, New York, (1970).
3. A. Haider and O. Levenspiel, "Drag coefficients and terminal velocity of spherical and nonspherical particles", *Powder Tech.*, 58, 63-70 (1989).
4. D.C. Chitester, R.M. Kornosky, L-S. Fan and J.P. Danko, "Characteristics of fluidization at high pressure", *Chem. Eng. Sci.*, 39, 253-261 (1984).
5. D. Kunii and O. Levenspiel, *Fluidization Engineering*, Butterworth-Heinemann, Boston (1991).
6. K.B. Mathur and N. Epstein, *Spouted Beds*, Academic Press, New York (1974).
7. ASAE, *Standards, American Society of Agricultural Engineers*, St. Joseph, MI (1991).
8. S.J. Kline and F.A. McClintock, "Describing uncertainties in single-sample experiments", *Mechanical Engineering*, 75, 3-9 (1953).
9. R.J. Moffat, "Describing uncertainties in experimental results", *Experimental Thermal and Fluid Science*, 1, 3-17 (1988).
10. H. Schenck, *Theories of Engineering Experimentation*, 2nd. Ed., McGraw-Hill, New York (1968)

Chapter 4

Aerodynamics of the Rotating Jet Spouted Bed

4.1 Introduction

The understanding of the flow characteristics of any gas-solid contactor is very useful owing to its importance in assessment of the effectiveness of gas-solid contact in any physical or chemical process application. The objectives of this chapter are:

- To describe the flow regimes with special reference to their suitability in relation to the operation of the rotating jets spouted bed (RJSB).
- To identify the optimum operating conditions required for stable spouting.
- To gain an understanding of the spouting mechanism in which the bed evolves from the packed structure into the fully developed spouting state.
- To obtain general design equations to describe such flow characteristics as minimum spouting velocity, peak pressure drop, and steady spouting pressure drop as functions of the fluid-solid properties and the main design and operating parameters of the system.

4.2 Flow Regime Diagrams

As in conventional spouted beds [1], spouting in a rotating spouted bed is a visually observable phenomenon which occurs over a definite range of gas velocity for a certain combination of gas, solids and equipment geometric and mechanical parameters. The parameters of interest are: gas flow rate, particle size and shape, particle density, gas inlet nozzle size, bed height and distributor rotational speed.

Various investigators have constructed charts to map the flow regimes encountered in conventional spouted beds. Each regime map has specific dimensional or nondimensional coordinates. Mathur and Gishler [2] used bed depth versus superficial gas velocity as the characteristic parameters of their flow regime map. Ye et al. [3] chose bed temperature versus superficial gas velocity in their study of spouting behavior at high temperatures. More generalized flow regime diagrams have been attempted by Németh et al. [4] who plotted pressure drop versus U/U_{mf} for different H/H_M, and by Becker [5] who used the same parameters normalized with respect to the condition of minimum spouting at H_M. However, as stated by Mathur and Epstein [1], these generalizations oversimplify the actual complex transition behavior between the different flow regimes. In this study, observations of spouting development in the bed have shown that the air distributor rotational speed has the greatest influence on the type of flow over the gas, solids and vessel parameters studied in this investigation.

When the rotational speed, N, of the air distributor is increased, the bed may be in different states at the same gas superficial velocity, U. Consequently, the studies of flow regimes for different material-vessel combinations are presented in N-U coordinates. Figures 4.1-4.2 show examples of such flow regime diagrams for both polyethylene and corn particles representing two ranges of particle size and density. These flow diagrams were obtained starting with the rotational speed at zero speed and then gradually

increasing the gas flowrate to obtain the onset of spouting. The gas flowrate was then kept constant while gradually increasing the rotational speed until the disappearance of the characteristic form of the spouted bed, and thus the development of another flow regime. This procedure was repeated for different values of the gas superficial velocity beyond the value required to initiate steady and stable spouting.

Three distinct flow regimes were observed within the operating parameter ranges studied:

I. Full rotating spouting (Figure 4.3 (a)):

Depending on the bed height, nozzle size and particles used, at low rotational speeds, stable spouting occurs in both central and annular regions of the bed over the entire range of gas superficial velocities higher than the incipient spouting velocity.

First, for a stationary air distributor (N = 0) two individual cells are formed each with its own annulus with more vigorous agitation and circulation inside the bed than the equivalent single-spout bed, but at the expense of higher gas consumption and the presence of dead zones surrounding the spouting cells. This might be attributed to the flat geometry of the supporting grid.

On the other hand, with the rotating air distributor a completely different gas-particle dynamics is established. The particles at the base of the bed receive a sudden impulse from one of the incoming rotating jets and accelerate from rest to their maximum velocity as result of the frictional drag of the high velocity ascending air jet, and then decelerate until they reach zero velocity at the top of the fountain(s), where they reverse their direction of movement and fall back into the bed surface. A temporary active cell in the bed assumes a loose packed orientation when the air jet is periodically and

continuously relocated to the following sections of the bed. However, particles from the layer surrounding other active cells continuously percolate towards the rotating core in both axial and radial directions, creating continuous motion in the entire bed cross section.

Depending on the gas flowrate and distributor rotational speed, particles of different size and density have different trajectories within the spouts and fountains and hence different radial and angular landing positions on the bed surface. Large and heavy particles like corn and soybeans tend to land more frequently at smaller positions and hence execute a higher proportion of cycle time than small and light particles like polyethylene and polystyrene.

The difference in the flow behavior might also reflect the increased relative importance of interparticle forces (electrostatic forces) in comparison with the aerodynamic or gravitational forces [6-10]. Polystyrene and polyethylene are dielectric polymeric particles and will become electrostatically charged during particle-particle contact, as well as particle-wall (glass) contact especially with the low relative humidity air used in the experiments. However, it is reasonable to suppose that the electrostatic effect on large particles (corn and soybean) is less significant. Similar behavior was observed by Passos [11] who tested wheat grains in a 2D spout-fluidized bed.

This regime clearly shows such spouted bed features as particle circulation, an ascending particle flow in the active spout region and downward-inward flow in the local annulus surrounding the rotating spout in both the central and annular regions of the bed. Moreover, this flow regime is characterized by certain distinct features:

a) The air distributor rotation causes the jets and hence the entrained solid particles to deviate in the opposite angular direction and this results in a rotating sprinkler-like distribution of the solids over the periphery of each cell. This phenomenon is more

pronounced in the case of the second jet covering the annular section of the bed because of its larger radius of rotation and hence higher circumferential velocity.

b) Intensive systematic particle circulation and hence short contact time between the solid particles and the gas with fast solids turnover.

c) The cyclic rotation of the spouts causes intensive mixing of the particles and their exchange between the rotating spouting cells and prevents dead zone formation in spite of the fact that the bed support screen is flat.

II. Rotating central spout- pulsating annulus(Figure 4.3 (b)):

If the rotational speed is high, the jet emerging from the second nozzle covering the annulus region of the bed cross-section with its larger radius of rotation, R, compared with the central jet, will have a higher circumferential velocity ($V_\theta = 2\pi RN$) and higher frequency of gas relocation. This produces an increase in the slope or deviation of the air jet from the vertical direction contributing to significant shear stresses and resistance forces in the direction of gas penetration proportional to the jet circumferential velocity. In such a case the annular spout will loose its kinetic energy and collapse leaving the annulus region in a no-spouting condition with local pulsation due to the internally rotating spout. This results in a second flow regime characterized by an external rotating central spouting and an internal rotating annular spouting with local bed pulsating. The solids circulation is significantly reduced compared to the first flow regime because most of the particles are in a nearly loose packed pulsating state with periodic aeration with only 20-25 % of the solid material (depending on the nozzle diameter, flowrate and rpm) in the rotating central spouting region. This causes a reduction of the time-averaged voids in the bed.

The effect of particle oscillation in the annulus region along with the rotating action of the central region causes continuous transfer and rolling of particles from the

surrounding sloped cone-shaped layers towards the core section. It is worth to noting that this flow regime possesses some features of the spout-fluid bed; gas passes through the bed as a central rotating jet and a pulsating annulus locally fluidized/aerated by the spent gas from the second rotating nozzle.

The gas and particle flow patterns in this flow regime lead to the hypothesis that both the magnitude and the direction of the momentum at the gas inlet are the governing parameters and that the vertical fluid drag is a monotonously decreasing function of the rotational speed. Hence, the state of dynamic equilibrium between the various forces acting on the spout-annulus interface that keep the spout stable in shape and direction does not exist. The resultant effect of this high rpm and the resulting resistances leads to the conclusion that while the spout is still developing, the gas jet is relocated and thus this spout will never pierce the annulus region of the bed even at a high gas flowrate and this will create an annular internal cavity inside the bed.

III. No spouting (Figure 4.3 (c)):

Above a rather high rotational speed (depending on the air flow rate, bed height , and particle properties) the central spout also collapses; the bed starts to oscillate in all directions, and the main body of the gas forms a vortex flow with its mouth directed toward the central region.

In this flow regime, because of bed inertia and particle interaction, the spouting air percolates through the bed in a vertical direction bringing the particles into local pulsation and hence the entire bed attains a "pseudo-fluidized" state.

A critical analysis of the flow regime diagrams shows that the full rotating spouting regime (regime I) is the most effective operating regime in terms of bed aerodynamics and

consequently performance in heat and mass transfer applications. This is because of the lower rpm and hence lower power requirements, more stable and uniform gas distribution, the systematic particle circulation across the entire bed and hence more vigorous mixing of particles. For these reasons, the discussion in the following sections will concentrate on experiments at low rpm values ($N < 14$ rpm).

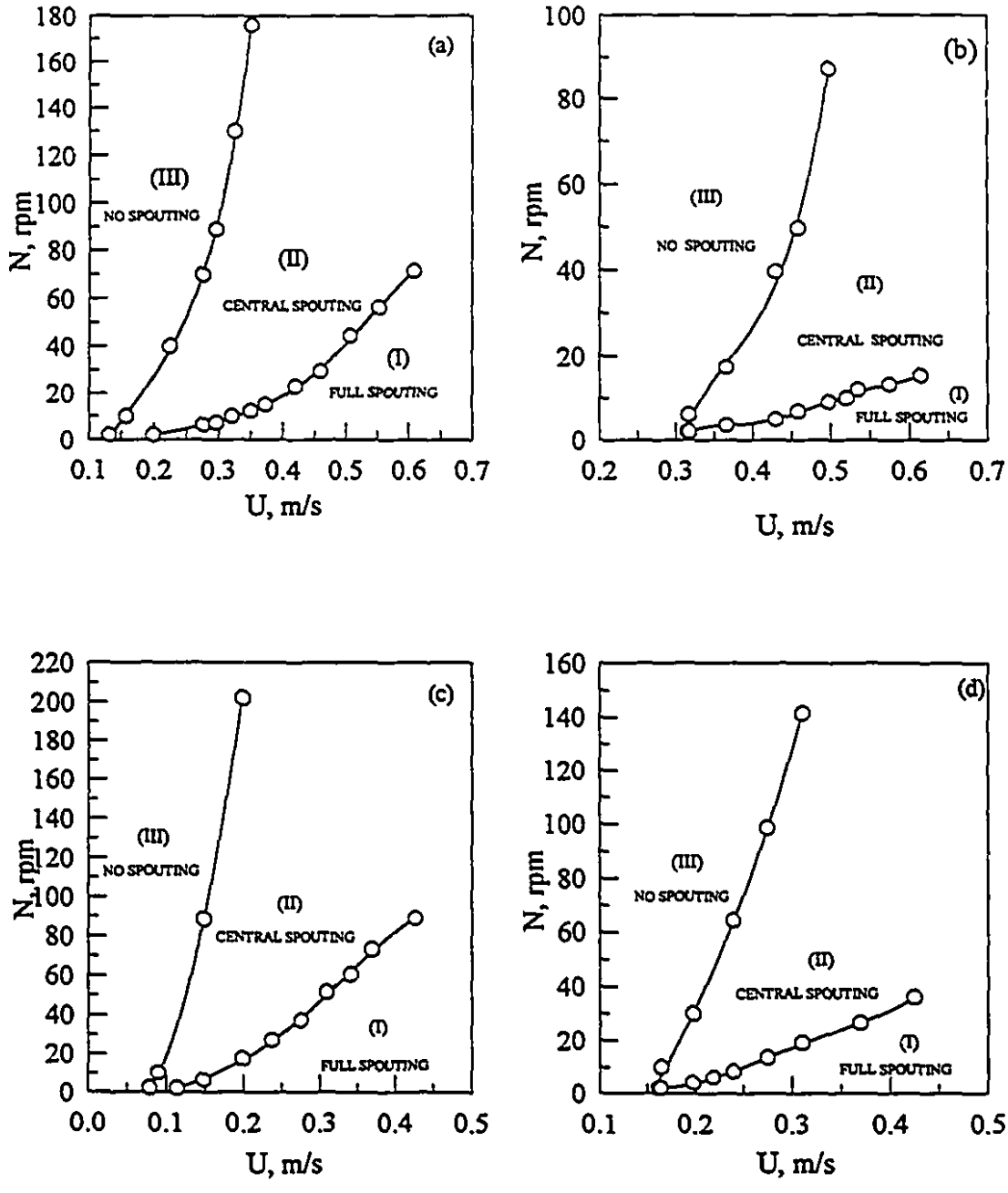

Figure 4.1: Flow regime maps for polyethylene particles: (a) D_n=3 cm, H= 10 cm, (b) D_n=3 cm, H=20 cm, (c) D_n=2 cm, H= 10 cm, (d) D_n=2 cm, H= 15 cm.

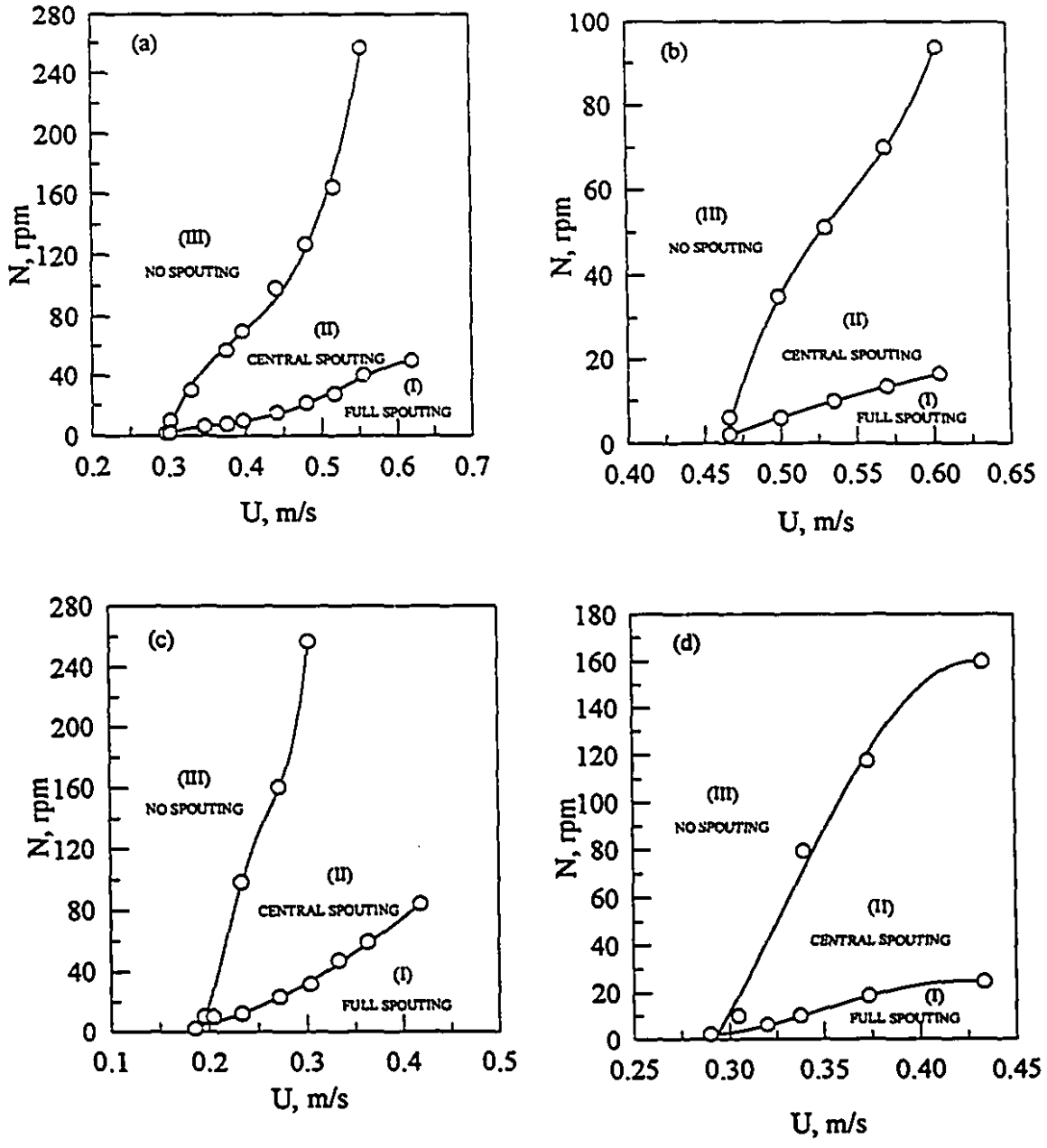

Figure 4.2: Flow regime maps for corn particles: (a) D_n=3 cm, H= 10 cm, (b) D_n=3 cm, H=15 cm, (c) D_n=2 cm, H= 10 cm, (d) D_n=2 cm, H= 15 cm.

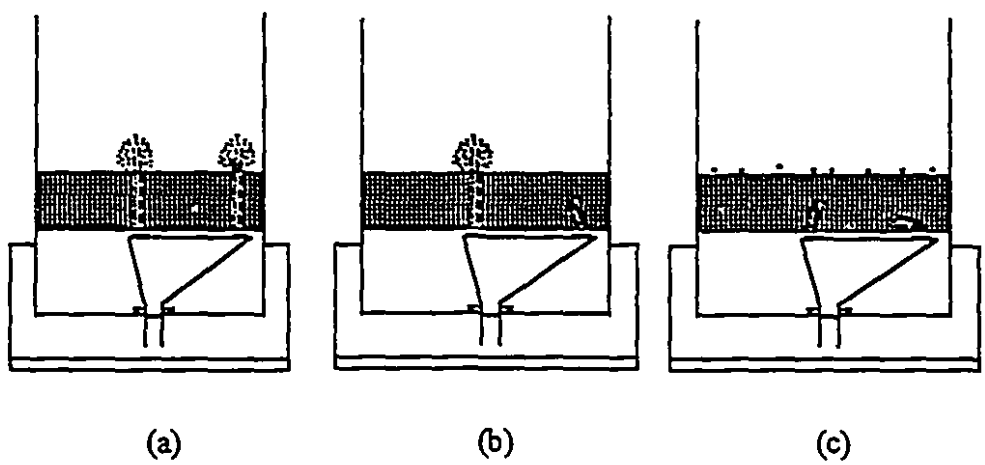

Figure 4.3: Schematic representation of the flow regimes in the RJSB (a) full spouting, (b) central spouting, (c) no spouting.

4.3 Spouting Mechanism

Generally the spouting mechanism in which the bed of particles changes from a packed state to fully developed spouting is best described with reference to plots of bed pressure drop versus superficial gas velocity. In order to generalize the analysis, the pressure drop and superficial gas velocity are written in dimensionless form, i.e., $\Delta P/\rho_b gH$ and Re. The former represents the ratio between the bed pressure drop and the bed weight per unit cross-sectional area while the latter represents the particle Reynolds number. Figures 4.4 and 4.5 show typical dimensionless pressure drop evolution traces for polyethylene particles at 0, 2, 6 and 10 rpm. The plots are supplemented by branches illustrating the reverse process, that is, the collapse of both central and annular spouts on decreasing the gas flowrate.

The following sequence of events are observed as the flow rate is increased:

I. Increasing flow

Curve A→B: As in conventional spouted beds, the pressure drop increases almost linearly with increasing gas flow rate while the fixed-bed state remains unchanged. For the stationary air distributor (Figure 4.4a), two small cavities and two internal spouts are formed. When the air distributor rotates (Figure 4.4b and Figure 4.5), two internally relocated annular cavities are formed along the path of the rotating internal spouts. An arch of compacted particles that offers high resistance to flow exists above the internal spouts so that the pressure drop rises until it reaches a peak value at point B.

Curve B→C: Beyond point B, the height of the internal spouts increases and the stationary or rotating jets have enough momentum to pierce the bed surface and hence spouting begins. Therefore, the pressure drop suddenly decreases to point C.

Curve B→C: Beyond point B, the height of the internal spouts increases and the stationary or rotating jets have enough momentum to pierce the bed surface and hence spouting begins. Therefore, the pressure drop suddenly decreases to point C.

Curve beyond C: Both spouts are fully developed and the pressure drop remains nearly constant.

II. Decreasing flow

Two different spout termination mechanisms were observed. In the case of stationary distributor and very low rotational (N = 2 rpm) speeds, the trend is similar to that found for conventional spouted beds. While the gas flowrate is decreased the pressure drop remains nearly constant and the bed remains in the spouting state until point D is reached; this represents the minimum spouting condition for both central and annular spouts (U_{ms} or Re_{ms}). A slight reduction of the air flowrate causes the spouts to collapse and the pressure drop to rise suddenly to point E.

When the rotational speed is higher (Figure 4.5) the annular spout collapses at a higher superficial velocity than the central one. This may be attributed to the fact that the annular spout has a higher velocity component in the angular direction because of its larger radius of rotation and hence larger deviation of the spout from the vertical direction. The spout failure locations are represented in Figure 4.5 by points D, E, F, G and H. Points D and G represent minimum spouting conditions for both annular (U_{ms2} or Re_{ms2}) and central (U_{ms1} or Re_{ms1}) spouts, point F designates the state when the central spout is still active and points E and H represent the secondary peaks after failure of the spouts.

Figures 4.4 and 4.5 also indicate that the pressure characteristics are different with increasing and decreasing gas flowrate at any rotational speed. This effect has already been cited in many investigations of conventional and non-conventional spouted bed

contactors. The decreasing flow curves fall below those for increasing flow as less energy is required by the spouting jets to penetrate the loose bed structure.

It has been observed that the rotational action of the spouting jets has a great influence on the onset of the spouting regime and hence in lowering the peak pressure drop values by about 30 % compared to the stationary spouting case (Figure 4.6). This can be explained by the pulsating action inside the bed that helps break interparticle forces, loosen the packed structure and hence facilitate spout evolution.

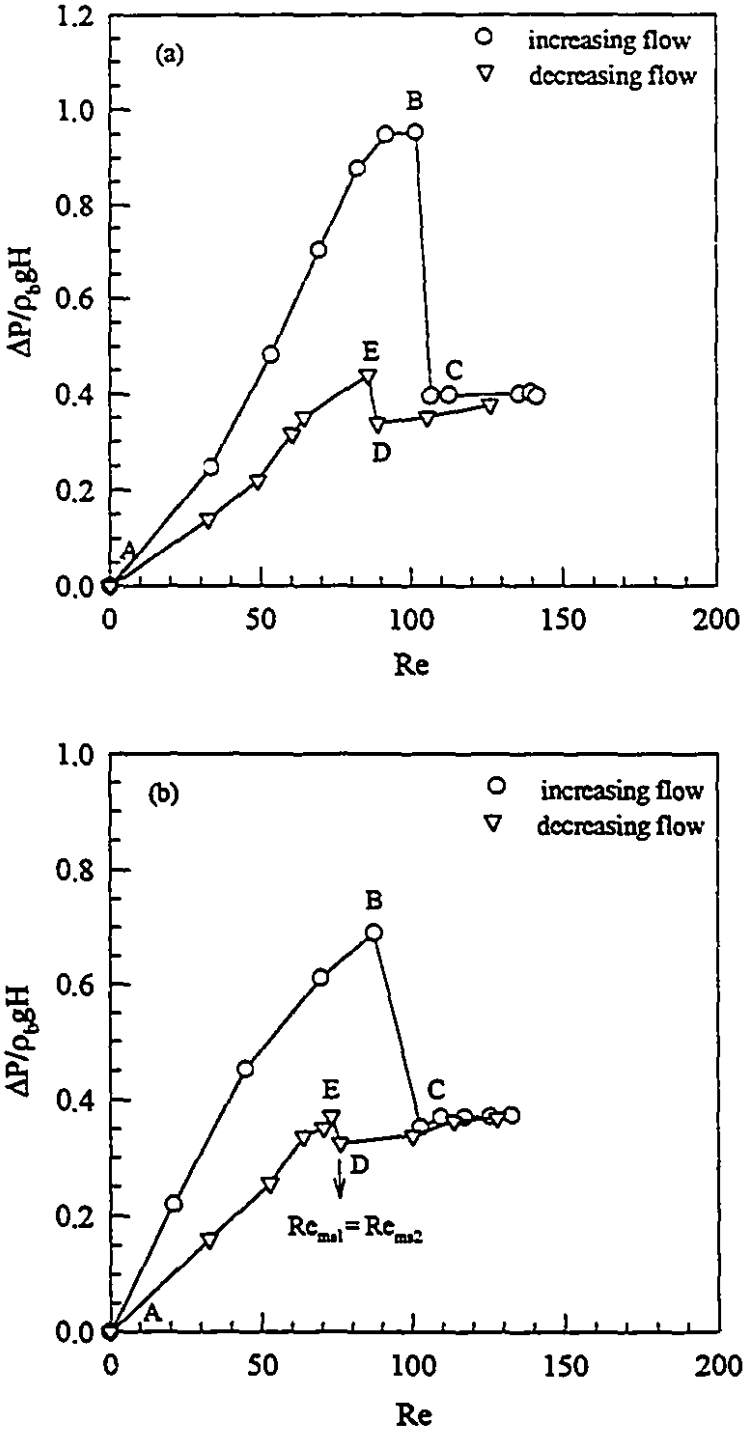

Figure 4.4: Spouting characteristics for polyethylene particles, H= 20 cm, D_n=3 cm. (a) N= 0 rpm, (b) N= 2 rpm. B: maximum spouting pressure drop; C: onset of spouting; D: minimum spouting condition; E: central and annular spout collapse.

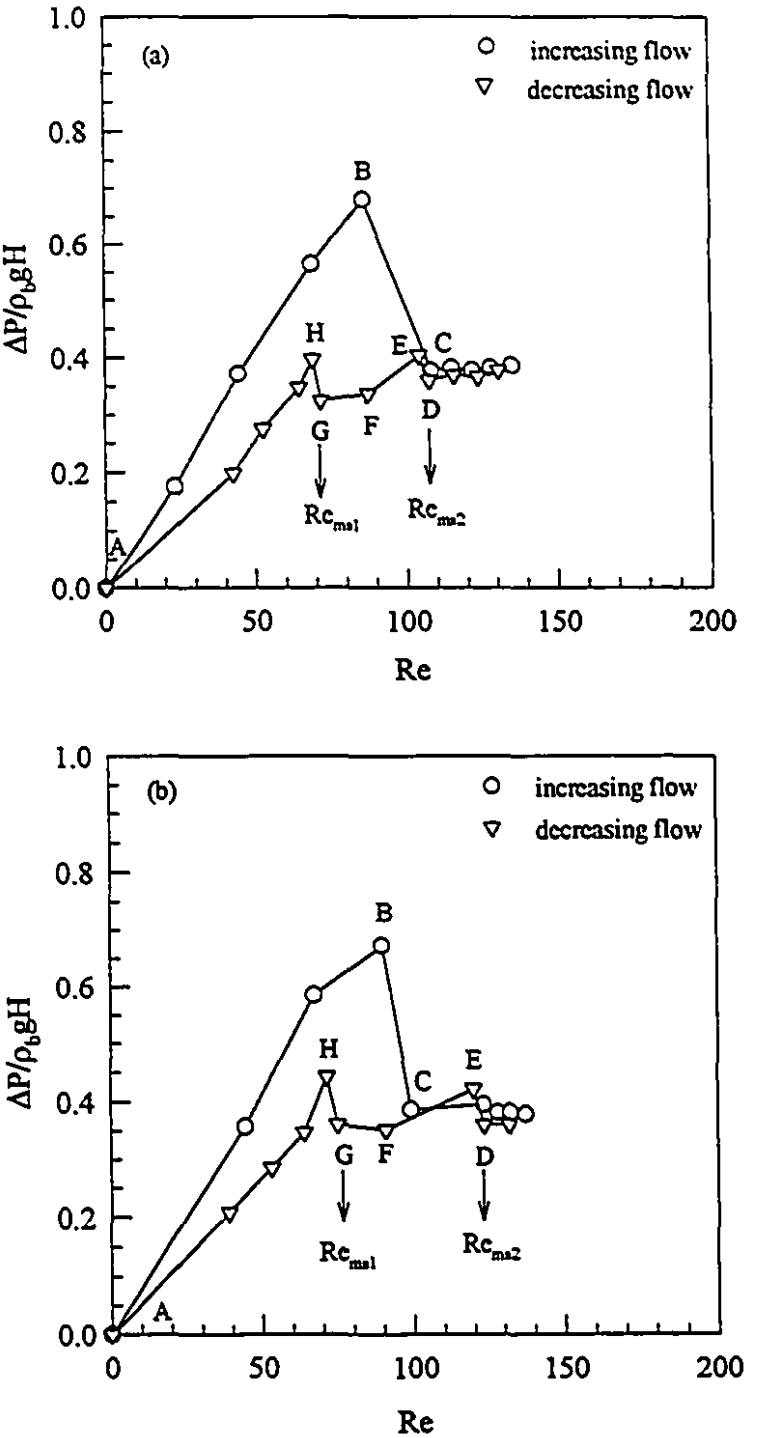

Figure 4.5: Spouting characteristics for polyethylene particles, H= 20 cm, D_n=3 cm. (a) N= 6 rpm, (b) N= 10 rpm. B: maximum spouting pressure drop; C: onset of spouting; D: annular minimum spouting; E: annular spout collapse; F: central spout active; G: central minimum spouting; H: central spout collapse.

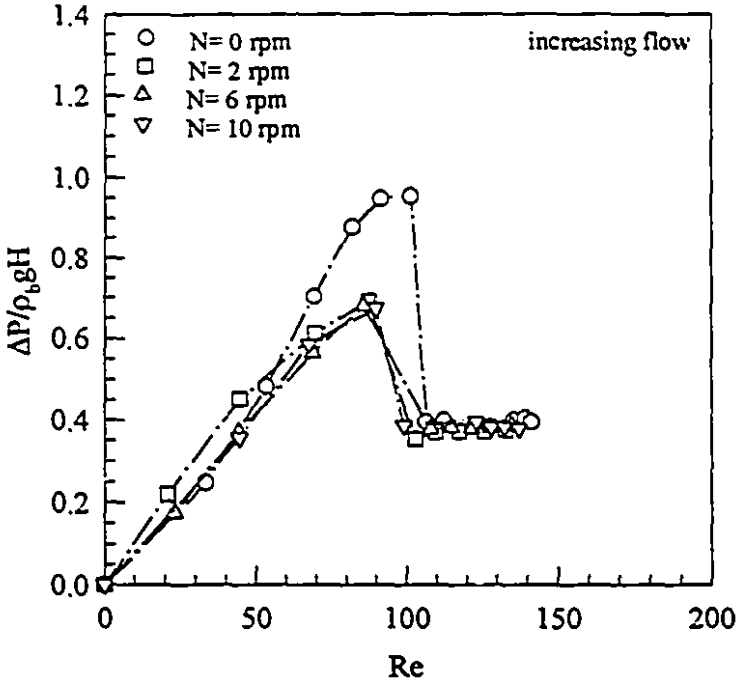

Figure 4.6: Effect of rotational speed on spouting characteristics curve for polyethylene particles, H= 20 cm, D_n=3 cm.

4.4 Flow Characteristics

Three main variables are commonly used to describe the flow characteristics in both conventional and non-conventional spouted beds. They are: minimum spouting velocity, peak pressure drop, and steady spouting pressure drop. In this work, extensive experiments were carried to study these variables and their relation with air, particle, and equipment parameters. To generalize the discussion and to present the experimental results in a useful and compact form empirical equations are developed using dimensional analysis.

4.4.1 Empirical Modeling

It is clear from sections 4.2 and 4.3 that the gas-particle dynamics in the RJSB is complicated and difficult to describe analytically. However, some qualitative reasoning based on the observations discussed earlier can be used to determine the dimensionless groups useful in correlating the experimental data. To accomplish this, the following postulates and assumptions are made:

1. The energy required to rupture the packed bed structure and to overcome the frictional resistance is responsible for the occurrence of a peak pressure drop before the onset of spouting.
2. When the rotating jets overcome gravity, friction and viscous forces, a steady spouting pressure drop is established during operation.
3. Particle geometry and density as well as the forces exerted thereon are responsible for the different particle trajectories in the spouts and fountains. These forces, including inertial, gravity and buoyancy, are best represented by the particle terminal velocity, U_t.

4. Superficial velocity at the minimum spouting condition for both spouts, steady spouting pressure drop, peak pressure drop are all functions of air properties, particle properties, and equipment related design parameters such as bed height, nozzle diameter and column diameter.
5. The particle density fulfills two roles. First, it is the source of particle weight in association with gravitational acceleration g, less the buoyancy force exerted by the fluid. Thus it is represented in the dimensional analysis by the specific weight of the particle $g(\rho_s-\rho_g)$. Second, the particle density is a multiplier of particle acceleration to produce particle inertia force during the unsteady motion in the spout.
6. Two separate expressions can be written for the circumferential velocity (θ-direction) of both the central and annular nozzles based on their radius of rotation, R and the distributor rotational speed, N (revolution per second):

$$V_{\theta 1} = 2\pi R_1 N \tag{4.1}$$

$$V_{\theta 2} = 2\pi R_2 N \tag{4.2}$$

7. When the air distributor is stationary (N = 0), both spouts collapse at the same time and hence they have equal minimum spouting velocities.
8. For N > 0, the spouts may have equal or different minimum spouting velocities depending on their circumferential velocities . Since $V_{\theta 2}$ is always greater than $V_{\theta 1}$ and for other reasons discussed in sections 4.1 and 4.2, the minimum spouting velocity of the annular region spout (U_{ms2}) will be equal or greater than the minimum spouting velocity of the central region spout (U_{ms1})

The method of obtaining dimensionless groups from the algebraic and/or differential equations based on basic principles is generally the preferred method. In this complex gas-particle system, however, a more general and simpler procedure based on the

Buckingham theorem [12,13] is used. Using this procedure and multiple nonlinear regression analysis based on the Marquardt method [14,15], the following empirical equations for the minimum spouting condition were derived (see Appendix):

$$Re_{mso} = 0.68\left(\frac{H}{D_c}\right)^{0.98}\left(\frac{D_n}{D_c}\right)^{0.82} Ar^{0.54} \tag{4.3}$$

$$Re_{ms1} = 0.59\left(\frac{H}{D_c}\right)^{1.02}\left(\frac{D_n}{D_c}\right)^{0.91} Ar^{0.57}\left(\frac{V_{\theta 1}}{U_t}\right)^{0.01} \tag{4.4}$$

$$Re_{ms2} = 8.46\left(\frac{H}{D_c}\right)^{0.83}\left(\frac{D_n}{D_c}\right)^{1.08} Ar^{0.45}\left(\frac{V_{\theta 2}}{U_t}\right)^{0.11} . \tag{4.5}$$

Equation (4.3) represents the minimum spouting condition for the case of stationary air distributor (Re_{ms1}=Re_{ms2}=Re_{mso}) while equations (4.4) and (4.5) represent minimum spouting conditions for the case of rotating air distributor for the central region spout and annular region spout, respectively. Comparison between the experimental and predicted Reynolds numbers at the minimum spouting condition is depicted in Figures 4.7-4.9 while Tables 4.1 - 4.3 show results of the analysis of variance for these estimations. The correlations could predict the experimental data with a standard deviation less than 6 and a standard error less than 10. The group $\frac{V_{\theta 1}}{U_t}$ has negligible contribution to Re_{ms1} indicating minor dependence of U_{ms1} on N over the range of rpm studied.

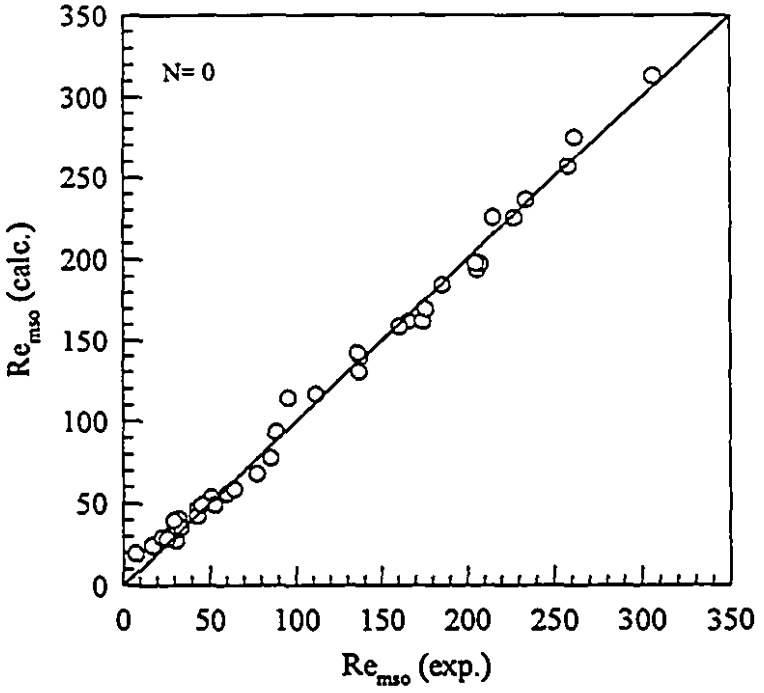

Figure 4.7: Comparison of experimental values of Re_{mso} with values calculated using equation 4.3.

Table 4.1 Analysis of Variance for Re_{mso}

Source	Sum of squares	Degrees of freedom	Mean squares	F value
Regression	2.75×10^5	3	9.17×10^4	1616.05
Error	2.04×10^3	36	56.77	
Total	2.77×10^5	39		
$R^2 = 0.9926$	Standard error = 7.535		Standard deviation = 3.96	

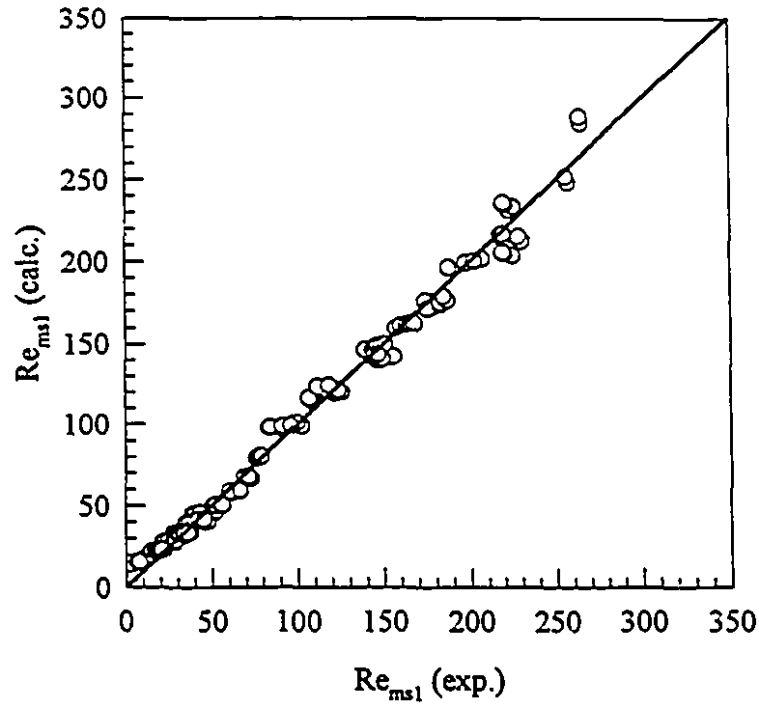

Figure 4.8: Comparison of experimental values of Re_{ms1} with values calculated using equation 4.4.

Table 4.2 Analysis of Variance for Re_{ms1}

Source	Sum of squares	Degrees of freedom	Mean squares	F value
Regression	8.36×10^5	4	2.09×10^5	4512.38
Error	7.18×10^3	155	46.34	
Total	8.43×10^5	159		
$R^2 = 0.9915$	Standard error = 6.807		Standard deviation = 4.33	

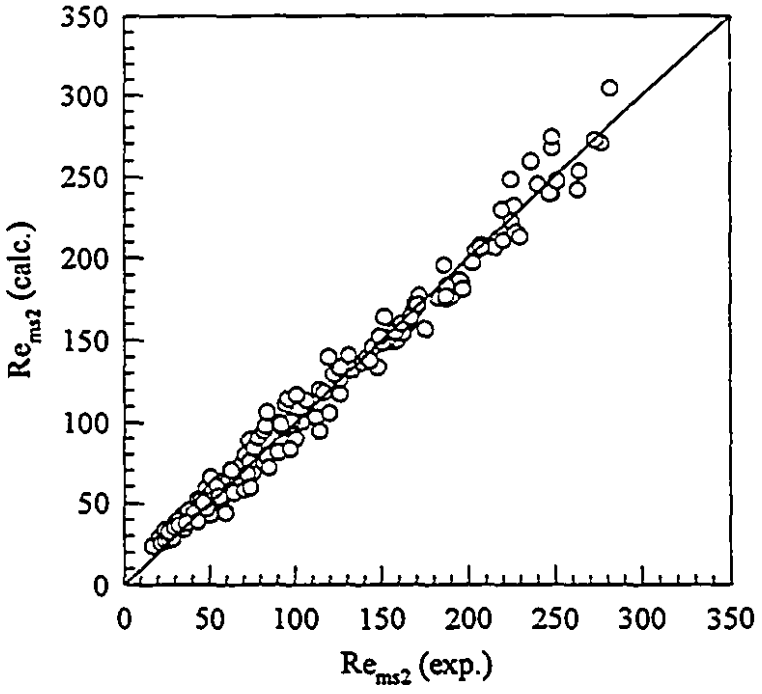

Figure 4.9: Comparison of experimental values of Re_{ms2} with values calculated using equation 4.5.

Table 4.3 Analysis of Variance for Re_{ms2}

Source	Sum of squares	Degrees of freedom	Mean squares	F value
Regression	8.19×10^5	4	2.05×10^5	2349.70
Error	1.35×10^4	155	87.18	
Total	8.33×10^5	159		
$R^2 = 0.9838$	Standard error = 9.337		Standard deviation = 5.66	

Using the same procedure the following empirical equations were derived for the peak pressure drop and the steady spouting pressure drop:

$$\frac{\Delta P_M}{\rho_b g H} = 2.12\left(\frac{H}{D_c}\right)^{0.47}\left(\frac{D_n}{D_c}\right)^{0.28} \tag{4.6}$$

$$\frac{\Delta P_s}{\rho_b g H} = 0.63\left(\frac{H}{D_c}\right)^{0.12}\left(\frac{D_n}{D_c}\right)^{0.16} \tag{4.7}$$

In order to illustrate the adequacy of the regression, a comparison between experimental and predicted pressure drop values is shown in Figures 4.10 and 4.11. Tables 4.4 and 4.4 show results of the analysis of variance based on these estimations. The range of applicability of Equations 4.3-4.7 is given in Table 4.6 in terms of the dimensionless variables.

Table 4.4 Analysis of Variance for $\Delta P_M/\rho_b gH$

Source	Sum of squares	Degrees of freedom	Mean squares	F value
Regression	0.2172	2	5.43×10^{-2}	385.87
Error	4.93×10^{-3}	37	1.41×10^{-4}	
Total	0.222	39		
$R^2 = 0.978$	Standard error = 0.0119		Standard deviation = 0.0058	

Table 4.5 Analysis of Variance for $\Delta P_s/\rho_b gH$

Source	Sum of squares	Degrees of freedom	Mean squares	F value
Regression	9.01×10^{-3}	2	2.25×10^{-3}	36.06
Error	2.19×10^{-3}	37	6.25×10^{-5}	
Total	0.0112	39		
$R^2 = 0.805$	Standard error = 0.0079		Standard deviation = 0.0050	

Table 4.6 The Range of Applicability of the Correlations for Minimum Spouting Velocity and Pressure Drop

Dimensionless group	Range
H/D_c	0.222 - 0.444
D_n/D_c	0.044 - 0.0667
Ar	8.18×10^5 - 2.17×10^7
$V_{\theta 1}/U_t$	0 - 8.0×10^{-3}
$V_{\theta 2}/U_t$	0 - 3.2×10^{-2}

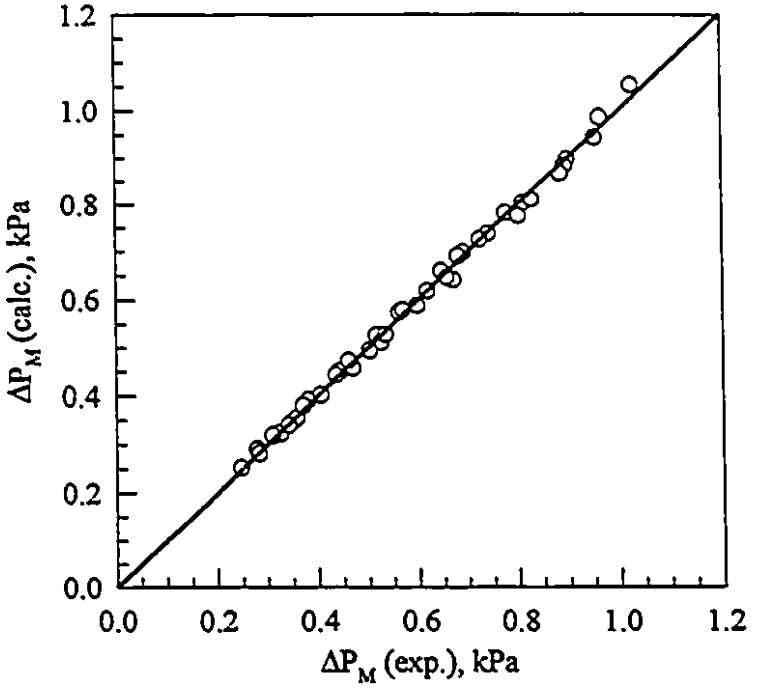

Figure 4.10: Comparison between experimental and calculated peak pressure drop.

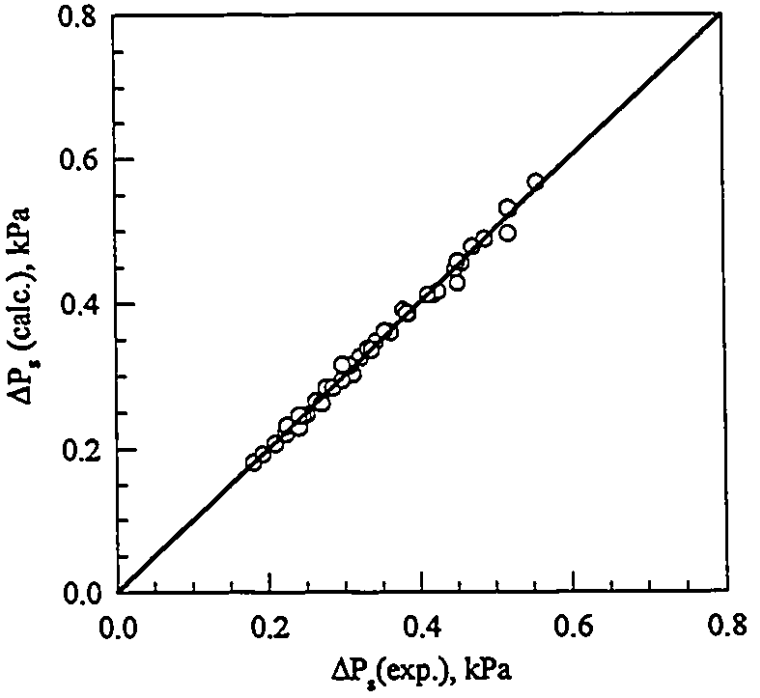

Figure 4.11: Comparison between experimental and calculated steady spouting pressure drop.

4.4.2 Minimum Spouting Velocity

A spouted bed system is characterized by its minimum flow requirement since a minimum air velocity is required for spouting. Knowing this quantity is important from the design point of view since it is used to specify the blower capacity. Minimum spouting velocity, U_{ms}, depends on the properties of the bed material and of the spouting agent, the bed height, and system geometry. Another added factor in the rotating jet spouted bed is the angular velocity of the air distributor. Experimental values of U_{ms} determined at the point where the spouts collapse as the air flowrate is decreased, are discussed in this section in terms of the dimensionless groups obtained in section 4.4.1. The corresponding correlations equations are also presented.

Effect of bed height

Figures 4.12 - 4.15 present examples of the variation of Re_{ms1} and Re_{ms2} with dimensionless bed height for different particles (different Ar) using two different nozzle diameters. The data for all particles show that U_{ms} and hence Re_{ms} increases almost linearly as the static bed height is increased. The deeper the bed the larger the amount of air needed to keep the central or annular bed regions at spouting condition and therefore the higher is U_{ms}. Similar observations have been reported in the literature for conventional spouted beds [1,2,5]. It is important to note that, unlike conventional spouted beds, the rotating jet spouted bed permits spouting of shallow beds as low as 10 cm (that is, $H/D_c = 0.22$). Conventional spouted beds with low bed depths ($H/D_c < 1$) exhibit poor quality of solids mixing and circulation and the greater part of the gas flow is localized around the spout [5,16].

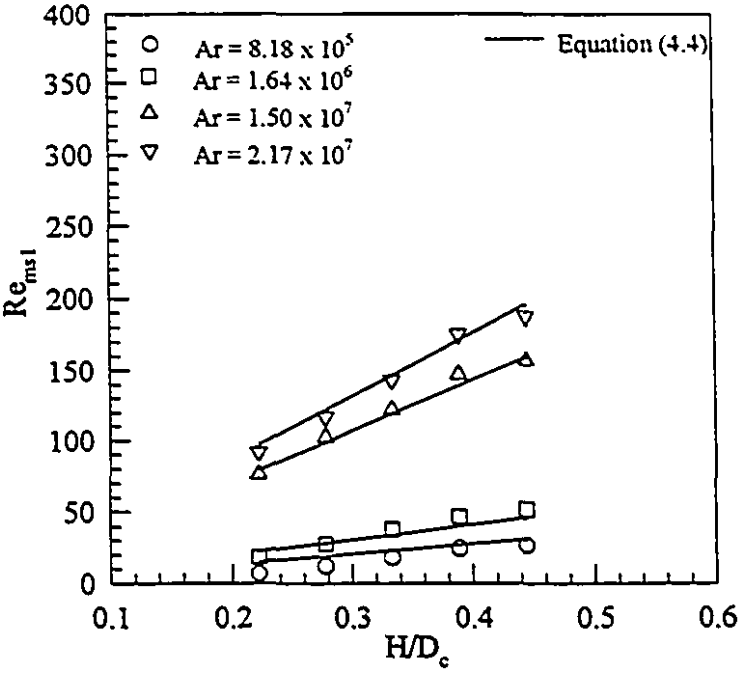

Figure 4.12: Effect of dimensionless bed height on Re_{ms1}, D_n/D_c= 0.0444, N=2 rpm.

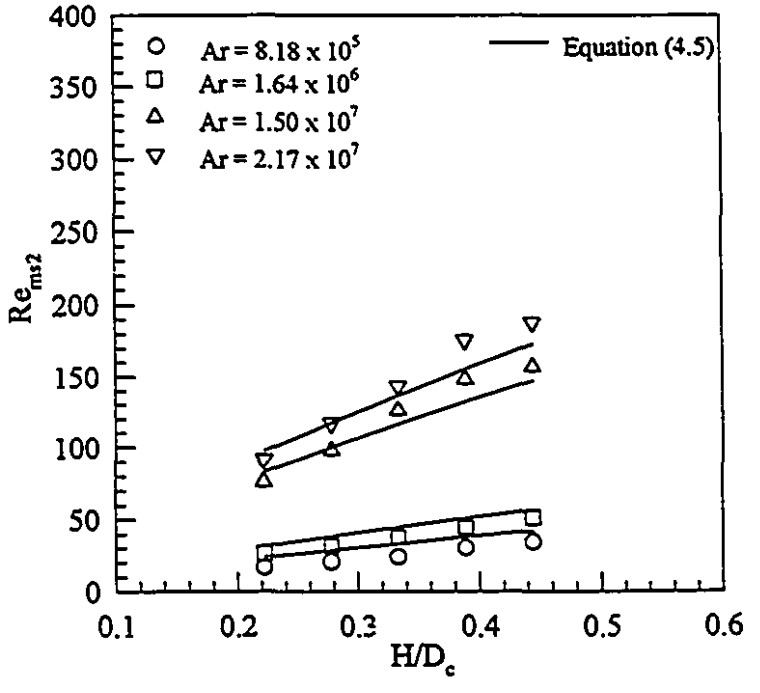

Figure 4.13: Effect of dimensionless bed height on Re_{ms2}, D_n/D_c= 0.0444, N= 2 rpm.

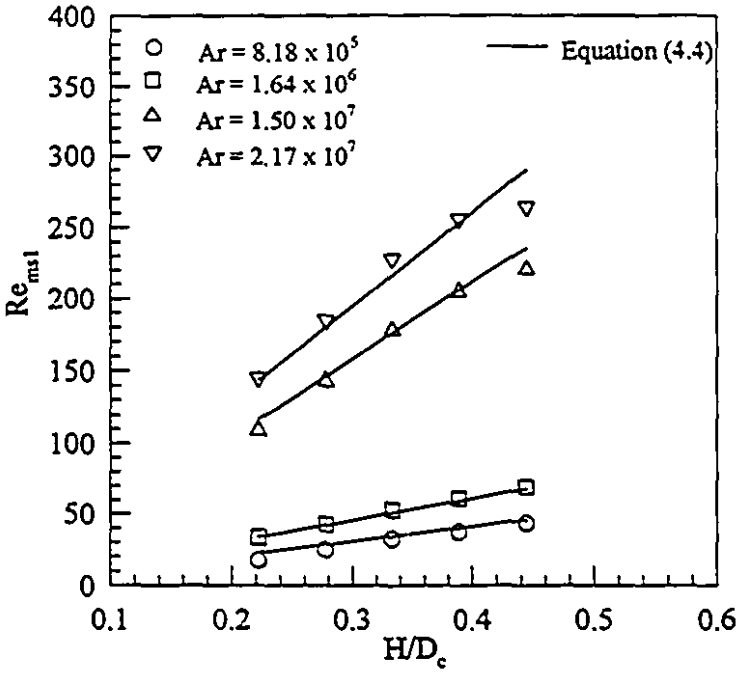

Figure 4.14: Effect of dimensionless bed height on Re_{ms1}, D_p/D_c= 0.0667, N= 6 rpm.

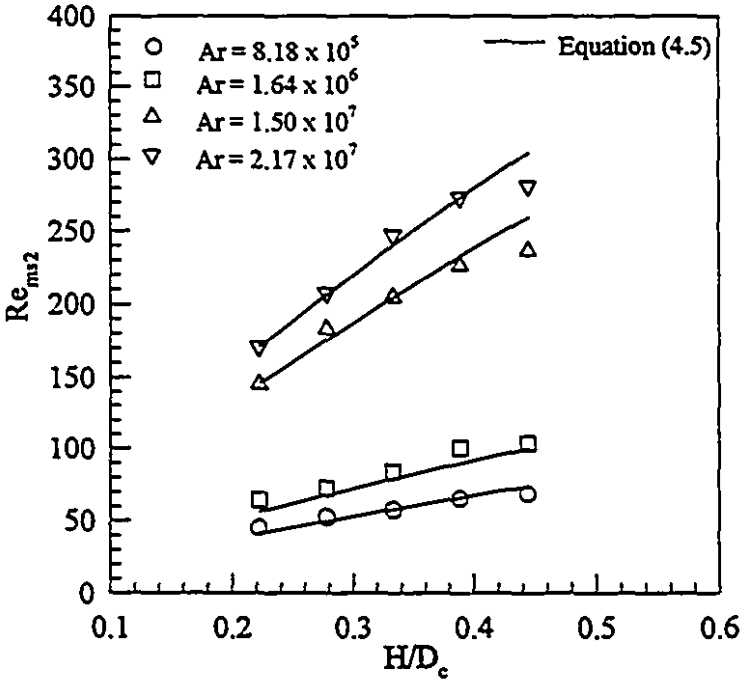

Figure 4.15: Effect of dimensionless bed height on Re_{ms2}, D_p/D_c= 0.0667, N= 6 rpm.

Effect of rotational speed

The effect of distributor rotational speed in terms of the dimensionless circumferential velocities, $V_{\theta 1}/U_t$ and $V_{\theta 2}/U_t$ on their corresponding Re_{ms} is presented in Figures 4.16 and 4.17 for $D_n/D_c = 0.067$ and $H/D_c = 0.22$ using different particles. Increasing $V_{\theta 1}/U_t$ from zero produces a slight decrease in both Re_{ms1} and Re_{ms2}. Further increases in the circumferential velocity show increases in Re_{ms2} while Re_{ms1} remain virtually constant. The small reduction in Re_{ms} when N is increased from zero might be explained by the pulsating action of the rotating jets which helps enhance the effectiveness of the spouting air streams. However, further increase in N introduces the effect of the resistance forces discussed earlier that tend to deviate the air jets from the vertical direction (particularly the annular jet), and thus more flow is required to maintain stable spouting and consequently higher Re_{ms2} values.

Effect of particle properties

Additional light was shed on the dynamic behavior of the RJSB by examining the effect of particle properties viz. diameter, shape, and density on the minimum spouting velocity. These properties along with the fluid properties are often combined into a single parameter- the Archimedes number Ar, which represents the ratio between gravity forces and viscous forces. The effect of this parameter on Re_{ms} is depicted in Figures 4.18 and 4.19 for different H/D_c ratios using $D_n/D_c = 0.044$ and N = 6 rpm. The main trend is for both Re_{ms1} and Re_{ms2} to increase with Ar. One possible explanation for this behavior is that materials with large Ar, in this case corn and soybeans, offer more resistance to flow than polystyrene and polyethylene (lower Ar). Large and heavy particles have large mass (inertia) and respond slowly to the change in fluid flow while small and light particles generally follow more closely the changes in fluid motion. Therefore, gravity forces are more significant than viscous forces for large particles under spouting conditions.

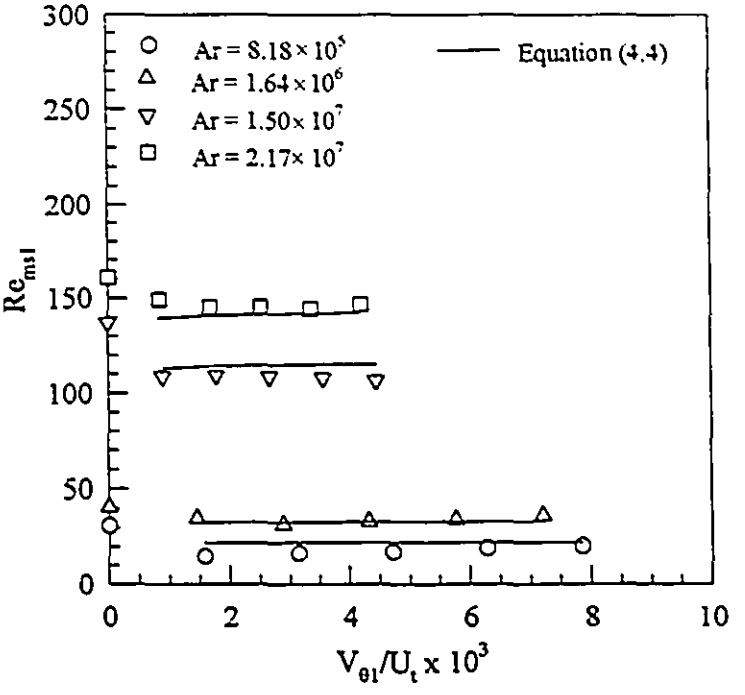

Figure 4.16: Effect of dimensionless circumferential velocity on Re_{ms1} for different Ar, D_n/D_c= 0.0667, H/D_c= 0.22.

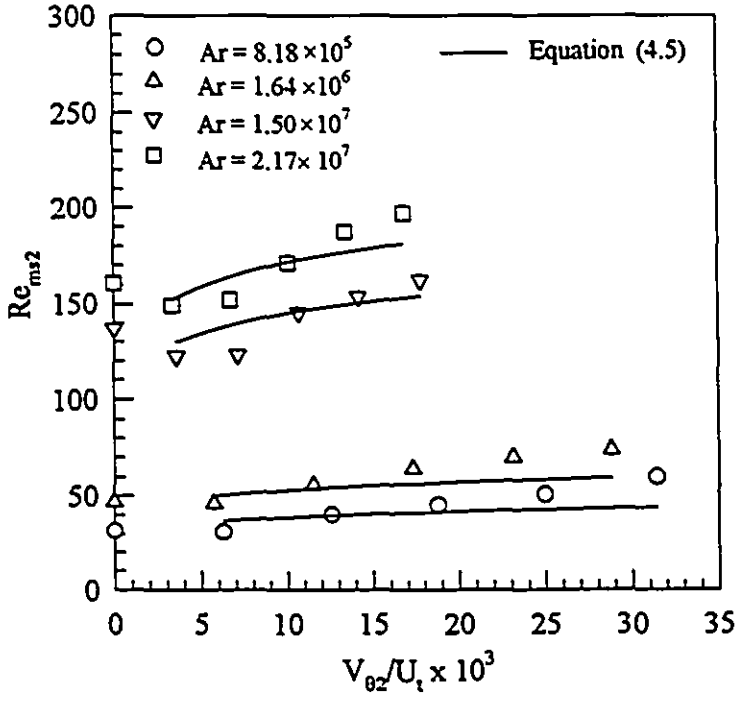

Figure 4.17: Effect of dimensionless circumferential velocity on Re_{ms2} for different Ar, D_n/D_c= 0.0667, H/D_c= 0.22.

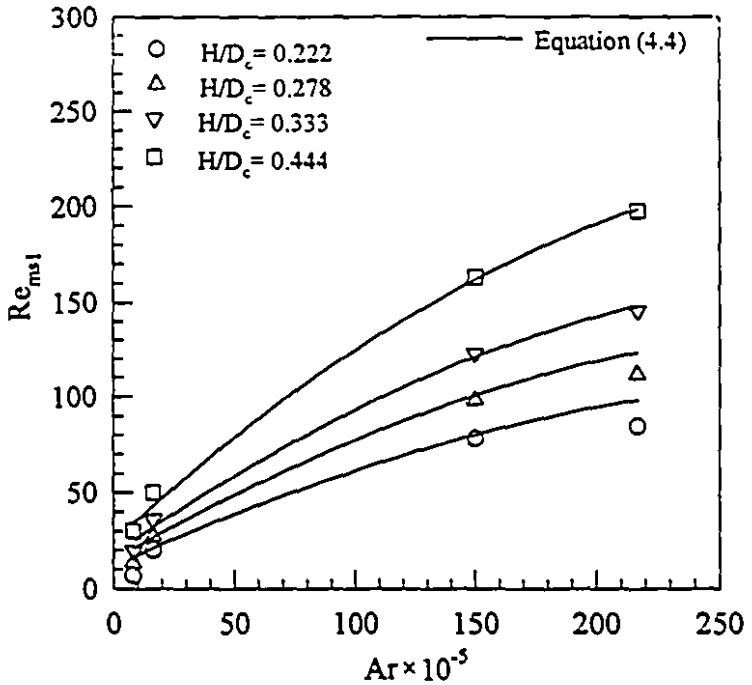

Figure 4.18: Effect of Archimedes number on Re_{ms1} for different H/D_c values, D_n/D_c= 0.0444, N= 6 rpm.

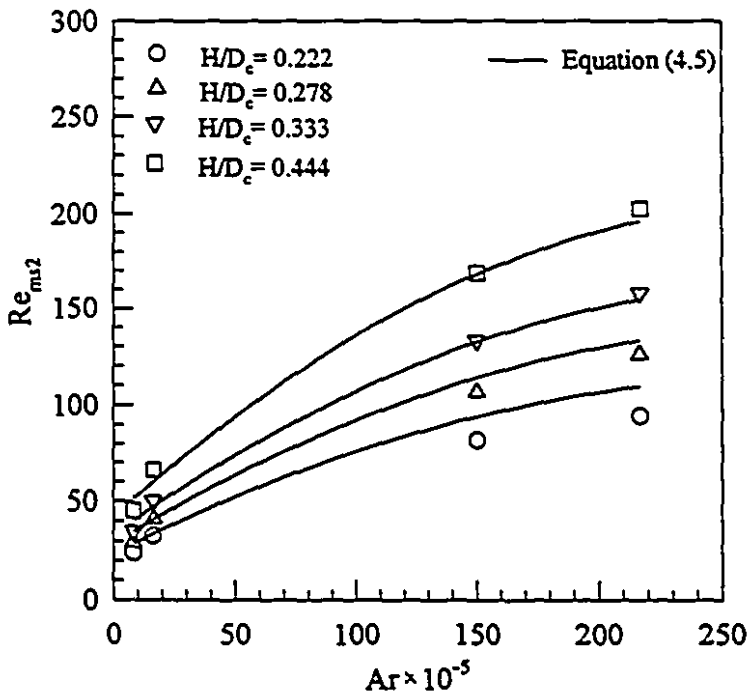

Figure 4.19: Effect of Archimedes number on Re_{ms2} for different H/D_c values, D_n/D_c= 0.0444, N= 6 rpm.

Effect of nozzle size

To examine the effect of nozzle diameter, several experiments were performed using two different nozzle sizes for different solid materials and distributor rotational speed. The results obtained are presented as Reynolds number versus dimensionless nozzle circumferential velocity with the dimensionless nozzle diameter as a parameter, Figures 4.20 and 4.21. Evidently the particle Reynolds number for both spouting cells increases as the dimensionless nozzle diameter increases from 0.044 to 0.067. This increase is due to the larger spout diameter and hence larger active cross-sectional area causing higher air flow requirements for transporting an increased volume of particles through the active spouting cells and for preserving stable dynamic conditions. Note that the difference is more pronounced at higher Archimedes number.

From the practical point of view, use of a larger nozzle size is recommended (i.e., $D_n = 3$ cm or $D_n/D_c = 0.067$) since at high air velocity the nozzle pressure drop increases significantly with decreasing the nozzle diameter and therefore increases the pumping power requirements. Also, using a small nozzle diameter limits the contact between air and particles because of the smaller active spouting area and higher air velocity.

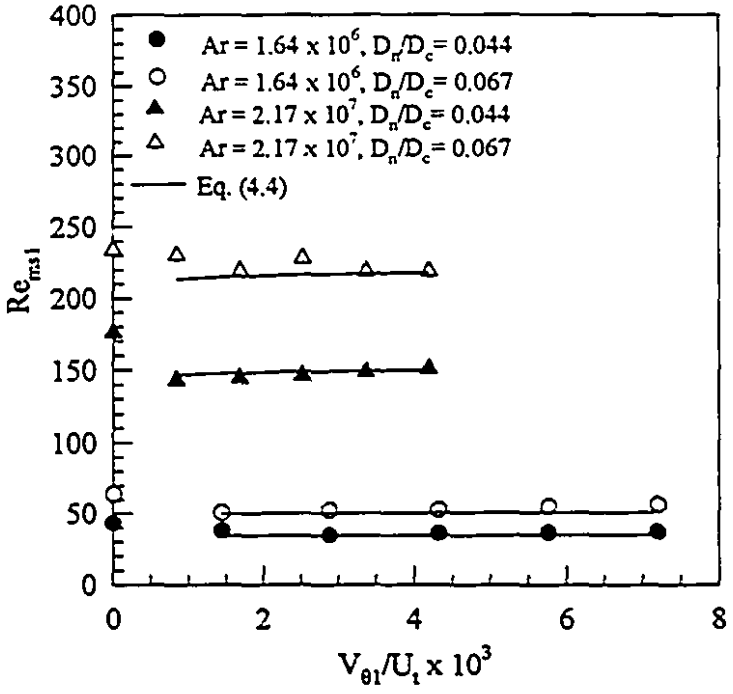

Figure 4.20: Effect of dimensionless nozzle diameter on Re_{ms1}, H/D_c= 0.333.

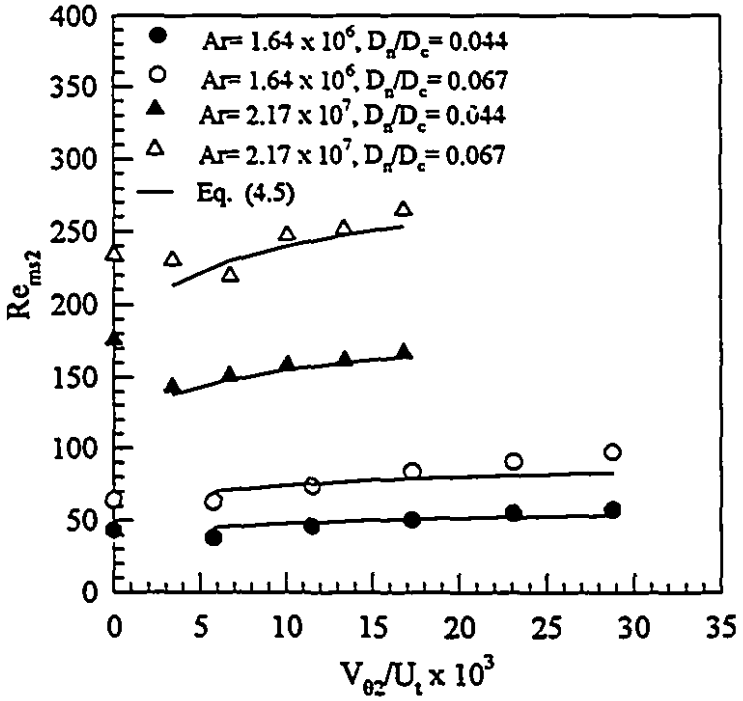

Figure 4.21: Effect of dimensionless nozzle diameter on Re_{ms2}, H/D_c= 0.333.

4.4.3 Pressure Drop

As in conventional spouted beds, two pressure drop values are of practical interest in the design and operation of the rotating jets spouted bed, namely the peak pressure drop ($-\Delta P_M$) and the steady (fully developed) spouting pressure drop ($-\Delta P_s$). The peak pressure drop, which depends on the initial bed compaction, corresponds to point B in Figures 4.4 and 4.5 (section 4.3) and it is encountered when starting up the bed and it is used, together with the air distributor pressure drop, in sizing the air blowing system. The steady spouting pressure drop corresponds to the constant pressure drop line beyond point C in Figures 4.4 and 4.5 and it is useful in estimating the operating power requirements.

Effect of distributor rotational speed

Figures 4.22 and 4.23 show the effect of distributor rotational speed, N, on the peak pressure drop and steady spouting pressure drop, respectively, for two bed heights of polyethylene particles. These figures show that neither the peak pressure drop nor the steady spouting pressure drop are affected by the rotational speed. It is clear, however, that the values for stationary distributor (N = 0 rpm) are slightly higher, especially for the dimensionless peak pressure drop which approximately approaches unity. The lower pressure drop values for N > 0 can be attributed to the pulsation and shaking actions introduced by the internal rotating jets. This causes disturbance in the stable packed bed structure by destroying the interparticle forces before the onset of spouting. Similar behavior was observed for beds of polystyrene, corn, and soybeans particles.

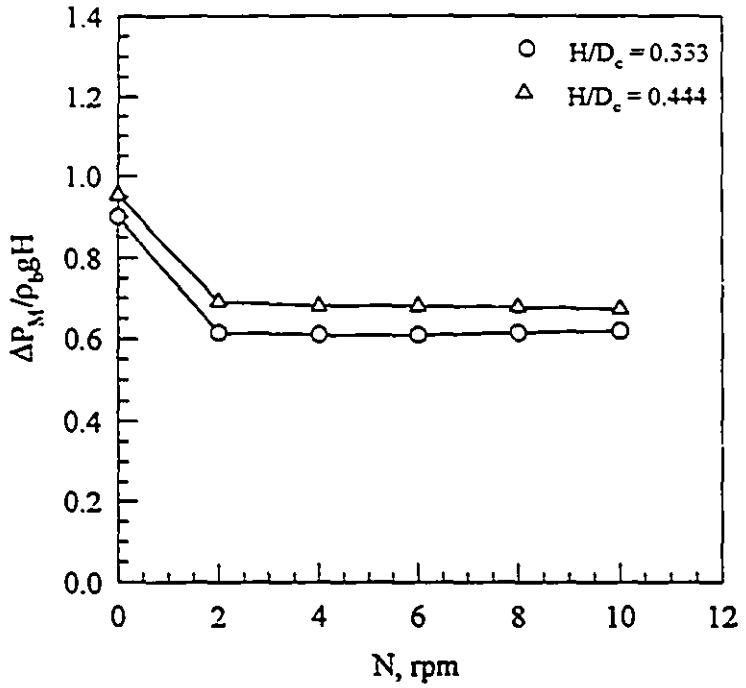

Figure 4.22: Effect of rotational speed on dimensionless peak pressure drop for polyethylene particles, $D_p/D_c = 0.0667$.

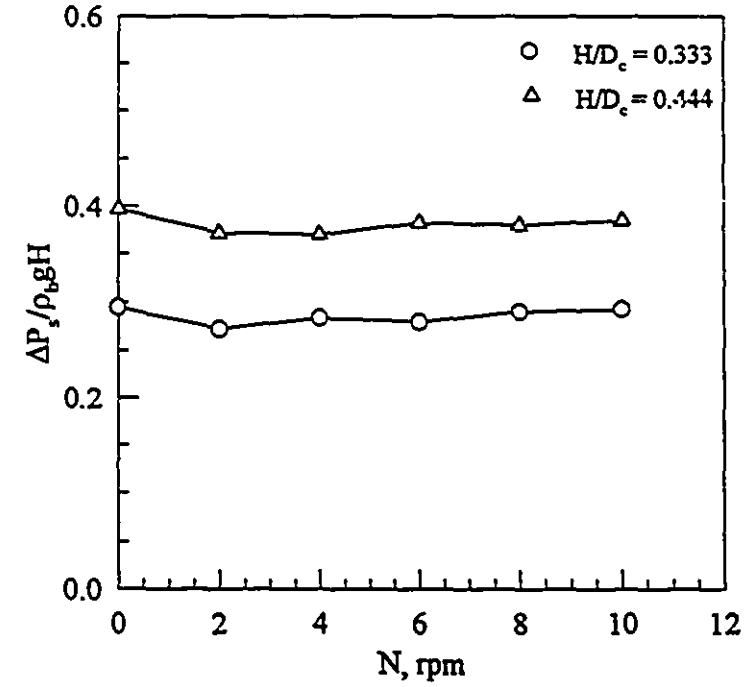

Figure 4.23: Effect of rotational speed on dimensionless steady spouting pressure drop for polyethylene particles, $D_p/D_c = 0.0667$.

Effect of bed height and nozzle size

In order to analyze the effect of the geometric parameters of the contactor, the values of dimensionless pressure drop, $\Delta P_M/\rho_b gH$ and $\Delta P_s/\rho_b gH$, are plotted in Figures 4.24 and 4.25 against the dimensionless bed height (H/D_c) for different dimensionless effective particle diameters (D_p/D_c) with the dimensionless nozzle diameter (D_n/D_c) as parameter. Both pressure drop values tend to increase with dimensionless bed height irrespective of the solid material; the effect is more pronounced on the peak pressure drop. It can be noticed that as the inlet air nozzle size increases, the pressure drop increases. Similar effects are reported in the literature for conventional spouted beds [1,17]. These figures also show a comparison between the experimental data and the calculated values using equations 4.6 and 4.7. This demonstrates that the agreement is good.

For the shallow bed heights ($H/D_c<1$) used in this work, the ratio of the peak pressure drop to that across a comparable fluidized bed at minimum fluidization,

$$\Delta P_{mf} = (1-\varepsilon)(\rho_p - \rho_g)gH = \rho_b gH \qquad (4.8)$$

is considerably less than unity for all dimensionless bed heights. In a conventional spouted bed, the peak pressure drop may be several times the bed weight per unit area [1,4], i.e.,

$$\Delta P_M = k\Delta P_{mf} \qquad (4.9)$$

where k= 1 to 3. The difference between the results obtained in this study and the values predicted by equation (4.9) highlights the impact of the rotating jets upon the spouting mechanism and, in particular, upon the bed structure before the onset of spouting. It should be noted also that the flat geometry of supporting grid and the periodic relocation of the spouting jets beneath, play an important role in lowering the peak pressure drop. Hence, the entire bed is not supported by the rising rotating jets; it is supported, in part by

the bottom screen or the walls. This means that the entire pressure drop at the air side can approach the pressure drop at the spouts themselves, which is known to be much smaller than the pressure drop caused by the entire bed. On the other hand, The pressure drop, ΔP_s across a fully developed spouted bed is always lower by at least 60 % than that required to support the weight of the bed.

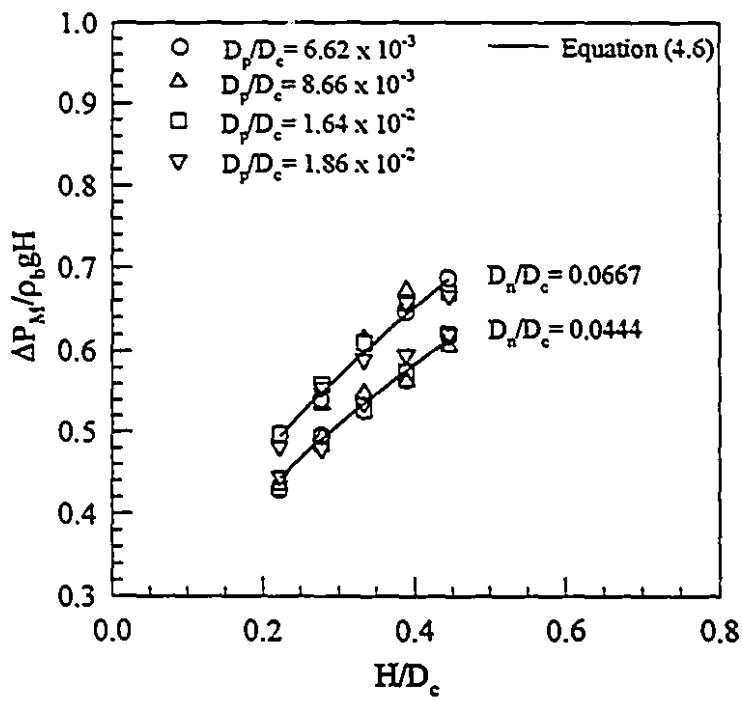

Figure 4.24: Variation of dimensionless peak pressure drop with H/D_c and D_n/D_c for different D_p/D_c,; $N > 0$.

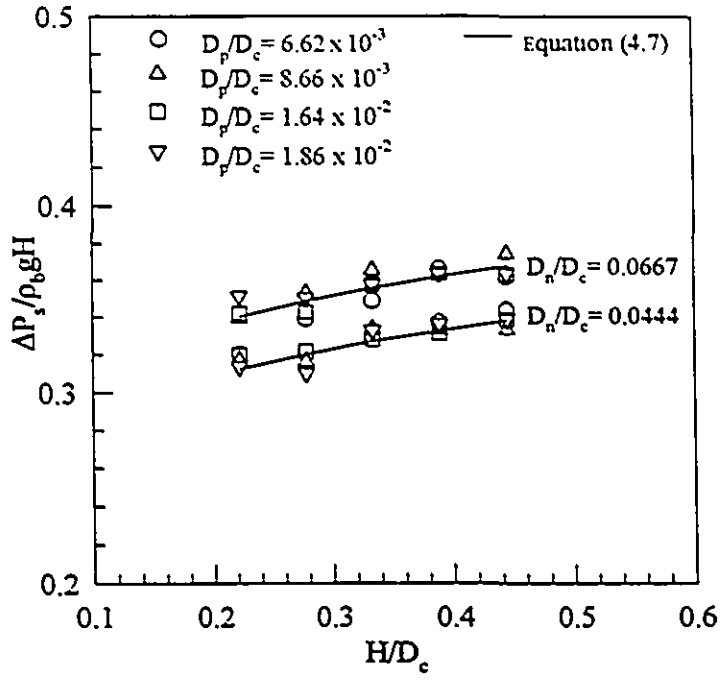

Figure 4.25: Variation of dimensionless steady spouting pressure drop with H/D_c and D_n/D_c for different D_p/D_c, $N > 0$

Effect of particle size

To analyze the effect of particle diameter, the dimensionless pressure drop parameters are further normalized by the (D_n/D_c) modulus obtained from the empirical equations 4.6 and 4.7 and thus the effect of dimensionless nozzle diameter is eliminated as shown in Figures 4.26 and 4.27. These plots demonstrate that the particle diameter has little or no effect on the pressure drop values and this can be explained by the fact that the bulk density and hence the bed weight is the most influential parameter on the pressure drop among other particle-related properties and this factor is already included in the pressure drop modulus, $\Delta P/\rho_b gH$. This is in agreement with the empirically estimated figures.

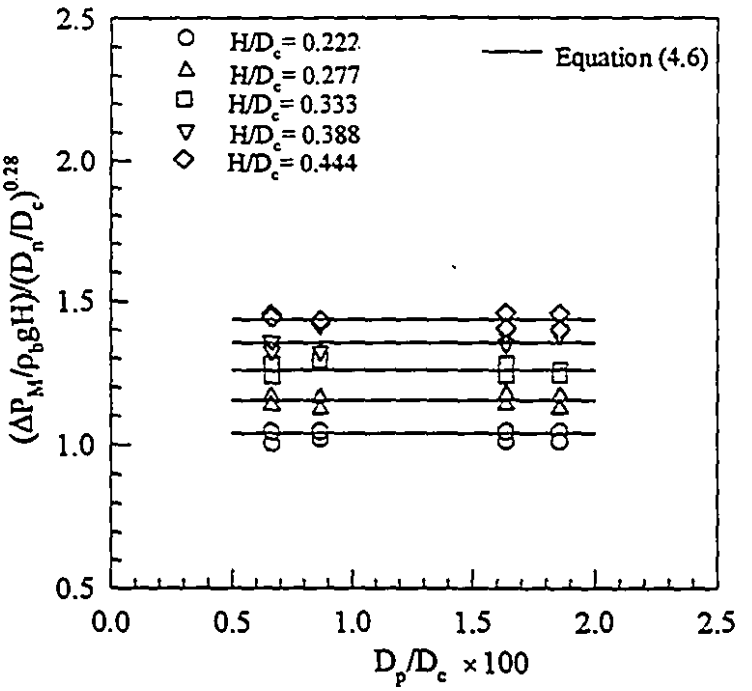

Figure 4.26: Variation of $(\Delta P_M/\rho_b gH)/ (D_n/D_c)^{0.28}$ modulus with D_p/D_c for different H/D_c, $N > 0$.

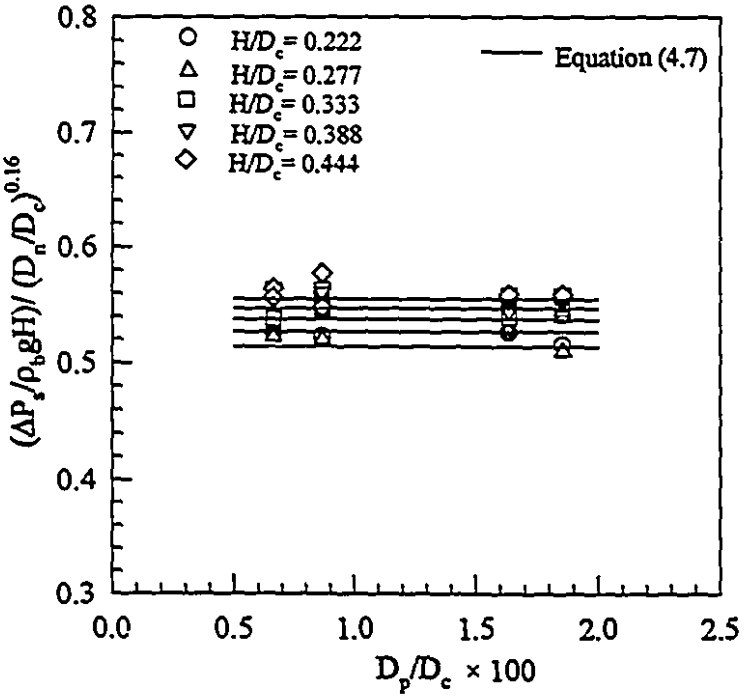

Figure 4.27: Variation of $(\Delta P_s/\rho_b gH) /(D_n/D_c)^{0.16}$ modulus with D_p/D_c for different H/D_c, $N > 0$.

4.5 A Note on the Spouting Stability and Scale-up

For conventional spouted beds, Becker [5] demonstrated that the critical value of the ratio D_c/D_n is 3. Ghosh [18] proposed that fine particles can be spouted as long as the ratio D_n/D_p does not exceed 30, while Chandnani and Epstein [19] indicated that D_n/D_p should be less than 25. Németh et al. [4] and Pallai et al. [20] stated that the optimum ranges for the ratios D_n/D_p, D_c/D_p, and D_c/D_n are 3-30, 25-200, and 6-10, respectively. The ratios D_n/D_p, D_c/D_p, and D_c/D_n employed in this study are listed in Table 4.7. The table also shows if the spouting criteria discussed above are achieved or not. It is clear from the table that stable spouting would not have been achievable if a single nozzle was used in the study. It is demonstrated also that D_c/D_n is higher than the upper limit required for stable spouting by 50 to 125 %.

The condition that the ratio D_c/D_n must be in the range 6 to 10 would also imply a maximum bed diameter of respectively 20 and 30 cm for the 2 and 3 cm nozzle diameters used in this study for stable spouting from a single nozzle. Noting that the column diameter (D_c) used in this study is 45 cm, It is obvious that it was possible to more than double the column diameter in the RJSB (with two nozzles) without any instability problems compared to the conventional spouted bed with only one stationary inlet nozzle. This gives another advantage of the RJSB in terms of capacity, efficiency, and scale-up.

Table 4.7 Expected stability of single nozzle spouting for the different nozzle and particle diameters used in the present study (✓ stability criteria satisfied, × stability criteria not satisfied)

D_p, mm	D_n, mm	D_n/D_p	D_c/D_n	D_c/D_p
2.981	20	6.71 ✓	22.5 ×	150.98 ✓
2.981	30	10.07 ✓	15.0 ×	150.98 ✓
3.898	20	5.13 ✓	22.5 ×	115.44 ✓
3.898	30	7.69 ✓	15.0 ×	115.44 ✓
7.367	20	2.71 ×	22.5 ×	61.08 ✓
7.367	30	4.07 ✓	15.0 ×	61.08 ✓
8.354	20	2.39 ×	22.5 ×	53.86 ✓
8.354	30	3.59 ✓	15.0 ×	53.86 ✓

Nomenclature

Symbols

Ar	Archimedes number = $\dfrac{D_p^3 \rho_g (\rho_s - \rho_g) g}{\mu_g^2}$
D_c	column diameter, m
D_n	nozzle diameter, m
D_p	effective particle diameter, m
g	acceleration of gravity, m/s^2
H	bed height, m
k	constant in eqn. (4.9)

N	distributor rotational speed, rpm
ΔP	pressure drop, Pa
ΔP_M	peak pressure drop, Pa
ΔP_{mf}	pressure drop at U_{mf}, Pa
ΔP_s	steady spouting pressure drop, Pa
R	radius of rotation, m
Re	particle Reynolds number = $\frac{D_p U \rho_g}{\mu_g}$
U	superficial air velocity, m/s
U_{mf}	minimum superficial air velocity for fluidization, m/s
U_{ms}	minimum superficial air velocity for spouting, m/s
U_t	particle terminal velocity, m/s
$V_{\theta 1}$	circumferential velocity of the central nozzle, m/s
$V_{\theta 2}$	circumferential velocity of the annular nozzle, m/s

Greek Letters

e	voidage, -
m_g	viscosity of gas, Pa s
r_b	bulk density, kg/m^3
r_s	solid density, kg/m^3
f	sphericity, -

Subscripts and Superscripts

o	stationary nozzle
1	first or central nozzle

2	second or annular nozzle
b	bed, bulk
c	column
g	gas
mf	minimum fluidization
ms	minimum spouting
n	nozzle
p	particle
s	solid
θ	circumferential

References

1. K. Mathur and N. Epstein, *Spouted Beds*, Academic Press, New York (1974).
2. K. Mathur and P. Gishler, " A technique for contacting gases with coarse solid particles", *A.I.Ch.E. Journal*, 1, 157-164 (1955).
3. B. Ye, C. Lim, and J. Grace, " Hydrodynamics of spouted and spout-fluidized beds at high temperature", *Can. J. Chem. Eng.*, 70, 840-847 (1992).
4. J. Nemeth, E. Pallai, and E. Aradi, " Scale-up examination of spouted bed dryers", *Can. J. Chem. Eng.*, 61, 419-425 (1983).
5. H. Becker, " An investigation of laws governing the spouting of coarse particles", *Chem. Eng. Sci.*, 13, 245-262 (1961).
6. A. Wolny and W. Kazmierczak, " Triboetrification in fluidized bed of polystyrene", *Chem. Eng. Sci.*, 44, 2607 (1989).
7. P. Jiang, H. Bi, S. Liang, and L. Fan, " Hydrodynamic behavior of circulating fluidized bed with polymeric particles", *AIChE Journal*, 40, 193-206 (1994).

8. B. White, Particle Dynamics in Two-phase Flows, in *Encyclopedia of Fluid Mechanics*, Vol. 4, N. Chermisinoff (Ed.), Gulf Publishing Company, Houston (1986).
9. D. Boland and D. Gildart, "Electrostatic charging in gas fluidized beds", *Proceedings of Int. Powder Tech. & Bulk Granular Solids Conference*, A.S. Goldberg (Ed.), Dorchester Harrogate, 243-249, 1971.
10. J. Ciborowski and A. Wlodarski, "On electrostatic effects in fluidized beds", *Chem. Eng. Sci.*, 17, 23-32, 1962.
11. M. Passos, *Flow Characteristics of Two-Dimensional Spouted and Spout-Fluidized Beds of Particles*, PhD Thesis, McGill University, Montreal, Canada, 1990.
12. E. Buckingham, " On physically similar systems: illustration of the use of dimensional equations", *Physical Review*, 4, 345-376 (1914).
13. E. Isaacson and M. Isaacson, *Dimensional Methods in Engineering and Physics*, John wily & Sons, Inc., New York (1975).
14. D. Marquardt, " An algorithm for least squares estimation of nonlinear parameters", *J. Soc. Ind. Appl. Math.*, 11, 431 (1963).
15. A. Constantinides, *Applied Numerical Methods with Personal Computers*, McGraw-Hill Company, New York (1987).
16. M. Anabtawi, B. Uysal, and R. Jumah, "Flow characteristics in a rectangular spout-fluid bed", *Powder Technology*, 69, 205-211 (1992).
17. F. Ogino, L. Zhang, and Y. Maehashi, " Minimum rate of spouting and peak pressure-drop in a spouted bed", *Int. Chem. Eng.*, 33, 265-272 (1993).
18. B. Ghosh, " A study on the spouted bed- a theoretical analysis", *Indian Chem. Eng.*, 7, 16 (1995).
19. P. Chandnani and N. Epstein, "Spoutability and spout destabilization of fine particles with a gas", in *Fluidization*, K. Ostergaard and Sorensen (eds.), Engineering Foundation, New York, 233-240 (1986).
20. E. Pallai, J. Nemeth, and E. Aradi, " Development of spouted bed dryer", *Drying'84*, A. S. Mujumdar (ed.), 158-165 (1984).

Chapter 5

Drying Kinetics in the Rotating Jet Spouted Bed

5.1 Introduction

This chapter contains the results and discussion of a sequence of experiments designed to investigate the drying kinetics of yellow dent corn grains used as a test material in the rotating jet spouted bed (RJSB). The chapter is divided into two main sections: continuous drying and intermittent drying. In continuous drying hot spouting air is supplied continuously to a batch of particles. In intermittent drying the supply of spouting air is interrupted to provide the bed a tempering period and thus the process consists of alternated convective heating and "rest" periods. The objectives of this chapter are:

- To investigate the kinetics of drying in the rotating jet spouted bed and compare the results with other spouted bed drying studies.
- To study the impact of operating variables such inlet air temperature, distributor rotational speed, bed height, superficial air velocity, and inlet nozzle diameter on the drying of yellow dent corn in the RJSB.
- To explore the feasibility of intermittent drying in the RJSB in terms of energy savings using different tempering periods.

5.2 Continuous Drying

Kinetics of continuous drying of corn grains in the rotating jet spouted bed are studied in terms of drying curves, drying rate, average bed temperature, exit air temperature, and exit air humidity curves. Drying curves represent the evolution of average material moisture content (X) with time (t). Drying rate curves are plotted as (-dX/dt) versus X where dX/dt values are obtained by numerical differentiation of the smoothed moisture content time data. It is assumed that the bed solids are well mixed and that the sampled material moisture content is, therefore, representative of the moisture content in the bed at any time. This assumption is supported by moisture content values of grain samples taken from various locations in the bed and the results showed that difference of the moisture content values is within the experimental uncertainty.

5.2.1 Effect of Inlet Air Temperature

Sets of drying and drying rate curves with the inlet air temperature as parameter are shown in Figure 5.1. It is clearly demonstrated that the drying kinetics in the RJSB follow the typical kinetics for convective drying. The results also show that the drying process is fully within the falling rate period where internal moisture diffusion dominates and the external convective mass transfer resistance has no measurable effect on the drying rate. This follows from the high mass transfer Biot number ($Bi_M = k_c R_p / \mathcal{D}$), relating the internal diffusion resistance to the external convective resistance, which is typically in the order of 10^6 - 10^7 for cereal grains under spouting drying conditions [1,2]. Similar trends are reported in the literature for corn drying in two-dimensional spouted beds with draft plates [3,4,5] and in fluidized beds of inert particles [6,7].

Figure 5.1 shows that the drying rate is considerably affected by the inlet gas temperature level throughout the whole drying period. This effect is especially significant during the final stages of drying when the release of moisture from the receded evaporation front requires a large temperature difference between the material surface and the evaporation front. Analysis of the results shows that in order to dry the corn grains to 15 % (d.b.) the drying time decreases by 30, 42, and 50 % when the inlet air temperature is increased from 60 °C to 70, 80, and 90 °C, respectively. However, this time saving is at the cost of the quality since some particle breakage was observed at T_{gi} = 90 °C, especially during the final stages of the drying process. It is recommended that inlet air temperatures be lower than 90 °C depending on the end use of the grains.

As the drying air temperature is increased there should be an increase in the temperature gradient within the solid and hence in the amount of heat transfer and its biasing effect on moisture diffusivity. The result will be an increase in the moisture gradient developed within the solid and hence an increase in the drying rate. Increasing the inlet air temperature also increases the vapor pressure of the moisture held in the solid material creating a higher vapor pressure gradient, which, in turn results in higher moisture vapor diffusion to the surface simultaneously with liquid diffusion.

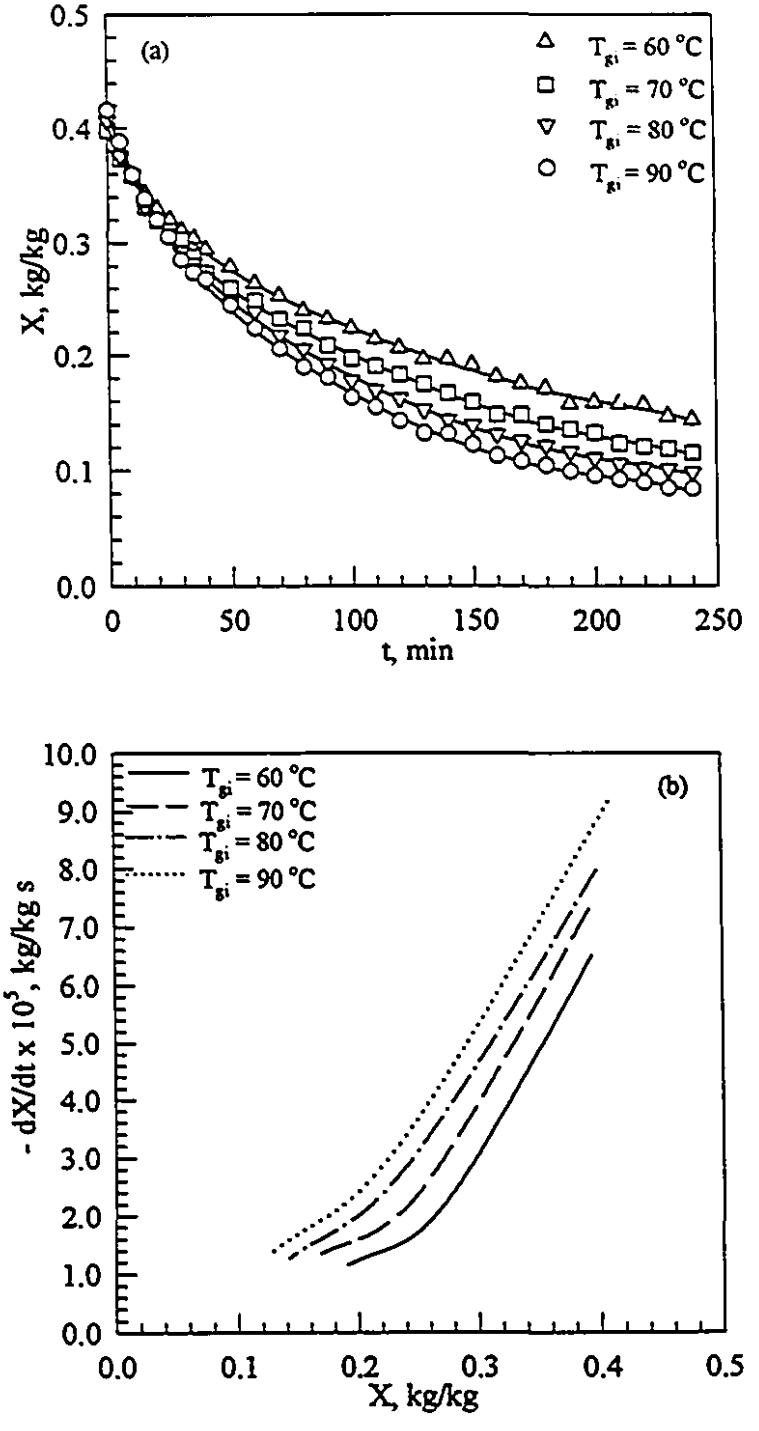

Figure 5.1: Effect of inlet air temperature on: (a) drying curve, (b) drying rate curve for corn grains. $D_n = 3$ cm, $H = 15$ cm, $X_o \cong 0.4$ kg/kg (d.b.), $N = 2$ rpm, $U = 0.514$ m/s.

Figure 5.2 shows plots of outlet gas temperature, bed temperature and outlet gas absolute humidity versus time at T_{gi} = 70 and 80 °C. In the initial warming-up period, the absolute gas humidity has a distinctive peak. As drying proceeds, the peak decreases rapidly indicating a continuous decrease in the drying rate.

Inspection of the temperature curves in Figure 5.2 shows that the outlet air temperature is higher than the bed temperature, especially in the first hour of drying. This suggests that the bed height is not high enough to assure thermal equilibrium between the drying medium leaving the spouted bed and the particles. Clearly, as drying proceeds thermal equilibrium is reached toward the end of the drying. An expression for the fractional approach to thermal equilibrium is derived in the following *approximate* analysis using an overall bed heat transfer coefficient, $\bar{h}_p$ [1,8]:

Neglecting heat used in moisture evaporation as well as heat losses and assuming plug flow for the air and quasi-steady state condition for the gas temperature profile with height, the following heat balance can be written for a differential height (dz) over which a temperature drop of dT_g occurs:

$$-\rho_g\left(c_{pg}+\bar{Y}_g c_{pv}\right)U dT_g = a\,\bar{h}_p\left(T_g - T_b\right)dz \qquad (5.1)$$

where $\bar{Y}_g$ is the average absolute air humidity over the whole drying time and a is the specific surface area for all bed particles,

$$a = \frac{\textit{total surface area of particles}}{\textit{total volume of particles}} = \frac{A_s}{V_s} \qquad (5.2)$$

A_s is related to a single particle surface area, A_p by the following equation

$$A_s = \frac{A_p m_s}{\rho_s V_p} \qquad (5.3)$$

where m_s is the mass of dry material in the bed. Equation (5.1), combined with equations (5.2) and (5.3) can be integrated to give

$$ln\left(\frac{T_{ge}-T_b}{T_{gi}-T_b}\right)=-\frac{A_p m_s \bar{h}_p H}{\rho_s V_p\left(c_{ps}+\bar{Y}_g c_{pv}\right)U\rho_g V_s} \tag{5.4}$$

noting that $V_s = A_c \times H$, equation (5.4) can be written as

$$\eta=\frac{T_{gi}-T_{ge}}{T_{gi}-T_b}=1-exp\left(\frac{A_p m_s \bar{h}_p}{\rho_s V_p\left(c_{ps}+\bar{Y}_g c_{pv}\right)U\rho_g A_c}\right) \tag{5.5}$$

where η is the fractional temperature approach to thermal equilibrium which is equal to 1.0 for exit air temperature equal to the bed temperature.

Using the experimental T_b and T_{ge} data, η averaged 0.8 while $\bar{h}_p$ ranged between 13 and 20 W/ m^2 K. It is interesting to note here that these overall bed heat transfer coefficient values are of the same order of magnitude as data reported by Uemaki and Kugo [9] (quoted from Mathur and Epstein [1]) and by Kmiec [10] for conventional spouted beds and based on the total surface area in the bed. Similar results are also recorded by Kudra et al. [11] using the drying rate method in a two dimensional spouted bed with and without draft plates under constant drying rate conditions.

These heat transfer coefficients only represent composite bed values and overlook the actual heat transfer mechanisms in both active spouting regions and static annular regions. This is due to the fact that the heat transfer area used in estimating $\bar{h}_p$, instead of being limited to the active spouting regions, is based on the total particle surface in the bed.

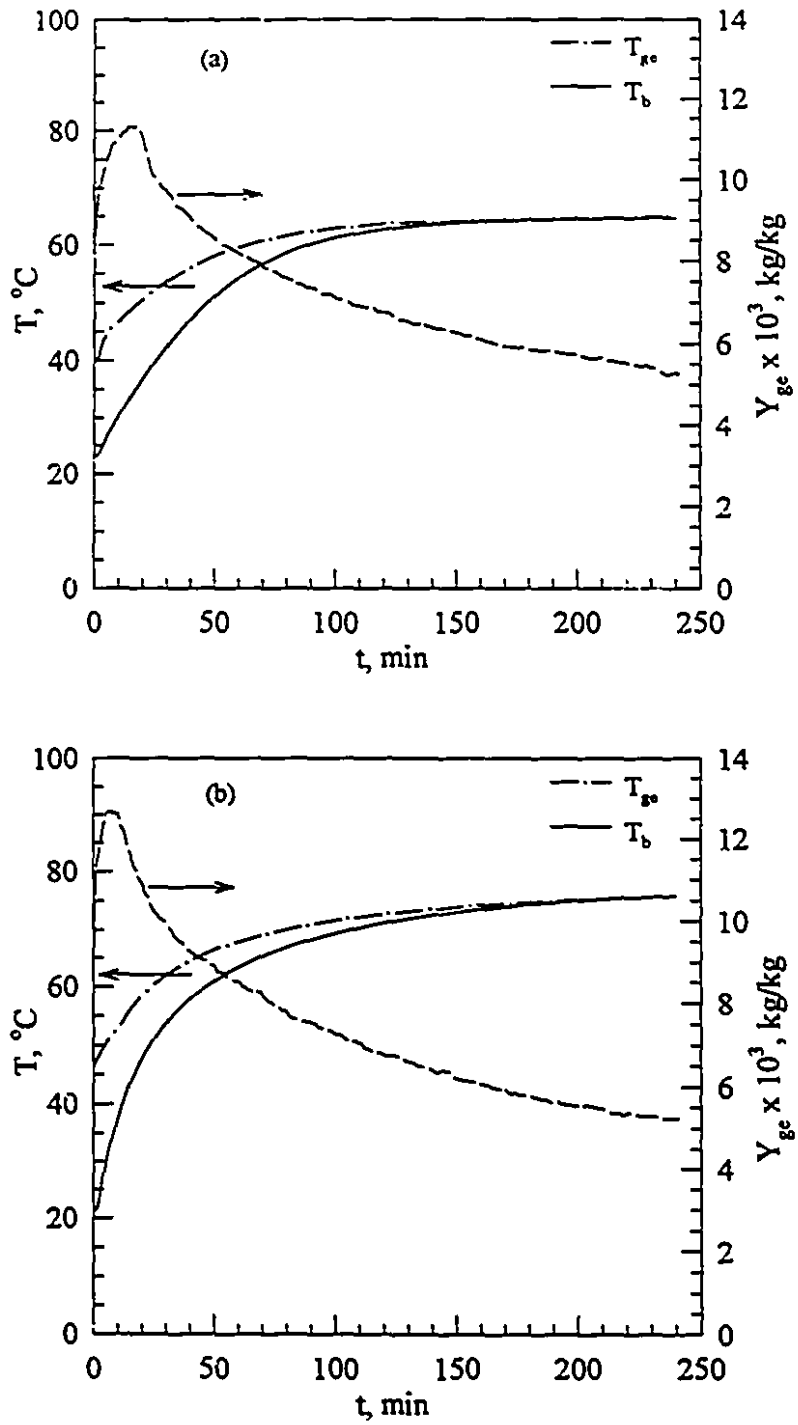

Figure 5.2: Evolution of exit air temperature, bed temperature, and exit air absolute humidity with drying time; (a) $T_{gi} = 70°C$, (b) $T_{gi} = 80°C$ for corn grains. $D_n = 3$ cm, $H = 15$ cm, $X_o \equiv 0.4$ kg/kg (d.b.), $N = 2$ rpm, $U = 0.514$ m/s.

5.2.2 Effect of Distributor Rotational Speed

The variation of the drying curves with distributor rotational speed is illustrated in Figure 5.3. The results reported in these figures are almost independent of the distributor rotational speed within the range tested. The selected rpm range was biased by the aerodynamic requirements to achieve a steady and stable rotating spouting state in both the central and the annular regions corresponding to the full spouting flow regime discussed in chapter 4. Similar behavior is reported by Jezowska [12] for the drying of beet and wheat seeds in a rectangular spouted bed with cyclically shifted gas stream with the frequency of pulsation ranging from 4 to 10 Hz.

For all the rpm values tested, visual observations during the drying process showed that there were no dead zones in the bed. This significantly diminishes the possibility of wet or hot spot formation inside the bed and improve the effectiveness of heat and mass transfer.

It is important here to mention the important role of the rotating spouting action in the heat and mass transfer mechanisms along with the advantageous aerodynamic characteristics presented in chapter 4. The rotating jets introduce pulses of hot air into the bed and prevent the set up of continuous large adverse temperature gradients. The formation of temporary loose packed sections in the bed as the air jets are periodically relocated to the following sections results in a "tempering period" during which moisture redistribution inside the particle occurs. Thus the intra-particle moisture and temperature gradients are relaxed. The degree of relaxation will depend on the rotational speed since using low rpm values results in lower exposure time to hot air pulses. It is expected that any drying during the tempering period will be marginal due to the short rest time and the low moisture diffusivity and thus low mass transfer Fourier number ($Fo_M = \mathcal{D}\ t/R_p^2$). Moreover, the heat and mass transfer coefficients during this short tempering period will

be considerably lower than those in the active spouts because of the minimal air flow in the "static" sections.

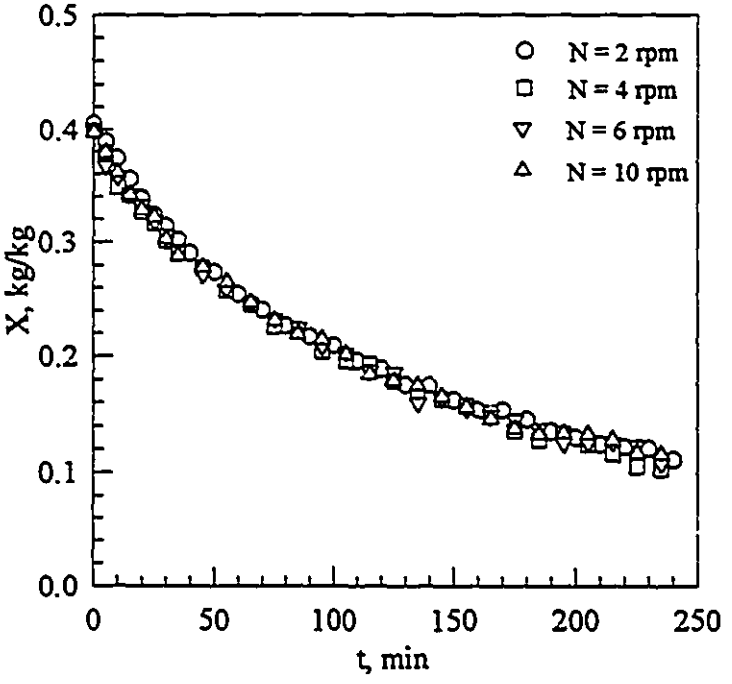

Figure 5.3: Effect of distributor rotational speed on drying curve.
D_n = 3 cm, H = 15 cm, T_{gi} = 70 °C, U = 0.57 m/s, X_o = 0.40 kg/kg.

5.2.3 Effect of Static Bed Height

The experimental data shown in Figure 5.4 indicate that the drying rate decreases slightly when the bed height is increased from 10 to 20 cm. The range tested was limited by the air blower capacity used in this study.

A reduction in bed height results in a shorter particle cycle time and thus higher temperature gradients inside the particle, higher surface temperature, hence higher moisture diffusivity and therefore higher drying rates.

Decreasing bed height leads also to a lower average vapor concentration in the gas phase, and therefore, the mean driving force for heat and mass transfer increases resulting in an increased drying rate.

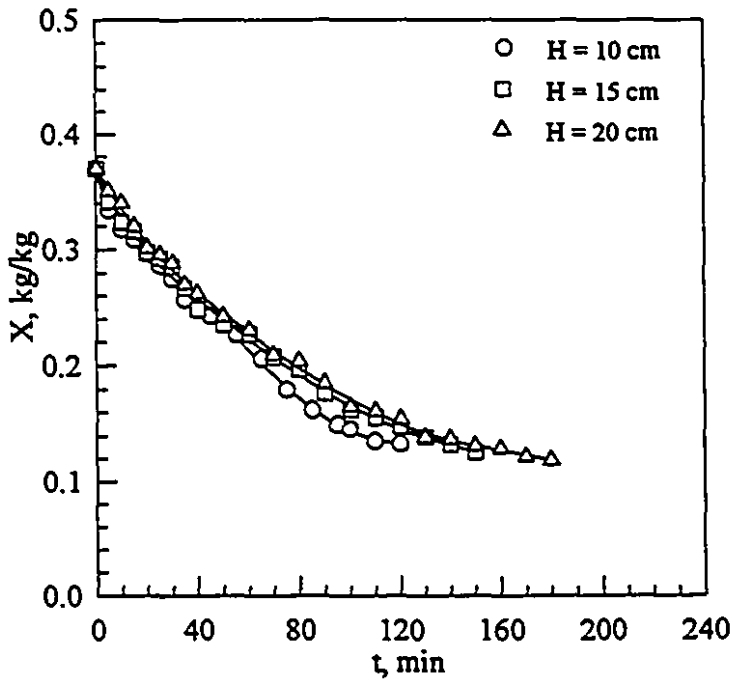

Figure 5.4: Effect of initial bed height on drying curve. $D_n = 2$ cm, $N = 4$ rpm, $T_{gi} = 80\ ^{\circ}C$, $X_o = 0.375$ kg/kg.

5.2.4 Effect of Air Velocity and Nozzle Diameter

The curves of moisture content versus drying time for different superficial air velocities are shown in Figure 5.5. The air velocity was varied in a narrow range above the minimum spouting velocity to achieve a steady spouting condition based on the experience gained from the aerodynamics experiments. The highest air velocity tested was limited by the risk of particle attrition. As drying proceeds, with continuous moisture loss and continuous reduction in bed height, the fountain's height will continuously increase since the gas velocity will be much higher than the minimum spouting value. This may lead to excessive entrainment and severe particle attrition.

Reference to Figure 5.5 shows that an increase in air velocity is accompanied by only a slight increase in the drying rate. This small effect can be attributed to the very low external resistance to heat and mass transfer relative to the internal diffusion which controls the process. This behavior suggests that, from both the aerodynamic and drying kinetics points of view, it is desirable to use low air superficial velocity (but $U>U_{ms}$) when drying material where drying kinetics are controlled by internal heat/mass transfer.

Similarly, the nozzle diameter has no discernible effect on the drying rate over the entire range of operating parameters covered in this study. An illustrative result is shown in Figure 5.6. This is despite the fact that increasing the nozzle diameter from 2 to 3 cm for the same air flow rate increases the average bed voidage and improves particle circulation. This is also due the drying rate being controlled by transport resistance inside the particle.

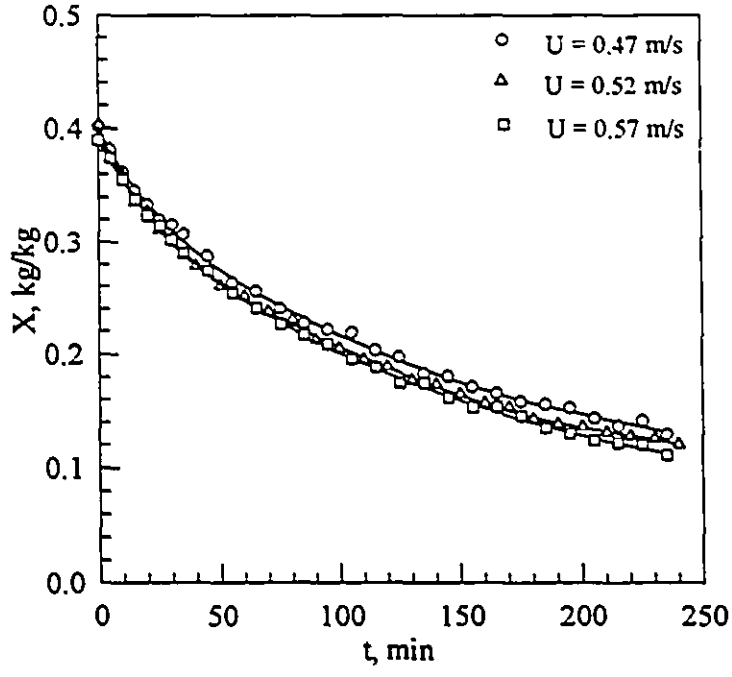

Figure 5.5: Effect of superficial air velocity on drying curve. $D_n = 3$ cm, $H = 15$ cm, $T_{gi} = 70\ ^{\circ}C$, $N = 2$ rpm, $X_o = 0.40$ kg/kg.

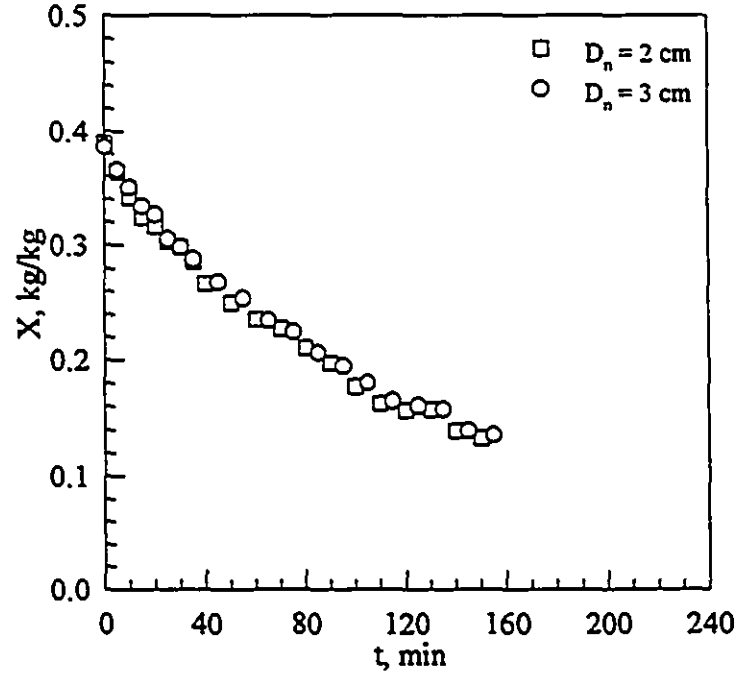

Figure 5.6: Effect of nozzle diameter on drying curve. $H = 15$ cm, $N = 4$ rpm, $T_{gi} = 80\ ^{\circ}C$, $U = 0.45$ m/s, $X_o = 0.39$ kg/kg.

5.3 Intermittent Drying

The rotating jet spouted bed is characterized by an inherently periodic gas-particle contact that generates intermittent drying conditions. In other words, the contact between gas and particles may be idealized as a series of active drying periods separated by tempering periods. However, these drying and tempering periods are short as a result of high frequency of gas relocation. This frequency is high enough that it does not affect the drying behavior of the slowly drying corn grains in which the limiting mechanism of heat and mass transfer is primarily internal. This fact is supported by the negligible effect of the distributor rotational speed on the corn drying rate as discussed in the previous section.

Preliminary experiments were carried out to test the hypothesis that corn as a slowly drying material can be dried to produce higher quality grain at lower energy consumption by providing external intermittency. This was achieved by using various drying periods alternated by long tempering periods. During the active period and as a result of the rotating spouts, the particles are subjected to very intense mixing and circulation and thus a high intensity of heat and mass transfer. While in the no flow period the temperature and moisture gradients are effectively relaxed with favorable moisture redistribution inside the particle.

Four intermittency patterns were compared with continuous drying using square-wave gas pulsing in which the superficial gas velocity is essentially constant during the active drying period (τ_{on}) of the pulsed cycle and zero during the rest or tempering period (τ_{off}) as shown schematically in Figure 5.7. One level of active period, 20 minutes and four levels of the tempering period, 10, 20, 40, and 60 minutes, were used in the intermittent drying experiments as shown in Table 5.1. The inetermittency, α, is defined as the fraction of cycle time during which spouting gas is supplied, i.e.,

$$\alpha = \frac{\tau_{on}}{\tau_{on} + \tau_{off}} \tag{5.6}$$

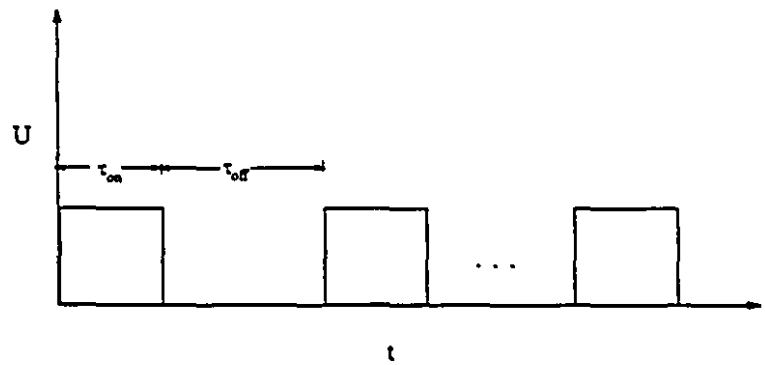

Figure 5.7: Schematic representation of square-wave (on/off) inlet air conditions used in the intermittent drying experiments.

Table 5.1: Summary of the Operating Conditions Applied in the Intermittent Experiments.

Drying period τ_{on}, min	Tempering period τ_{off}, min	Intermittency α	Process conditions
20	60	1/4	T_{gi} = 80 °C
20	40	1/3	U = 0.475 m/s
20	20	1/2	X_o = 0.4 kg/kg
20	10	2/3	m_s = 12 kg
continuous	0	1	N = 4 rpm

The effect of the intermittency, α on the drying curves is displayed in Figure 5.8. This figure was constructed using the total process time, that is, the cumulative sum of both drying and tempering periods. To highlight the effect of the intermittency in a more informative way, these drying curves are then replotted using the effective or net drying time, i.e., the cumulative sum of the drying periods. The results are shown in Figures 5.9.

It is clear from Figures 5.8 that the continuous drying curve (α=1) shows very rapid loss of moisture initially with the rate falling off thereafter. The initial high drying rate is not maintained because the surface zone of the material is rapidly dried to its equilibrium value and the process is controlled largely by internal moisture diffusion. In this case, intensified and continuous heating has little effect on speeding up the drying process.

In the intermittent drying experiments ($\alpha < 1$) the drying curves show that the initial high rate of moisture loss is repeated in each active drying period so that steeper drying curve segments are obtained compared to the corresponding continuous drying curve, particularly for $\alpha < 2/3$, i.e., long tempering periods. This proves that moisture leveling occurs during the tempering periods with moisture migration to the kernel surface.

As the tempering period increases (α decreases), the drying rate decreases if the total process time including the tempering periods is used to calculate the drying time (Figure 5.8). On the other hand, if the net or cumulative active drying time is used (Figure 5.9), the drying rate increases. This proves that the net drying rate after a tempering period is higher than that of a corresponding period for the continuous drying process. Similar trends are reported by Zhang and Litchfield [13] who dried corn in a thin layer dryer using 20 minutes drying periods separated by tempering periods between 10 and 120 minutes.

Samples collected during the tempering periods demonstrate the occurrence of some partial drying, although marginal, as shown in Figure 5.8. This can be attributed to the fact that as a result of moisture redistribution and migration towards the grain surface, part of the sensible heat gained during the active period is used to evaporate this moisture from the surface of the grain, especially with long tempering period, i.e., low α values. Similar conclusions were reported by Hemati et al. [7] using a flotation fluidized bed.

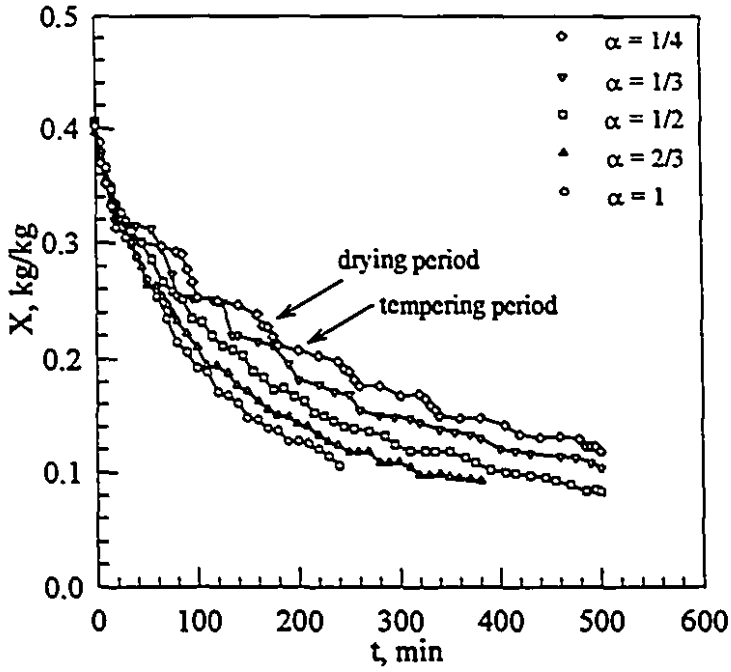

Figure 5.8: Effect of intermittency on the evolution of moisture content with total time. H= 15 cm, N = 4 rpm, T_{gi} = 80 °C, U = 0.475 m/s, X_o = 0.40 kg/kg.

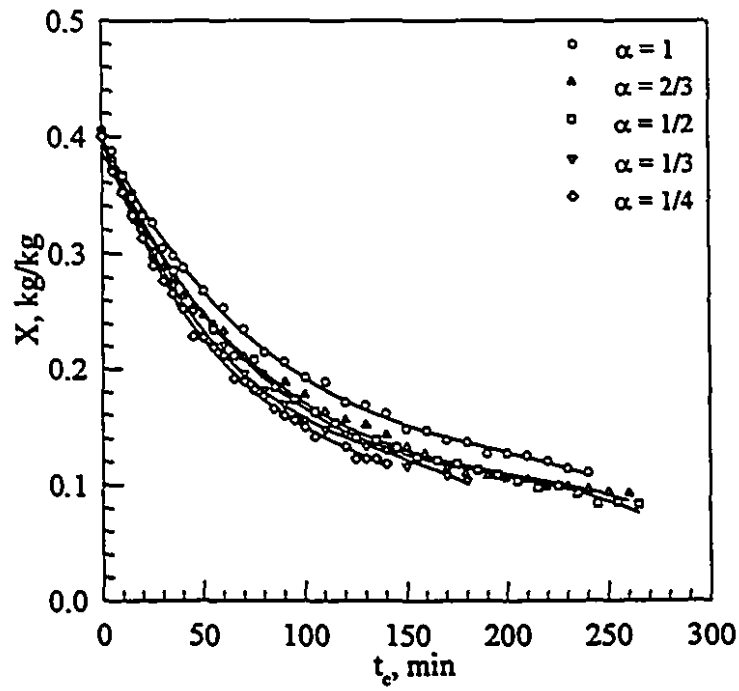

Figure 5.9: Effect of intermittency on the evolution of moisture content with the effective drying time. H= 15 cm, N = 4 rpm, T_{gi} = 80 °C, U = 0.475 m/s, X_o = 0.40 kg/kg.

To evaluate the intermittent drying process as compared to the continuous one, the following performance factors are defined:

1. Specific thermal energy consumption ratio,

$$\text{STER} = \frac{\text{specific thermal energy consumption of intermittent process}}{\text{specific thermal energy consumption of continuous process}}$$

2. Specific fan energy consumption ratio,

$$\text{SFER} = \frac{\text{specific fan energy consumption of intermittent process}}{\text{specific fan energy consumption of continuous process}}$$

3. Effective drying time ratio,

$$\text{EDTR} = \frac{\text{effective drying time of intermittent process}}{\text{effective drying time of continuous process}}$$

4. Total process time ratio,

$$\text{TPTR} = \frac{\text{total process time of intermittent process}}{\text{total process time of continuous process}}$$

In this preliminary study where the inlet air temperature, superficial air velocity, and bed load are fixed as listed in Table 5.1, both the specific thermal energy consumption (STER) and the specific fan energy consumption (SFER) are equivalent to the effective drying time ratio if the material is dried to the same final moisture content. Table 5.2 summarizes the performance results of the intermittent drying process in comparison with the continuos process. The final moisture content is taken as 13 % (d.b.) which is the recommended value for safe storage [14].

Table 5.2: Effect of the Intermittency on the Performance of the Drying Process.

α	Total process time ratio	Effective drying time ratio = energy consumption ratio	Percent energy saving over continuous drying
1/4	2.32	0.63	37
1/3	1.95	0.70	30
1/2	1.48	0.77	23
2/3	1.19	0.81	19
1	1	1	-

As depicted in Table 5.2, for any α value, intermittent drying takes a longer time than the continuous one when the total time is considered and shorter time in terms of the effective spouting time required to dry the material to a particular final moisture content. The total process time needed to reach 13 % (d. b.) final moisture content increases by 19 % when a 10 minute tempering period (α =2/3) was used relative to the continuous drying with no tempering periods. However, the effective or net drying time decreases by 19 %. Furthermore, the total process time no more than doubled when the tempering period was increased by a factor of 6, i.e., increasing τ_{off} from 10 to 60 minutes or decreasing α from 2/3 to 1/4. However, the effective drying time decreases by 22 %. All these time savings are translated directly to energy savings as shown in Table 5.2 and equations 5.2 - 5.4 with a maximum energy saving of 37 % using 60 minutes tempering period (α =1/4).

Figures 5.10-5.13 display the evolution of the corresponding bed temperature and exit air temperature for different intermittency values. The figures clearly show the cyclic response of the temperature during the successive drying and tempering periods. Thermal equilibrium with the outlet air temperature is attained even with the relatively short drying period used in these experiments (i.e., τ_{on} = 20 min), especially after 2 to 4 drying periods depending on the intermittency α. This is a result of the thermal inertia of the corn kernels.

The bed temperature in the case of intermittent drying is lower than that in the continuous case as depicted in Figure 5.14. This is because of the cooling effect during the tempering period that results in a lower particle surface temperature. It is worth pointing out that observations made during the experiments have shown that intermittent drying prevents particle damage from occurring as compared to the continuous process at the same inlet air temperature and superficial velocity. This means that short-time drying periods separated with equal or longer tempering periods yield better product quality than long-time continuous drying as result of the reduced exposure to hot air streams with the resulting lower temperature and moisture gradients inside the particles. The latter also reduces drying-induced stresses and hence stress-cracking of the kernels.

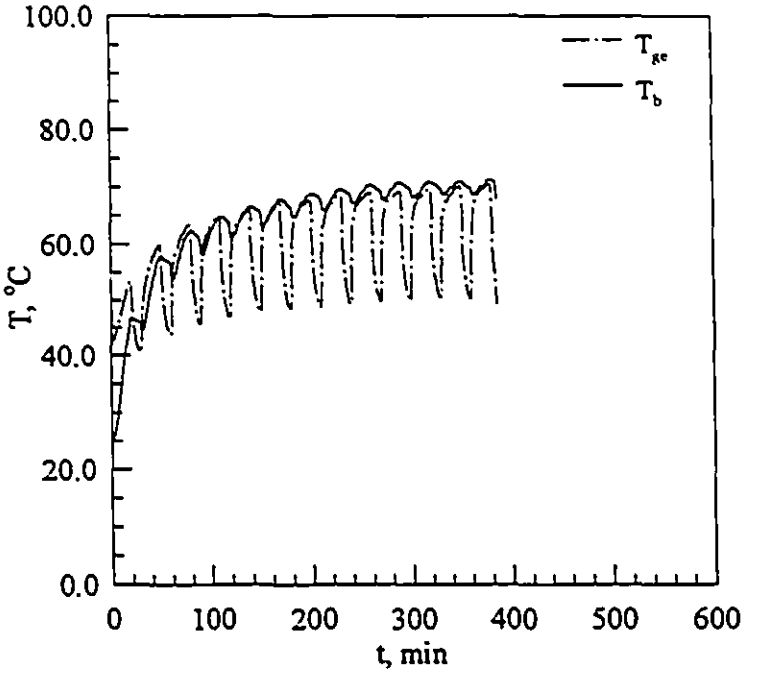

Figure 5.10: Evolution of exit air temperature and bed temperature with time for α =2/3.

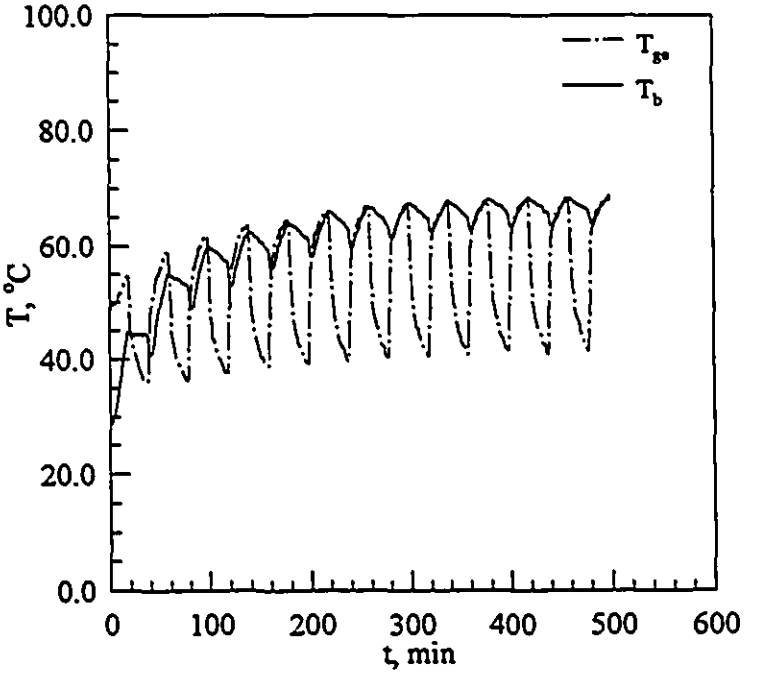

Figure 5.11: Evolution of exit air temperature and bed temperature with time for α =1/2.

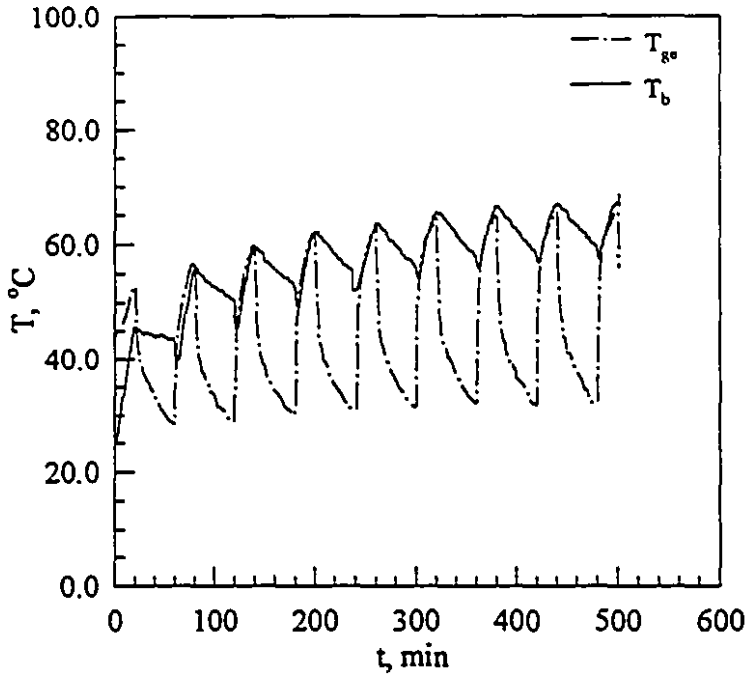

Figure 5.12: Evolution of exit air temperature and bed temperature with time for α =1/3.

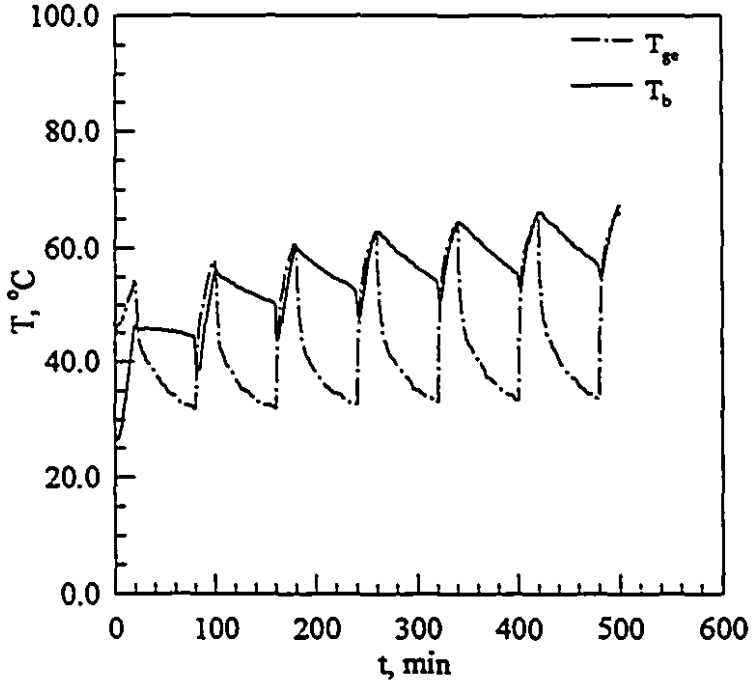

Figure 5.13: Evolution of exit air temperature and bed temperature with time for α =1/4.

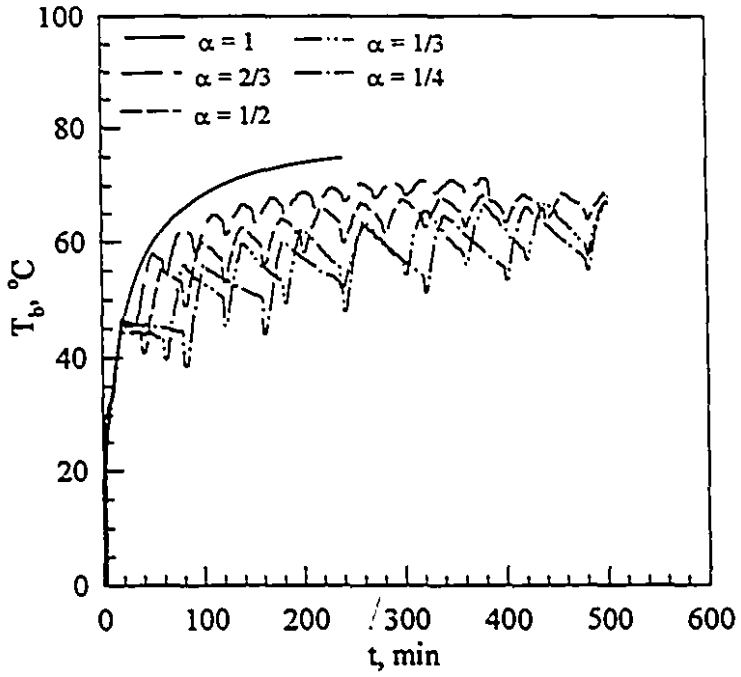

Figure 5.14: Comparison between continuous (α =1) and intermittent bed temperature evolution.

5.4 Implication for Design and Operation

On the basis of the experimental results discussed above, it can be concluded that with the proper design and selection of the operating parameters the batch RJSB dryer lends itself to a wide range of drying applications. Fast drying materials or materials with surface moisture can be dried in the RJSB using continuous spouting/heating scheme without the risk of thermal damage. This is because of the periodic relocation of the air jets inside the bed which provides rest periods for moisture diffusion. Slow drying materials and materials with bound moisture such as foodstuffs, pharmaceuticals, and synthetic products can be dried in the system using either continuous or intermittent spouting /heating schemes by adjusting the operating parameters depending the type and the quality of the product.

If the material being dried is sensitive to mechanical stresses or the drying kinetics are controlled by internal heat/mass transfer, a low superficial air velocity (but $> U_{ms}$) should be used. For heat sensitive agricultural products (e.g., corn in this study), inlet air temperatures between 50 and 80 °C are recommended. Using higher temperatures results in excessive thermal damage of the product. Using nozzle diameter of 3 cm satisfies both the pumping power and product quality demands. Smaller nozzle diameters result in high jet velocity and nozzle pressure drop and hence high power requirements and risk of product damage while larger nozzle diameters require large air flow rates. Since for slow drying materials the effect of the distributor rotational speed on the drying rate is negligible, low rpm values ($0 < N < 6$) should be used in order to obtain the steady full rotating spouting characteristics at low power requirement.

It is worth pointing out that the practical value of the intermittent spouting/heating process can be realized if it can be applied in an economical and efficient way. One possible method is use of a battery of similar units in parallel with the number of units

equal to $1/\alpha$, where α is the intermittency. In this configuration (Figure 5.15) the air supply is periodically switched from the first unit to the next after the end of one on period (τ_{on}). At the end of one spouting/heating cycle ($\tau = \tau_{on} + \tau_{off}$), the air supply is switched from the last unit back to the first unit and so on. However, such a system should be optimized in terms of the capital cost, operating cost, and other factors.

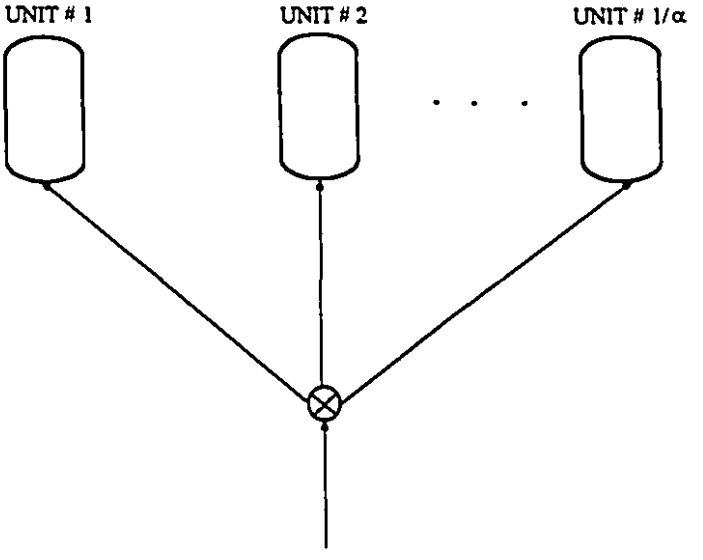

Figure 5.15 A battery of RJSBs operating in a periodic spouting/heating scheme.

Nomenclature

Symbols

a	specific surface area, m^2/m^3
A	area, m^2
A_c	cross-sectional area of column, m^2
A_p	surface area of single particle, m^2
A_s	total surface area of bed particles, m^2
Bi_M	mass transfer Biot number $= \frac{k_c R_p}{\mathcal{D}}$, -
c_{pg}	heat capacity of dry air, J/kg K
c_{pv}	heat capacity of water vapor, J/kg K
$\mathcal{D}$	effective moisture diffusivity in solid, m^2/s
D	diameter, m
Fo_M	mass transfer Fourier number $= \mathcal{D}\, t/R_p^2$
$\bar{h}_p$	overall bed heat transfer coefficient, W/m^2 K
H	bed height, m
k_c	mass transfer coefficient, m/s
m_s	mass of solids in bed, kg
N	distributor rotational speed, rpm
R_p	effective particle radius, m
t	time, s
T_b	bed temperature, °C
T_g	air temperature, °C
T_{ge}	exit air temperature, °C
T_{gi}	inlet air temperature, °C
U	superficial air velocity, m/s

V_p	volume of a single particle, m^3
V_s	total volume of solids in bed, m^3
X	moisture content (dry basis), kg/kg
X_o	initial moisture content (dry basis), kg/kg
Y	absolute humidity, kg/kg

Greek Letters

α	intermittency, -
η	fractional temperature approach to thermal equilibrium, -
ρ_g	gas density, kg/m^3
ρ_s	solid density, kg/m^3
τ	cycle period, s
τ_{on}	on period, s
τ_{off}	off period, s

Subscripts and Superscripts

b	bed
c	column
e	exit
g	gas
i	inlet
ms	minimum spouting
n	nozzle
o	initial
p	particle
s	solid
v	vapor

References

1. K. Mathur and N. Epstein, *Spouted Beds*, Academic Press, New York (1974).
2. N. Epstein and K. Mathur, "Heat and mass transfer in spouted beds- a review", *Can. J. Chem. Eng.*, 49, 467-476 (1971).
3. T. Kudra, A. S. Mujumdar, G.S.V. Raghavan, and M. Kalwar, Two-Dimensional Spouted-Beds: Some Hydrodynamic, Heat Transfer and Drying Characteristics, In: A.S. Mujumdar (Ed.), *Drying of Solids*, Oxford and IBH Publishing Company, New Delhi, India, 65-85 (1992).
4. M. Kalwar, T. Kudra, G.S.V. Raghavan, and A. S. Mujumdar, "Drying of grains in a drafted two dimensional spouted bed", *J. Food Process Engineering* , 13, 321-332 (1991).
5. M. Kalwar and G.V.S. Raghavan, "Batch drying of shelled corn in two-dimensional spouted beds with draft plates", *Drying Technology*, 11, 339-354 (1993).
6. M. Abid, R. Gibert, and C. Laguerie, " An experimental and theoretical analysis of the mechanisms of heat and mass transfer during the drying of corn grain in a fluidized bed", *Int. Chem. Eng.*, 30, 632-642 (1990).
7. M. Hemati, M. Mourad, D. Steinmetz and C. Laguerie, "Continuous and intermittent drying of maize on a flotation fluidized bed", *Fluidization VII, Engineering Foundation for International Fluidization Conference*, Australia, (1992).
8. D. Kunni and O. Levenspiel, *Fluidization Engineering*, 2nd ed., Butterworth-Heinemann, Boston, MA (1991).
9. O. Uemaki and M. Kugo, "Heat transfer in spouted beds", *Kagaku Kogaku*, 31, 348 (1967).
10. A. Kmiec, "Simultaneous heat and mass transfer in spouted beds", *Can. J. Chem. Eng.*, 53, 18-24 (1975).

11. T. Kudra, A. S. Mujumdar, and G. S. V. Raghavan, "Gas-to-particle heat transfer in two-dimentional spouted beds", *Int. Comm. Heat Mass Transfer*, 16, 731-741 (1989).
12. A. Jezouska, "Kinetics of drying in cyclically shifted spouted bed", *Drying Technology*, 11, 319-337 (1993).
13. Q. Zhang and J. Litchfield, "An optimization of intermittent corn drying in a laboratory scale thin layer dryer", *Drying Technology*, 9, 383-395, (1991).
14. Raghavan, Drying of Agricultural Products, Chapter 19 in: A.S. Mujumdar (Ed.), *Handbook of Industrial Drying*, 2nd ed., Marcel Dekker, Inc., New York (1995).

Chapter 6

Mathematical Model for Continuous and Intermittent Drying

6.1 Introduction

This chapter provides an analysis of the heat and mass transfer mechanisms during the drying of grains in the RJSB. The overall macroscopic balances and the diffusion-based internal transport equations together with published empirical relations have been utilized to establish the governing equations. Both continuous and time-dependent spouting/heating schemes have been simulated. The model predictions are compared with experimental drying data of yellow dent corn.

The first attempt to model conventional spouted-bed (CSB) dryers goes back to 1960 when Becker and Sallans [1] developed a model to simulate the drying of wheat in a continuous, well-mixed, isothermal CSB. Assuming thermal equilibrium between the bed particles and the exit air and constant surface moisture content, the liquid diffusion equation is solved assuming a constant moisture diffusion coefficient.

From overall energy and mass balances, Becker and Isaacson [2] extended the above analysis to well-stirred batch and continuous moving-bed dryers. While Brunello et al. [3] noted that liquid diffusion did not correlate with their drying data for barley malt in a

batch CSB. Instead, they developed a semiempirical model based on a semipermeable membrane concept.

Viswanathan et al. [4-6] investigated the dynamics of both batch and continuous (start-up period) spouted bed dryers. Analytical expressions are presented for the time required to reach steady state, the solids moisture content, and temperature at steady state which are useful for control of these dryers.

Zuritz and Singh [7] improved Becker and Isaacson [2] analysis to describe the batch drying of rough rice by relating the equilibrium surface moisture content to the changing outlet air humidity by an empirical moisture content equation developed by the authors. Instead of using a constant average value, they used a semi-theoretical equation for the heat desorption-vaporization as a function of temperature and moisture content.

In an attempt to optimize the performance of both continuous spouted and spout-fluidized beds for grain drying, Passos et al. [8] combined Becker and Sallans' model [1], Viswanathan's model [6], and semiempirical correlations available in the literature as well as information obtained in the authors' laboratory to describe the aerodynamic parameters. The results are presented in terms of the drying efficiency, dryer size, energy consumption, and air handling requirements for different cereal grains.

In a recent study, Zahed and Epstein [9,10] refined Zuritz and Singh [7] analysis by using empirical equations relating the moisture diffusivity to temperature and moisture content for three cereal grains. The model was also extended to predict product temperature and moisture content for continuous spouted bed drying and the agreement with literature data was good especially under the assumption of isothermicity and imperfect mixing in the spouted bed.

A close examination of the previous theoretical studies reveals that two assumptions have been made in order to simplify the analysis. First, it is assumed that the spouted bed is deep enough to assure thermal equilibrium between the particles and the air leaving the bed. The second assumptions is based on the fact that temperature gradients inside the particles can be neglected. With these assumptions, there is no need for a single particle heat transfer equation and the exit air temperature is taken to be equal to the bed temperature in the overall energy balance. In addition, these studies used constant thermal and physical properties for both solid material and air-water system. This is at odds with the physical reality that particle thermophysical properties are functions of moisture content and/or temperature and air-water system properties are affected by temperature.

The above mentioned simplifications are not employed in the present model. This follows from the results obtained in our experimental study in which the exit air temperature was found to be higher than or equal to the bed temperature and hence thermal equilibrium was not attained especially in the first hour of drying. Furthermore, the model will be extended to include different periodic boundary conditions.

The objectives of this chapter are:

- To develop a general model for the batch drying of grains in the rotating jet spouted bed (RJSB).
- To compare the model predictions with experimental data obtained for drying of yellow dent corn using both continuous and intermittent spouting-heating schemes.
- To explore, by simulation, the feasibility of using continuous spouting air with different heating schemes, e.g., on/off, sinusoidal, and saw tooth.
- To study the effect of the operating parameters on average particle moisture content, particle surface temperature, and moisture and temperature profiles inside the particle.

6.2 Development of the Model

Assumptions

The following assumptions are made in the model:

1. The corn kernels are uniform in size, homogeneous, and can be approximated as isotropic spheres.
2. The grains are perfectly mixed such that all particles within the bed are at the same temperature and have the same moisture content at any instant during the drying process.
3. The diffusional resistance to moisture transport inside the particle significantly exceeds the diffusional resistance of the gas-layer surrounding the particle during the removal of moisture from the surface to the ambient medium. For the RJSB this assumptions implies that the diffusional time scale in the kernel is much longer than the period of rotation of the spout.
4. Conduction of heat and moisture between bed particles is negligible.
5. Heat losses are negligible.
6. Particle shrinkage is negligible

With the aforementioned assumptions, the equations governing the coupled heat and mass transfer mechanisms for both equipment and material are derived as follows:

Macroscopic Balances:

The macroscopic balances on the gas and solid phases in RJSB dryer (Fig. 6.1) are performed using the conservation law:

$$\begin{pmatrix}\textit{rate of mass}\\ \textit{or energy in}\end{pmatrix}-\begin{pmatrix}\textit{rate of mass}\\ \textit{or energy out}\end{pmatrix}=\begin{pmatrix}\textit{rate of mass or}\\ \textit{energy accumulation}\end{pmatrix} \qquad (6.1)$$

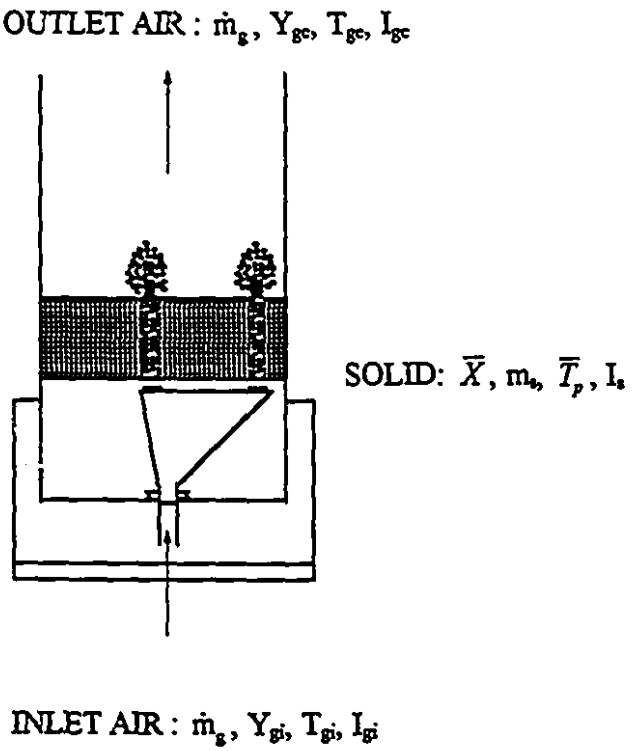

Figure 6.1 Schematic of a batch RJSB dryer.

Solid Phase

The mass balance in the solid phase is given by

$$-\dot{m}_w = m_s \frac{dX}{dt} \quad . \tag{6.2}$$

The corresponding energy balance can be written as

$$Q - \dot{m}_w I_v = m_s \frac{dI_s}{dt} \tag{6.3}$$

where

$$I_s = c_{ps}\left(\overline{T}_p - T_p^\circ\right) + \overline{X} c_{pw}\left(\overline{T}_p - T_p^\circ\right) \tag{6.4}$$

and hence

$$\frac{dI_s}{dt} = \left(c_{ps} + \overline{X} c_{pw}\right)\frac{d\overline{T}_p}{dt} + I_w \frac{d\overline{X}}{dt} \tag{6.5}$$

in which

$$I_w = c_{pw}\left(\overline{T}_p - T_p^\circ\right). \tag{6.6}$$

Substituting equations (6.2) and (6.5) into equation (6.3) yields

$$Q + m_s I_v \frac{d\overline{X}}{dt} = m_s\left(c_{ps} + \overline{X} c_{pw}\right)\frac{d\overline{T}_p}{dt} + m_s I_w \frac{d\overline{X}}{dt} \tag{6.7}$$

or

$$Q + m_s \Delta \overline{H}_{d-v} \frac{d\overline{X}}{dt} = m_s \left(c_{ps} + \overline{X} c_{pw} \right) \frac{d\overline{T}_p}{dt}. \tag{6.8}$$

Gas Phase

Assuming that the terms involving the rate of change of the humidity and the temperature of the gas with time are negligible compared to the corresponding convective terms, the mass and energy balances in the gas phase are:

$$\dot{m}_g Y_{gi} + \dot{m}_w - \dot{m}_g Y_{ge} = 0. \tag{6.9}$$

Introducing equation (6.2) into equation (6.9) gives

$$\dot{m}_g \left(Y_{ge} - Y_{gi} \right) = -m_s \frac{d\overline{X}}{dt}. \tag{6.10}$$

The corresponding energy balance equation is

$$\dot{m}_g I_{gi} + \dot{m}_w I_w - \dot{m}_g I_{ge} - Q = 0 \tag{6.11}$$

Substituting equation (6.9) into equation (6.11) yields

$$\dot{m}_g I_{gi} + \dot{m}_g (Y_{ge} - Y_{gi}) I_w - \dot{m}_g I_{ge} - Q = 0 \tag{6.12}$$

where

$$I_g = c_{pg}\left(T_g - T_g^o\right) + Y_g\left[\lambda_o + c_{pv}\left(T_g - T_g^o\right)\right] \tag{6.13}$$

and

$$I_v = \lambda_o + c_{pv}\left(T_g - T_g^o\right) \tag{6.14}$$

Combining equations (6.12), (6.13) and (6.14) one obtains

$$\dot{m}_g\left(c_{pg} + c_{pv}Y_{gi}\right)\left(T_{gi} - T_{ge}\right) = Q \tag{6.15}$$

Substituting equation (6.15) into equation (6.8) gives

$$\dot{m}_g\left(c_{pg} + c_{pv}Y_{gi}\right)\left(T_{gi} - T_{ge}\right) - m_s\Delta\overline{H}_{d-v}\frac{d\overline{X}}{dt} = m_s\left(c_{ps} + \overline{X}c_{pw}\right)\frac{d\overline{T}_p}{dt}. \tag{6.16}$$

Equation (6.16) expresses the exit gas temperature (i.e., T_{ge}) as a function of the unknown quantities $\overline{X}$, $\frac{d\overline{X}}{dt}$, $\frac{d\overline{T}_p}{dt}$, $\Delta\overline{H}_{d-v}$. Expressions for each of these unknown variables are developed below.

Drying and Thermal Kinetics of a Single Particle

For a differential control volume of the particle, the mass and energy transport equations are:

$$\rho_s\frac{\partial X}{\partial t} = -\vec{\nabla}.\vec{n}_w; \tag{6.17}$$

$$\rho_s c_{ps} \frac{\partial T}{\partial t} = -\bar{\nabla}.\bar{q}. \tag{6.18}$$

where $\vec{n}_w$ is the diffusion mass flux and $\bar{q}$ is the heat flux.

Generally diffusion mass flux is related not only to moisture content gradient, but also to the temperature gradient (thermodiffusion) [11,12]. Whilst the heat flux is related to the temperature gradient and, although weakly, to the moisture gradient (Dufour effect) [11-13]. However, both thermodiffusion and Dufour effects are usually insignificant compared to concentration gradient driven mass diffusion during grain drying at normal conditions [14-16]. We can, therefore, write the mass and heat fluxes as

$$\vec{n}_w = -\rho_s \mathcal{D} \bar{\nabla} X; \tag{6.19}$$

$$\bar{q} = -k_{ws} \bar{\nabla} T. \tag{6.20}$$

Combining equations (6.17) - (6.20), the transient evolution of moisture content and temperature in a single particle can be written as follows

$$\frac{\partial X}{\partial t} = \bar{\nabla}.\left(\mathcal{D} \bar{\nabla} X\right); \tag{6.21}$$

$$\rho_s c_{pws} \frac{\partial T}{\partial t} = \bar{\nabla}.\left(k_{ws} \bar{\nabla} T\right). \tag{6.22}$$

For spherical, unidimensional (radial) heat and mass diffusion, equations (6.21) and (6.22) can be written as follows

$$\frac{\partial X}{\partial t} = \frac{1}{r^2} \frac{\partial}{\partial r}\left(r^2 \mathcal{D} \frac{\partial X}{\partial r}\right); \tag{6.23}$$

$$\rho_s c_{pws} \frac{\partial T}{\partial t} = \frac{1}{r^2} \frac{\partial}{\partial r} \left(r^2 k_{ws} \frac{\partial T}{\partial r} \right). \qquad (6.24)$$

$\mathcal{D}$ and k_{ws} represent the effective moisture diffusivity and the effective thermal conductivity, respectively.

Initial and boundary conditions

The initial profiles of moisture content and temperature in the particle are assumed to be uniform:

$$@\ t = 0 \ and \ 0 \le r \le R_{pe}, \quad X = X_o \ and \ T = T_{po} \ . \qquad (6.25)$$

Because of symmetry, the moisture content and temperature gradients at the center of the spherically assumed particle are zero:

$$@\ t \ge 0 \ and \ r = 0, \quad \frac{\partial X}{\partial r} = 0 \ and \ \frac{\partial T}{\partial r} = 0 \ . \qquad (6.26)$$

Various types of surface boundary conditions representing different spouting and heating patterns are considered :

I. Continuous spouting and heating :

The mass transfer surface boundary condition is written based on the assumption that the surface of the particle is in moisture content equilibrium with the surrounding gas [7,9]:

$$@\ r = R_{pe},\quad -\mathcal{D}A_p\rho_s\frac{\partial X}{\partial r} = -\frac{m_s}{n_p}\frac{d\overline{X}}{dt}. \tag{6.27}$$

where n_p, the number of bed particles is given by

$$n_p = \frac{m_s}{\rho_s V_p}. \tag{6.28}$$

Combining equations (6.10), (6.27) and (6.28), the moisture transfer surface boundary condition is finally written as follows

$$@\ r = R_{pe},\quad -\frac{\partial X}{\partial r} = \frac{V_p\dot{m}_g}{m_s\mathcal{D}A_p}\left(Y_g - Y_{gi}\right). \tag{6.29}$$

The amount of heat supplied to the particle surface equals that which penetrates by conduction and that spent for moisture desorption-vaporization,

$$k_{ws}\frac{\partial T}{\partial r} = \overline{h}_p\left(T_{gi} - T\right) - n_w\Delta H_{d-v}. \tag{6.30}$$

The mass flux from a single particle, n_w, is related to the total bed mass rate of evaporation by the following expression

$$n_w = \frac{\dot{m}_w}{n_p A_p}. \tag{6.31}$$

Substituting equations (6.10), (6.27), (6.29), (6.31) into equation (6.30), the heat transfer surface boundary condition is written as follows:

$$@\ r = R_{pe}:\ k_{ws}\frac{\partial T}{\partial r} = \bar{h}_p\left(T_{gi} - T\right) - \frac{\dot{m}_s \rho_s V_p}{m_s A_p}\Delta H_{d-v}\left(Y_s - Y_{gi}\right). \qquad (6.32)$$

A correlation developed by Kmiec [17] for conventional spouted beds is used to estimate the overall bed heat transfer coefficient, $\bar{h}_p$,

$$Nu = \frac{\bar{h}_p d}{k_g} = 0.897\, Re^{0.464}\, Pr^{1/3}\, Ar^{0.116}\left(H/d\right)^{-1.19}\varphi^{2.261}. \qquad (6.33)$$

where d is the geometric average from the diameters of adjacent screens and φ is the particle shape factor. $\bar{h}_p$ represents a spouting cycle-average heat transfer coefficient during which the particle travels in the active and static zones.

II. Continuous spouting-sinusoidal heating (fig. 6.2(a))

The surface boundary heat and mass transfer conditions are still governed by equations (6.29) and (6.32) with the inlet air temperature described by

$$T_{gi} = T_m + T_a \sin\left(2\pi t/\tau\right). \qquad (6.34)$$

where T_m and T_a are the mean and amplitude of variation of inlet air temperature and τ is the period (i.e., time for one cycle).

III. Intermittent or on/off spouting and heating (figure 6.2(b))

In this drying pattern, the spouting air flowrate is periodically interrupted to allow for a rest or tempering period. In the rest periods, the particle is assumed to be sealed [18-21]:

$$@\ \tau n \le t \le \tau(n+\alpha): \quad \frac{\partial X}{\partial r} \text{ and } \frac{\partial T}{\partial r} \text{ are given by eqns. (6.29) and (6.32)}$$
$$@\ \tau(n+\alpha) \le t \le \tau(n+1): \quad \frac{\partial X}{\partial r},\ \frac{\partial T}{\partial r} = 0 \tag{6.35}$$

where τ is the cycle period, α is the intermittency (fraction of cycle when heating is on), and n is the number of heating cycles done (n = 0,1,2, ...).

IV. Continuous spouting- on/off heating (figure 6.2(c))

Spouting air is continuous while heating is periodically on and off. T_{gi} in equations (6.29) and (6.32) are given by

$$@\ \tau n \le t \le \tau(n+\alpha): \quad T_{gi} = T_h$$
$$@\ \tau(n+\alpha) \le t \le \tau(n+1): \quad T_{gi} = T_c \tag{6.36}$$

where T_h and T_c denote hot and cool temperatures, respectively,

V. Continuous spouting- saw tooth heating (figure 6.2(d))

The inlet air temperature in equations (6.29) and (6.32) rises linearly from T_c to T_h and drops back to T_c at the end of the cycle:

$$T_{gi} = T_c + (T_h - T_c)(t - n\tau)/\tau. \tag{6.37}$$

The average particle temperature, moisture content, and enthalpy of desorption-vaporization are obtained by integrating over the particle volume:

$$\overline{T}_p(t) = \frac{4\pi}{V_p}\int_0^{R_p} r^2 T(r,t)dr\,. \tag{6.38}$$

$$\overline{X}(t) = \frac{4\pi}{V_p}\int_0^{R_p} r^2 X(r,t)dr\,. \tag{6.39}$$

$$\Delta\overline{H}_{d-v}(t) = \frac{4\pi}{V_p}\int_0^{R_p} r^2 \Delta H_{d-v}\{T(r,t), X(r,t)\}dr\,. \tag{6.40}$$

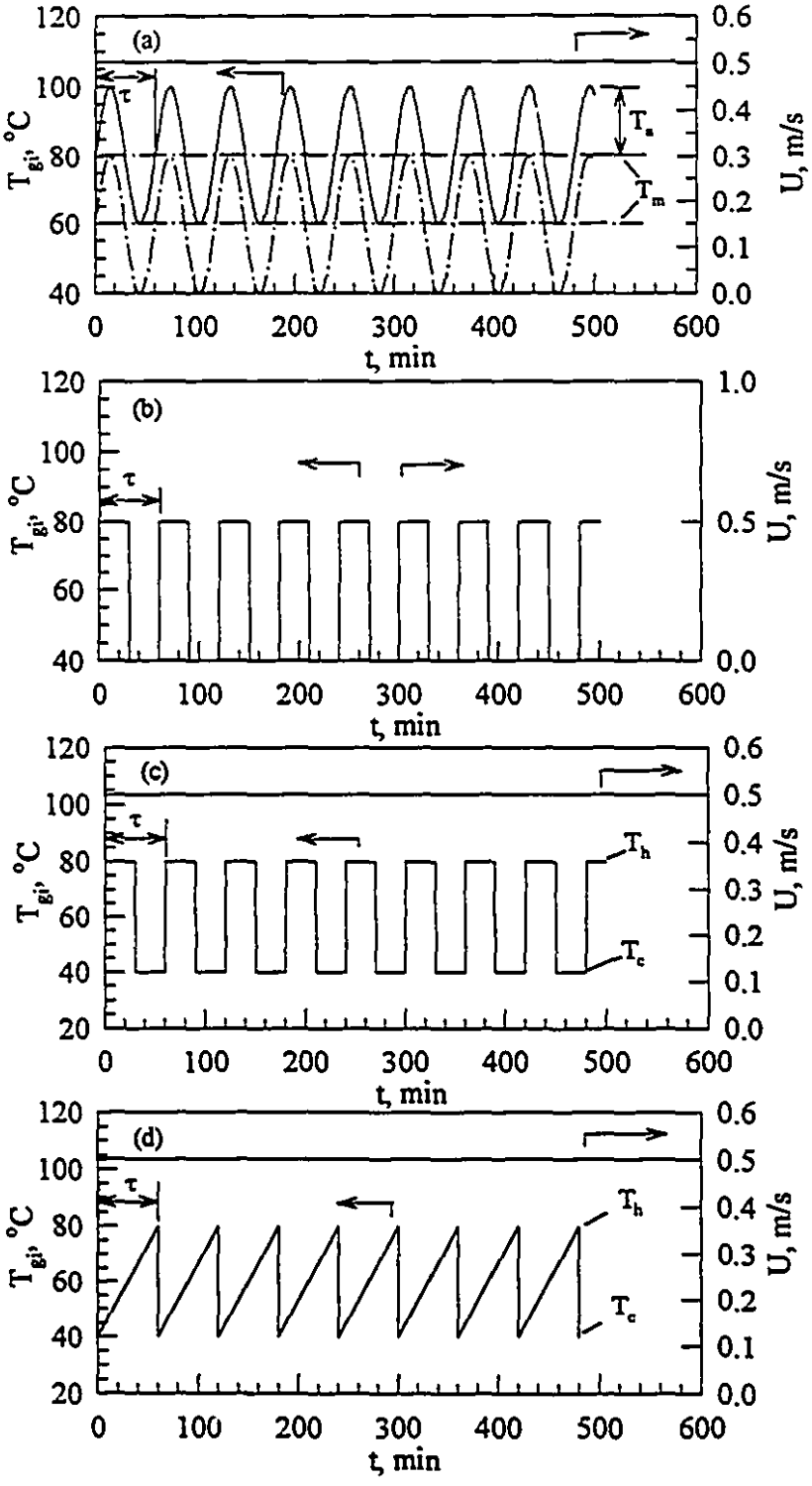

Figure 6.2: Spouting and heating schemes. (a) continuous spouting-sinusoidal heating, (b) on/off spouting-heating, (c) continuous spouting-on/off heating, (d) continuous spouting-saw tooth heating.

Transport and Equilibrium Relationships

Expressions for the transport and thermodynamic equations obtained from literature equations for yellow dent corn and air-water system are listed in Tables 6.1 and 6.2.

Table 6.1: Transport and Equilibrium Properties of Yellow Dent Corn

Eqn. #	Property	Expression	Reference
(6.41)	$\mathcal{D}$	$\mathcal{D} = 4.203\times10^{-8}\exp\left[(-2513/T_{abs})+(0.045T_{abs}-5.485)X\right]$	[22]
(6.42)	ΔH_{v-d}	$\Delta H_{d-v} = R_v T_{abs}^2\left[(6887/T_{abs}^2)-(5.31/T_{abs})+(1-RH)c_1(100X_e)^{c_2}/RH\right]$	[9]
(6.43)	RH	$RH = 1-\exp\left[-c_1(100X_e)^{c_2}(T+c_3)\right]$ $c_1 = 8.6541\times10^{-5}$, $c_2 = 1.8634$, $c_3 = 49.81$ *in (6.42) & (6.43)*	[23]
(6.44)	c_{pws}	$c_{pws} = 1.465\times10^3 + 3.56\times10^3\left(X/(1+X)\right)$	[24,25]
(6.45)	k_{ws}	$k_{ws} = 0.1409 + 0.112\left(X/(1+X)\right)$	[24,25]

Table 6.2: Thermodynamic and Transport Properties of Air and Water Systems [26,27].

Eqn. #	Property	Expression
(6.46)	P_v	$P_v = 100\exp\left[27.0214-(6887/T_{abs})-5.31\ln(T_{abs}/273.16)\right]$
(6.47)	Y	$Y = 0.622\,RH\,P_v/(P-RH\,P_v)$
(6.48)	c_{pg}	$c_{pg} = 1.00926\times10^3 - 4.0403\times10^{-2}T + 6.1759\times10^{-4}T^2 - 4.097\times10^{-7}T^3$
(6.49)	k_g	$k_g = 2.425\times10^{-2} + 7.889\times10^{-5}T - 1.790\times10^{-8}T^2 - 8.570\times10^{-12}T^3$
(6.50)	ρ_g	$\rho_g = PM_g/(RT_{abs})$
(6.51)	μ_g	$\mu_g = 1.691\times10^{-5} + 4.984\times10^{-8}T - 3.187\times10^{-11}T^2 + 1.319\times10^{-14}T^3$
(6.52)	c_{pv}	$c_{pv} = 1.883 - 1.6737\times10^{-4}T + 8.4386\times10^{-7}T^2 - 2.6966\times10^{-10}T^3$
(6.53)	c_{pw}	$c_{pw} = 2.8223 + 1.1828\times10^{-2}T - 3.5043\times10^{-5}T^2 + 3.601\times10^{-8}T^3$

6.3 Numerical Solution

The governing equations with their initial and boundary conditions are solved using the following numerical procedure steps:

1. Discretization of the spatial variables according to the method of lines, Sincovec and Madsen [28-30]:

Equations (6.23) and (6.24) can be written in the following general form

$$\frac{\partial u_j}{\partial t} = f_j\left(\frac{1}{r^2}\frac{\partial}{\partial r}\left(r^2 \mathcal{D}_j \frac{\partial u_j}{\partial r}\right)\right). \tag{6.54}$$

where j =1,2 representing X and T.

The boundary conditions (equations 6.26, 6.29, and 6.32) are of the form

$$\alpha_j u_j + \beta_j \frac{\partial u_j}{\partial r} = \gamma_j \,. \tag{6.55}$$

Using centered difference approximations, the discretized equations are:

$$\frac{1}{r^2}\frac{\partial}{\partial r}\left(r^2 \mathcal{D}_j(u_j)\frac{\partial u_j(t,r)}{\partial r}\right)$$

$$\approx \frac{3}{\left(r_{i+1/2}\right)^3 - \left(r_{i-1/2}\right)^3}\left[\left(r_{i+1/2}\right)^2 \mathcal{D}_{j,i+1/2}\left(\frac{u_{j,i+1} - u_{j,i}}{h_i}\right) - \left(r_{i-1/2}\right)^2 \mathcal{D}_{j,i-1/2}\left(\frac{u_{j,i} - u_{j,i-1}}{h_{i-1}}\right)\right].$$

(6.56)

where

$$r_{i\pm1/2} = \frac{r_{i\pm1} + r_i}{2}$$

$$\mathcal{D}_{j,i\pm1/2} = \mathcal{D}_j\left(r_{i\pm1/2}, \mathbf{u}_{i\pm1/2}\right)$$

$$\mathbf{u}_{i\pm1/2} = \left(\frac{u_{1,i\pm1} + u_{1,i}}{2}, \frac{u_{2,i\pm1} + u_{2,i}}{2}\right)$$

$$h_i = r_{i+1} - r_i$$

Boundary conditions:

$$at\ r = r_1 :\ u_j(t,r) \approx u_{j,1}. \tag{6.57}$$

$$\frac{\partial u_j(t,r)}{\partial r} \approx \left\{ \begin{array}{l} \dfrac{u_{j,2} - u_{j,1}}{h_1} \quad \text{if } \beta_j = 0 \\ \dfrac{\gamma_j - \alpha_j u_{j,1}}{\beta_j} \quad \text{if } \beta_j \neq 0 \end{array} \right\}. \tag{6.58}$$

$$\frac{1}{r^2}\frac{\partial}{\partial r}\left(r^2 \mathcal{D}_j(r,\mathbf{u})\frac{\partial u_j(t,r)}{\partial r}\right)$$

$$\approx \left\{ \begin{array}{l} \dfrac{3}{r_{i+1/2}^3 - r_1^3}\left[\left(r_{i+1/2}^2 \mathcal{D}_{j,i+1/2} - r_1^2 \mathcal{D}_{j,1}\right)\left(\dfrac{u_{j,2} - u_{j,1}}{h_1}\right)\right] \quad \text{if } \beta_j = 0 \\ \dfrac{3}{r_{i+1/2}^3 - r_1^3}\left[r_{i+1/2}^2 \mathcal{D}_{j,i+1/2}\left(\dfrac{u_{j,2} - u_{j,1}}{h_1}\right) - r_1^2 \mathcal{D}_{j,1}\left(\dfrac{\gamma_j - \alpha_j u_{j,1}}{\beta_j}\right) \text{if } \beta_j \neq 0\right] \end{array} \right\}. \tag{6.59}$$

a uniform mesh of 40 points was used in the spatial discretization.

2. The resulting semidiscrete system of nonlinear ordinary differential equations is integrated with respect to time using the software package LSODE [31]. This routine contains a set of integration algorithms based on the variable-order, multi-step, fully-

implicit Gear's method [32] for stiff and nonstiff problems. Time intervals of 10 s and absolute time integration error tolerance of 1×10^{-6} were used in the computation.

3. To obtain $\overline{X}, \overline{T}_p$, *and* $\Delta\overline{H}_{d\text{-}v}$, the integral equations ((6.38)-(6.40)) are evaluated using the Simpson numerical integration technique.

4. T_{gc} is calculated using equation (6.16) after making a simple finite-difference approximation for $\frac{d\overline{X}}{dt}$ and $\frac{d\overline{T}_p}{dt}$.

Figure 6.3 shows the flow diagram of the computer program. It indicates the main subprograms, their interrelations, and their functions.

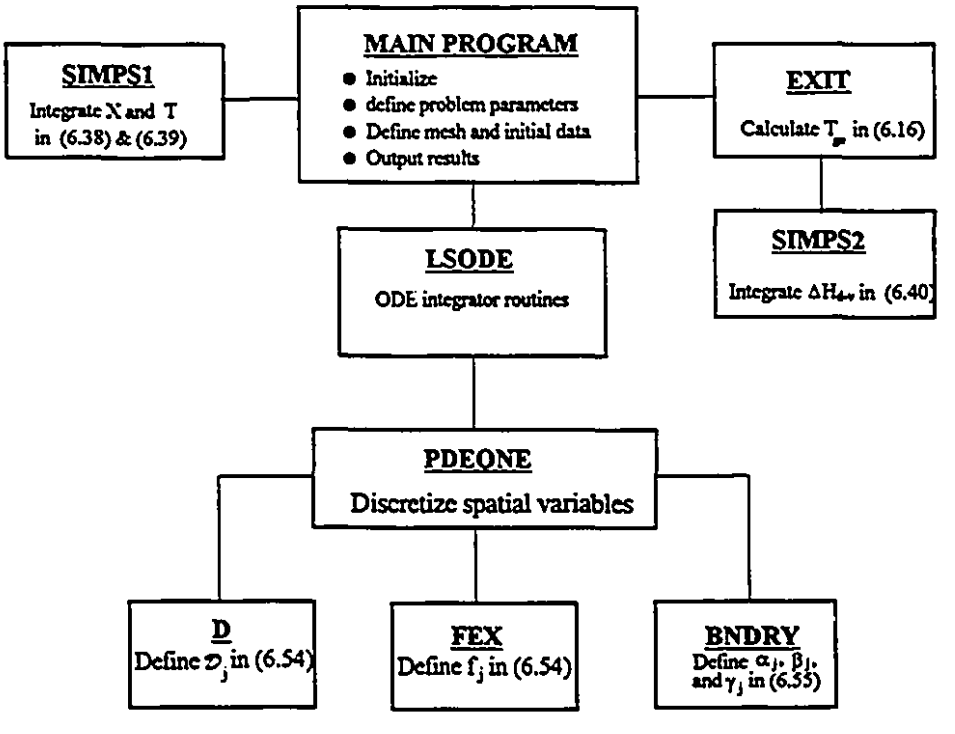

Figure 6.3 Flow diagram of the computer program.

6.4 Results and Discussion

In order to assess the accuracy of the model predictions, the numerical solutions are compared with experimental data of corn drying in the rotating jet spouted bed using continuous and intermittent spouting-heating patterns. These correspond to surface boundary condition patterns I and III, respectively. Only inlet air temperature and intermittency effects are verified as other parameters showed little or no effect on the drying kinetics of slow drying materials such as agricultural grains within the range tested.

The relevant fixed experimental parameters used in the model validation are listed in the following table:

Table 6.3: Values of Fixed Experimental Parameters used for Model Validation

Parameter	Value	Unit
Y_{gi}	0.040 - 0.045	kg/kg
T_{po}	20 - 21	°C
m_s	12.0	kg
H	0.15	m
X_o	0.4	kg/kg
R_{pc}	4.70×10^{-3}	m
A_p	3.89×10^{-4}	m^2
V_p	4.35×10^{-7}	m^3
φ	1.4	-

6.4.1 Sensitivity of the Model to $\mathcal{D}$ and $\bar{h}_p$

Many empirical correlations are available in the literature for the estimation of mass diffusion coefficient, $\mathcal{D}$ of yellow dent corn [22,33-35]. These correlations have been developed based on experimental drying data using many different types of equipment. In the present study and based on preliminary screening simulation, the correlation proposed by Chu and Hustrulid [22] (Table 6.1) was selected to obtain an expression for the mass diffusion coefficient as a function of moisture content and temperature.

The simulation results indicated that there is a very small difference (< 0.5 %) when estimating $\mathcal{D}$ using either local or average particle temperature in both the governing mass diffusion equation (Eqn. 6.23) or the surface boundary condition equation (Eqn. 6.29). This is because of the uniform particle temperature as will be discussed later. However, estimating $\mathcal{D}$ using local or average moisture content values shows a remarkable effect on the model prediction of both the average moisture content and surface temperature as depicted in Figure 6.4. The sensitivity analysis presented in Table 6.4 reveals that the best results are obtained when $\mathcal{D}$ is calculated using the particle average moisture content. It should be noted that the method by which the moisture diffusivity correlations are developed is based on the average particle moisture content and does not take into account the non-uniform moisture profiles inside the particle which is difficult, if not impossible, to be measured experimentally.

Figure 6.5 shows the effect of the characteristic particle dimension d used in estimating $\bar{h}_p$ from equation (6.33) on model predictions of both particle moisture content and surface temperature, respectively. Four particle diameters are used in the comparison: the smaller diameter (D_{ps}), the geometric diameter (D_{pgm}), the equivolume-sphere diameter (D_{pc}), and the effective diameter ($D_p = \phi\, D_{pc}$),. Table 6.5 presents error estimates between

experimental and theoretical values for a typical drying run. The results indicate that the experimental data are best predicted when d is taken as the smaller diameter of the corn grain. This is justified by the observed fact that the kernels align themselves in the spout in such a way that the smallest diameter is normal to the flow of air. In fact, the smaller diameter was also used by Mathur and Gishler [36,37] to correlate the minimum spouting velocity of wheat particles. This clearly indicates the important effect of the flow behavior of the particles on the heat and mass transfer mechanisms in the system.

Table 6.4: Sensitivity of numerical model solution to $\mathcal{D}$ evaluation, T_{gi} = 80 °C, U = 0.514 m/s

Legends in Fig. 6.4	$\mathcal{D}$	Mean relative error in X (%)	Max. relative error in X (%)	Mean relative error in T_s (%)	Max. relative error in T_s (%)
1	$\mathcal{D}_{r=r} = f(\overline{X})$ $\mathcal{D}_{r=R_{ps}} = f(X)$	14.77	25.69	17.52	60.54
2	$\mathcal{D}_{r=r} = f(\overline{X})$ $\mathcal{D}_{r=R_{ps}} = f(\overline{X})$	5.08	12.37	3.81	15.49
3	$\mathcal{D}_{r=r} = f(X)$ $\mathcal{D}_{r=R_{ps}} = f(X)$	19.64	35.05	3.25	12.6
4	$\mathcal{D}_{r=r} = f(X)$ $\mathcal{D}_{r=R_{ps}} = f(\overline{X})$	61.26	100.00	35.07	45.4

Table 6.5: Sensitivity of numerical model solution to $\overline{h}_p$ evaluation T_{gi} = 80 °C, U = 0.514 m/s

$\overline{h}_p$	Mean relative error in X (%)	Max. relative error in X (%)	Mean relative error in T_s (%)	Max. relative error in T_s (%)
$\overline{h}_p = f(D_{ps})$	5.08	12.37	3.81	15.49
$\overline{h}_p = f(D_p)$	6.71	12.78	7.39	25.96
$\overline{h}_p = f(D_{p_{sm}})$	7.45	14.6	9.12	31.12
$\overline{h}_p = f(D_{pg})$	8.95	12.37	11.99	41.83

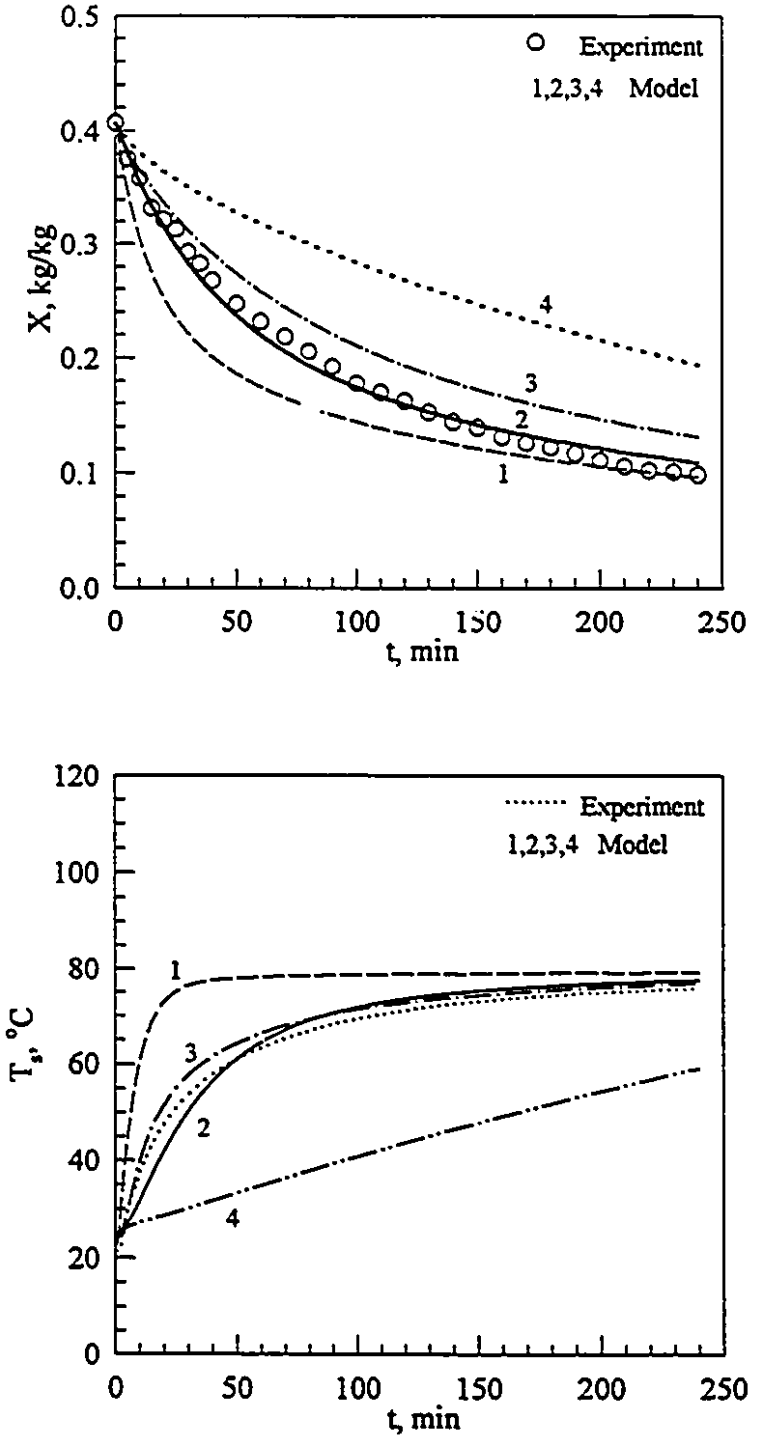

Figure 6.4: Effect of $\mathcal{D}$ evaluation on model predictions. T_{gi} = 80 °C, U = 0.514 m/s. (Legends 1,2,3,4 are described in Table 6.4)

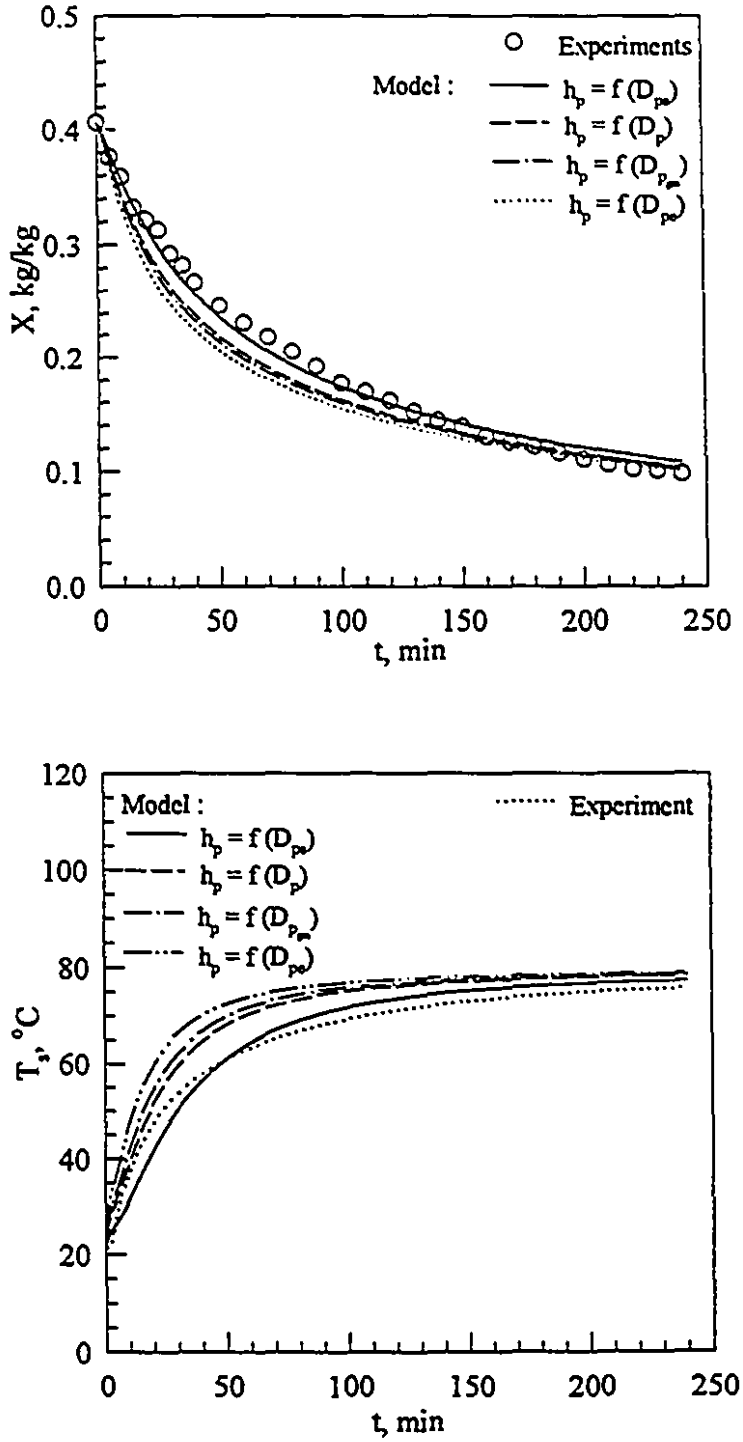

Figure 6.5: Effect of $\overline{h}_p$ evaluation on model predictions. $T_{gi} = 80\ ^{\circ}C$, U = 0.514 m/s.

6.4.2 Continuous Spouting-Heating

Figure 6.6 presents a comparison of the model predictions of the moisture content evolution with the experimental results for inlet air temperatures ranging between 60 °C and 90 °C. The results exhibit a very good match as indicated by visual comparison of the plotted data. Although curve fitting is not desirable to validate a model, error analysis performed on the curve fitted experimental data and the model solutions indicates that the mean absolute relative error is less than 5 % and the maximum absolute error is less than 11 % for all the tested data. These results witness the reliability of the model and the method by which $\mathcal{D}$ and $\bar{h}_p$ are estimated as discussed in section 6.4.1.

A test of data calculated on the basis of the computation model with experimental particle surface temperature and exit air temperature is shown in Figure 6.7. The maximum absolute deviations between the experimental and predicted values are, respectively, 16 and 13 %, while the mean relative error is less than 7 % for both particle surface and exit air temperatures. The discrepancy might be attributed to the uncertain definition and measurement of the particle surface temperature, the simplifying assumptions which are made in the development of the model (e.g., ignoring heat losses), and errors in estimating air-water system properties.

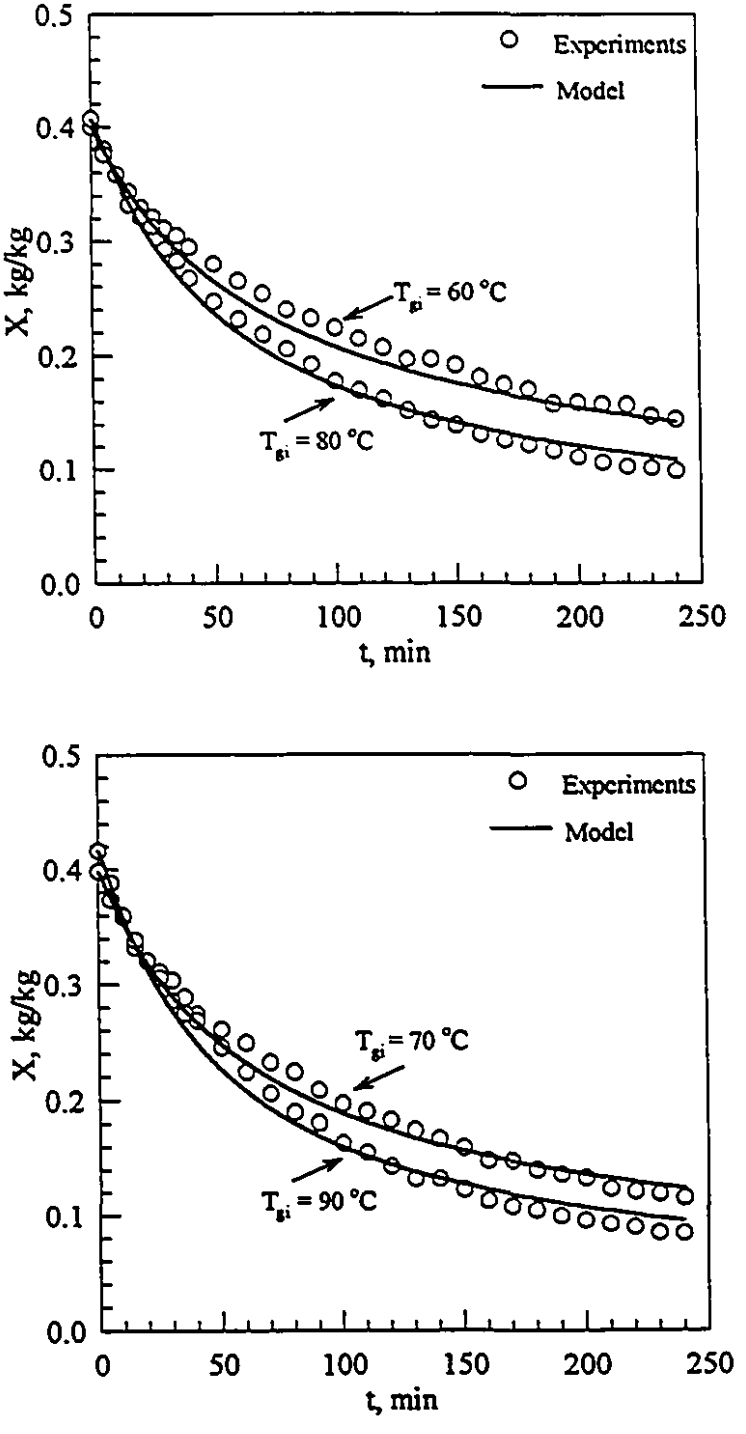

Figure 6.6: Comparison between theoretical and experimental drying curves for different inlet air temperatures. $D_n = 3$ cm, $N = 2$ rpm, $U = 0.514$ m/s.

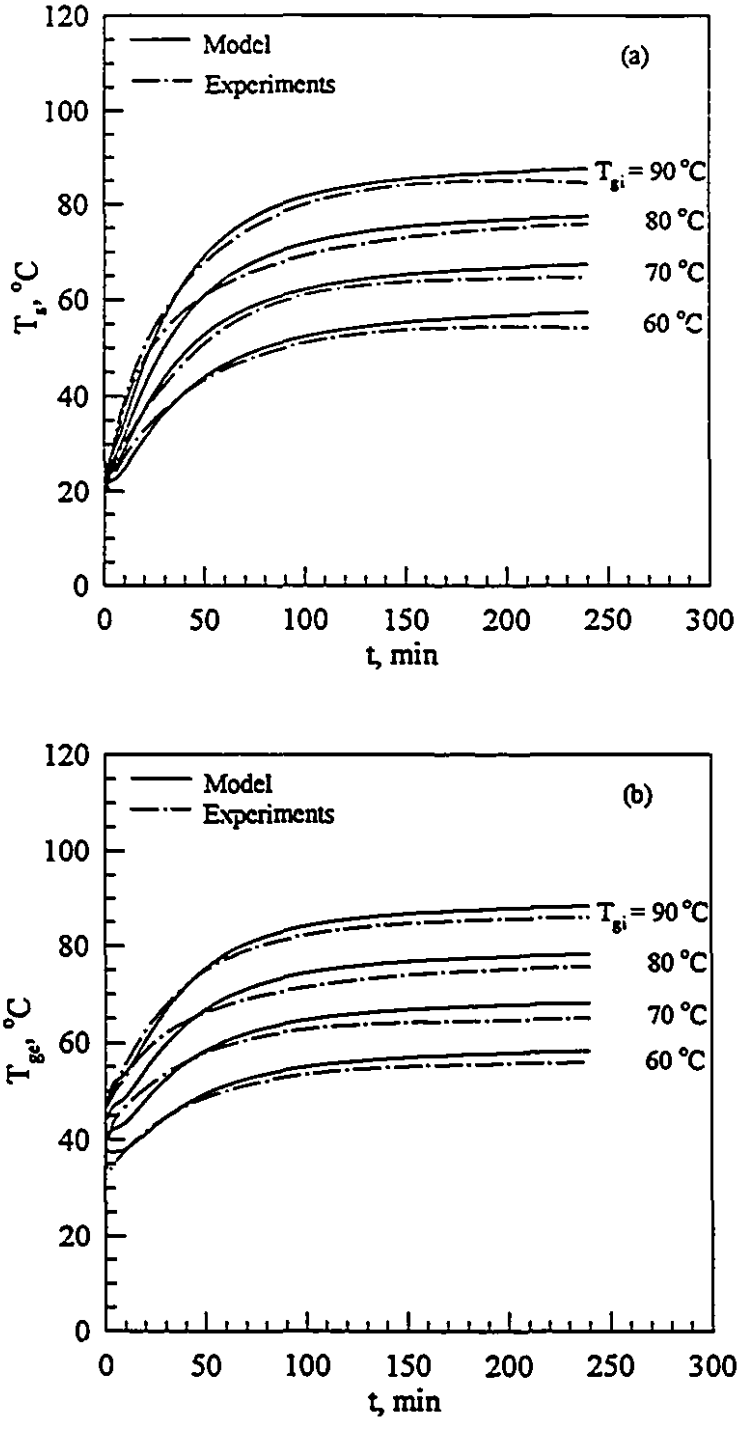

Figure 6.7: Comparison between theoretical and experimental: (a) surface temperature and (b) exit air temperature for different inlet air temperatures. D_n = 3 cm, N = 2 rpm, U = 0.514 m/s.

Numerical results of the transient moisture and temperature profiles inside the particle are shown in Figures 6.8-6.10 for different inlet air temperatures. While temperature profiles show negligible temperature gradients, moisture content profiles show the existence of relatively large concentration gradients inside the particle. This might be explained with reference to the Lewis number, Le = $\alpha_T/\mathcal{D}$ or [Luikov number, Lu = $\mathcal{D}/\alpha_T$]. The Lewis number represents the ratio of the thermal diffusivity and mass diffusivity of the material. In other words, the ratio of the relaxation rates of the mass to heat transfer potentials. During simulation runs, it was observed that Le is much greater the unity and increases with decreasing moisture content reaching a maximum value of about 1200. This means that the rate of internal heat transfer is fast compared to the rate of mass transfer.

The predicted results demonstrate high moisture concentration around the center of the particle while the surface moisture content drops gradually, but not instantaneously, to an equilibrium value with the drying air. This is also displayed in Figure 6.11 in which the surface moisture content is plotted against the drying time for different inlet air temperature. The trend proves that assuming a constant surface moisture content, based on a constant "dynamic" equilibrium moisture content [1,2], during the entire drying process is inappropriate [7,9], especially in the first 30 minutes of the drying process.

The transient temperature distribution curves (Figure 6.10) show that the temperature profiles inside the particle "linearize" after the initial heating-up period. After that, the slope of the linear temperature profiles decreases, as the center and surface temperatures approach each other and thereafter remain virtually flat. These profiles, which are calculated based on the concept of the overall bed heat transfer coefficient, confirms the hypotheses that any temperature gradients developed during the particle journey in the spouts (high heat transfer coefficients) are effectively relaxed in the static annular regions (low heat transfer coefficients). This is by virtue of the low average heat transfer Biot number, $\overline{Bi}_H = \overline{h}_p R_{pe} / k_{ms}$ (ranged between from 0.24 to 0.28 in this study)

which can be thought of as the ratio of internal to external heat transfer resistances. This implies that the air-solid interface resistance is higher than the internal heat conduction resistance of the material and therefore very small temperature gradients.

The computed results for surface mass and heat fluxes for T_{gi} varying from 60 to 90 °C are shown in Figure 6.12. The results show that as T_{gi} increases the surface heat and mass fluxes increase. Physically, increasing the inlet air temperature increases the effective thermal and mass diffusivities of the solid material. There is an initial disturbance period in the heat flux curves. This is because of the time-temperature response of the system to adjust to the new condition imposed at t = 0. After which q start to rise up reaching a peak around t = 10-15 min. The mass flux profiles also show a similar, but less pronounced, peak in this heating-up period. In this period during which the heat and mass transfer gradients (deriving forces) are still developing, the heat supplied by the inlet air is more than sufficient to evaporate the moisture which instead goes to heat the solids. As time elapses, both heat and mass fluxes drop to very low values especially after the first hour of the drying process.

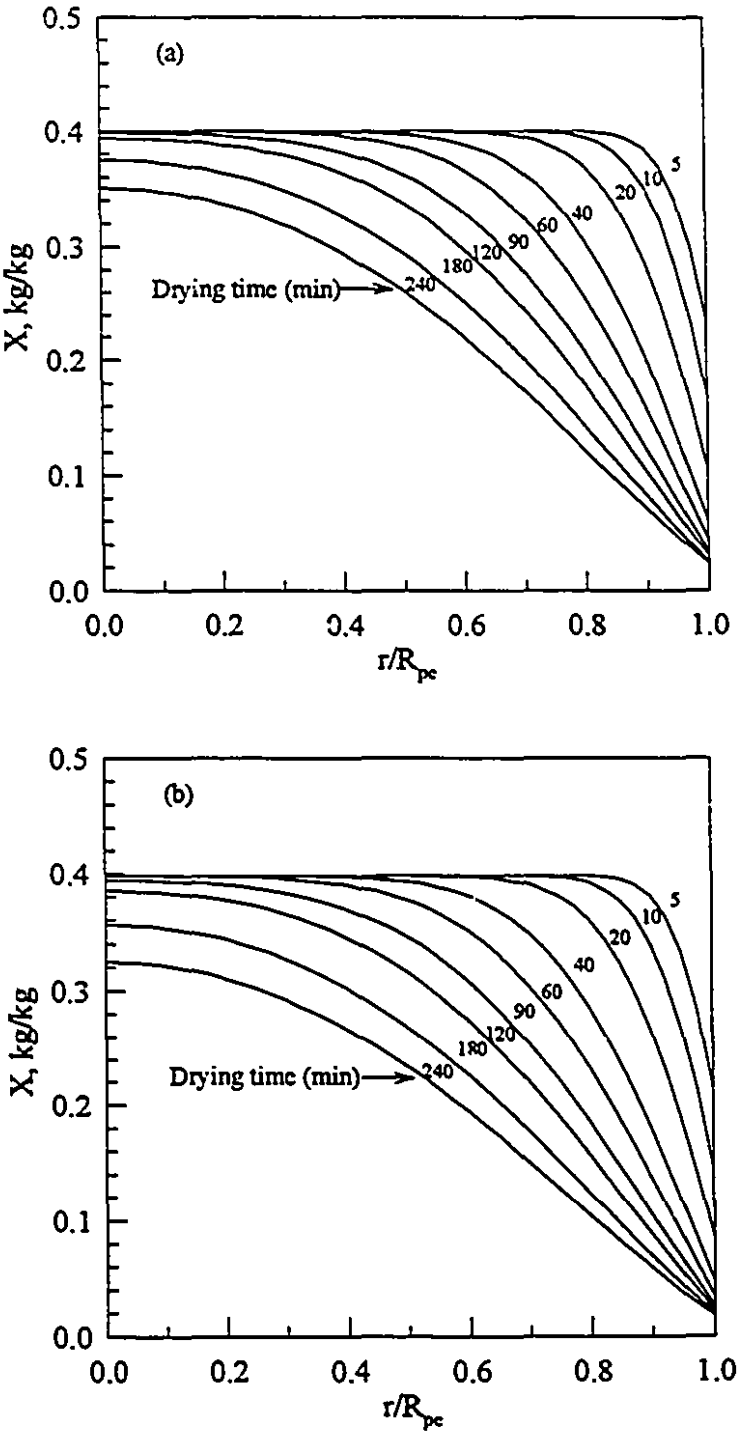

Figure 6.8: Predicted transient moisture profiles inside the corn kernel. (a) $T_{gi} = 60\ ^{\circ}C$, (b) $T_{gi} = 70\ ^{\circ}C$, $D_n = 3$ cm, N = 2 rpm, U = 0.514 m/s.

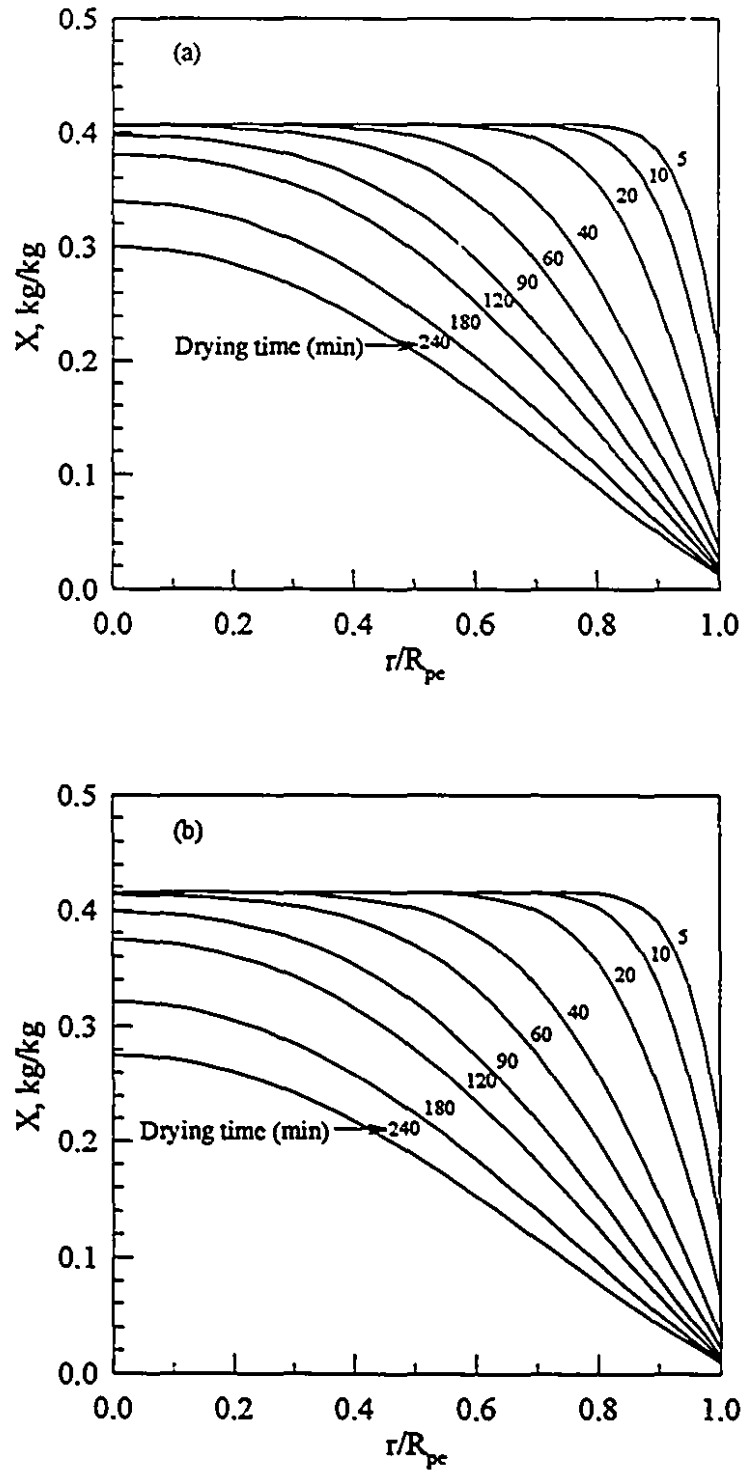

Figure 6.9: Predicted transient moisture profiles inside the corn kernel. (a) $T_{gi} = 80\ ^{\circ}C$, (b) $T_{gi} = 90\ ^{\circ}C$, $D_n = 3$ cm, $N = 2$ rpm, $U = 0.514$ m/s.

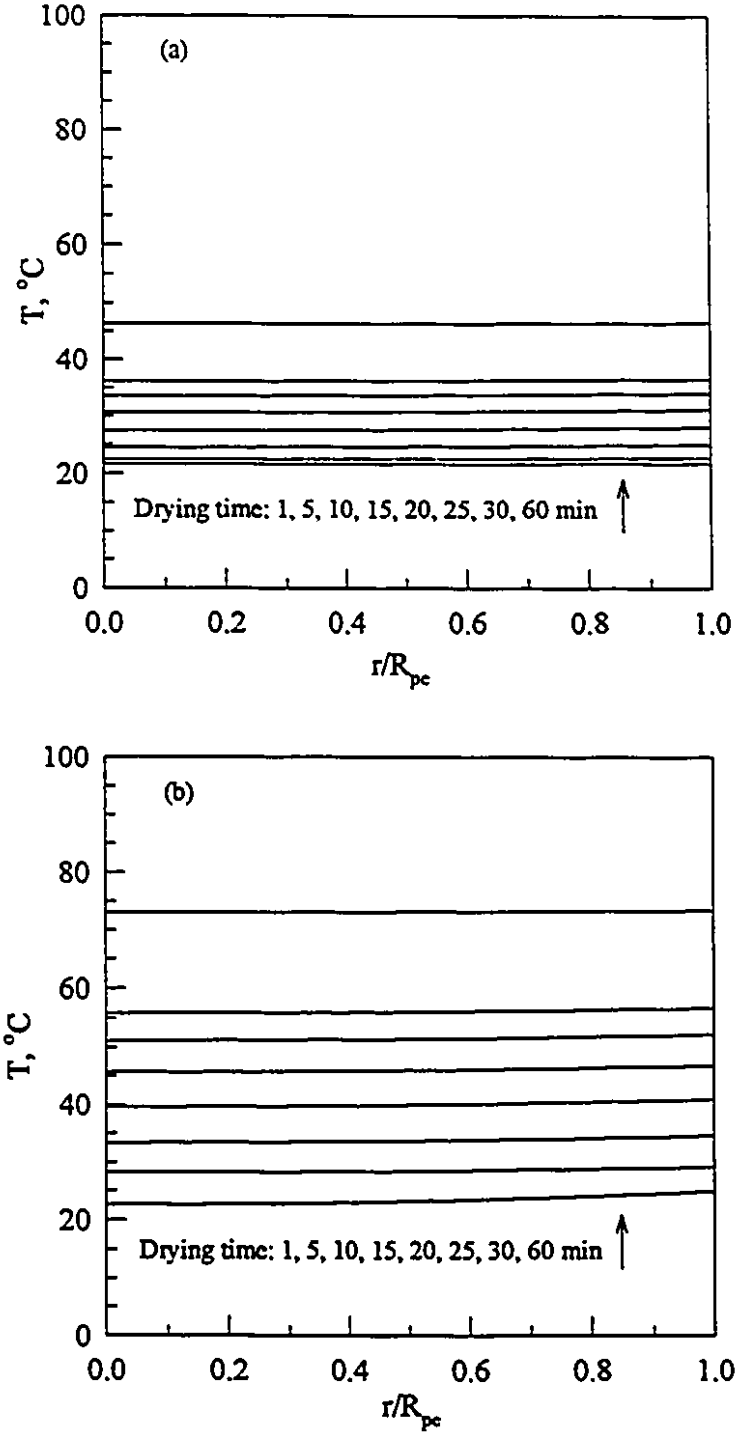

Figure 6.10: Predicted transient temperature profiles inside the corn kernel. (a) $T_{gi} = 60\ ^{\circ}C$, (b) $T_{gi} = 90\ ^{\circ}C$, $D_n = 3$ cm, $N = 2$ rpm, $U = 0.514$ m/s.

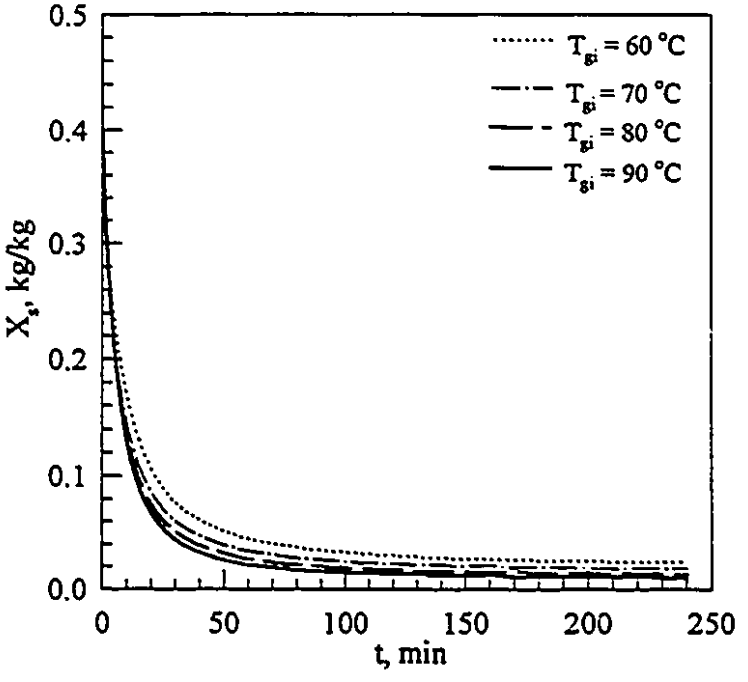

Figure 6.11: Predicted surface moisture content profiles for different inlet air temperatures. D_n = 3 cm, N = 2 rpm, U = 0.514 m/s.

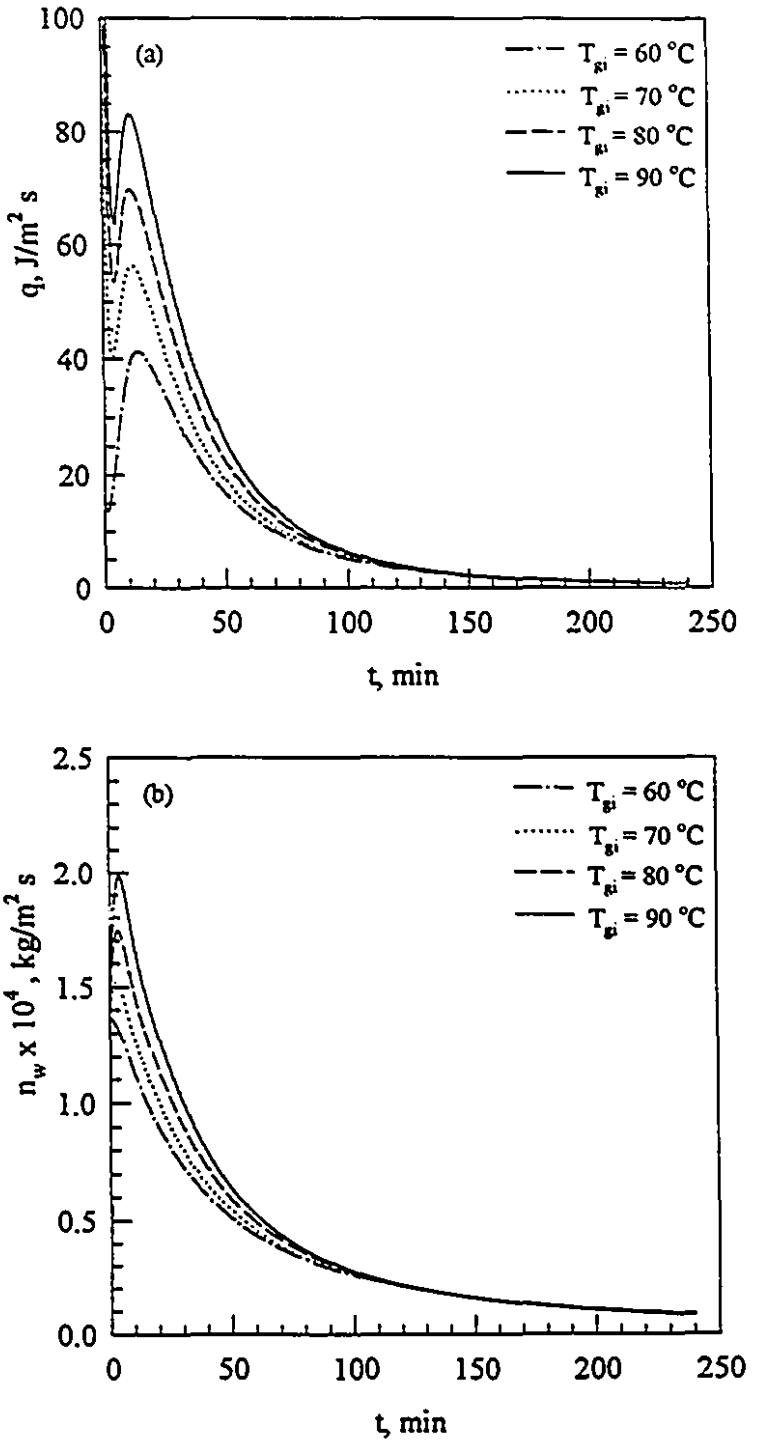

Figure 6.12: Predicted heat and mass fluxes at the corn kernel surface for different inlet air temperatures. D_n = 3 cm, N = 2 rpm, U = 0.514 m/s.

6.4.3 Intermittent or On/Off Spouting-Heating

In Figure 6.13, model predictions and experimental data are presented for the effect of intermittency, α, on the particle average moisture content evolution with time. No numerical error estimate is performed in this case to compare between the theoretical and experimental results because of the difficulty in curve fitting the periodic behavior of the drying curves. Nevertheless, the dominant agreement is clear in all cases.

Figure 6.14 shows the calculated transient behavior of the moisture content at the surface of the particle for different intermittency values. The profiles clearly demonstrate the periodic response of X_s during which it reaches a peak value at the end of a tempering or rest period and then falls down to a very small equilibrium value at the beginning of the following spouting period and thus approaches the continuous spouting/heating curve. Furthermore, the tendency is to raise the peak values with a decrease α. This suggests that long rest periods (low α) provide more time for the moisture to diffuse from the interior to the surface of the particle. This is supported by the observed moisture condensation on the surface of the particles during the experiments especially in the case of long rest periods.

The predicted and experimental results of the particle surface temperature profiles are shown in Figure 6.15 for α = 1/4, 2/3, and 1. Although the agreement between experiment and model for α = 1 (continuous spouting) is acceptable. A systematic discrepancy is observed when on/off spouting (α = 1/4, 2/3) is applied. This difference is most likely due to one or a combination of the following reasons:

1. The use of inappropriate heat transfer boundary condition at the surface of the kernel during the rest period, i.e., zero temperature gradient. This means that particle is sealed and it has a constant temperature during the off period. In reality, however, the particle looses heat and hence the temperature decreases as shown in Figure 6.15. In

the case of mass transfer boundary condition, applying a zero concentration gradient at the surface of the particle has no effect on the model prediction. This is due to the negligible drying during the rest periods. In fact, the use of zero gradients as boundary conditions was motivated by the lack of information regarding heat and mass transfer coefficients for an aggregate of particles in a static bed at no flow. In this case the value of Nusselt number (Nu) and Sherwood number (Sh) is expected to be several order of magnitudes less than 2, the value of an isolated particle [38].

2. The unreliable experimental data for the particle surface temperature. The complex and cyclic aerodynamic patterns inside the bed make it difficult to measure the actual surface temperature.
3. Neglect of heat losses from the dryer.

It is worth pointing out that both experiments and model predictions display a disturbance period at the beginning of each spouting period. In this very short period, the surface temperature suddenly drops to a low value and then starts to rise. This represents the system response to the new conditions imposed at the beginning of the on period.

Representative moisture content profiles using on/off spouting-heating scheme are shown in Figures 6.16 for α =1/4 and 1/2, i.e., 20 min. drying followed by 60 and 20 min. tempering (spouting air off), respectively in each cycle. The solid lines denote the moisture profiles at the end of an "on" spouting-heating period while the dashed-dotted lines denote the corresponding profiles at the end of a "rest" or "off" period. It is shown that tempering periods allow gradual moisture redistribution inside the particle that ensures leveling of the concentration field and moisture supply to the outer drier portions of the kernel. The longer the rest period (lower α), the more reduction of the slope of the moisture profiles with time and thus the more evenly the moisture is distributed.

The general behavior of the on/off spouting-heating process is characterized by alternate development and reduction of moisture gradients inside the particle. This means

flatter moisture profiles compared to the continuous spouting process. Thereby the material is protected against drying-induced stresses, shrinkage, and cracking [39-42].

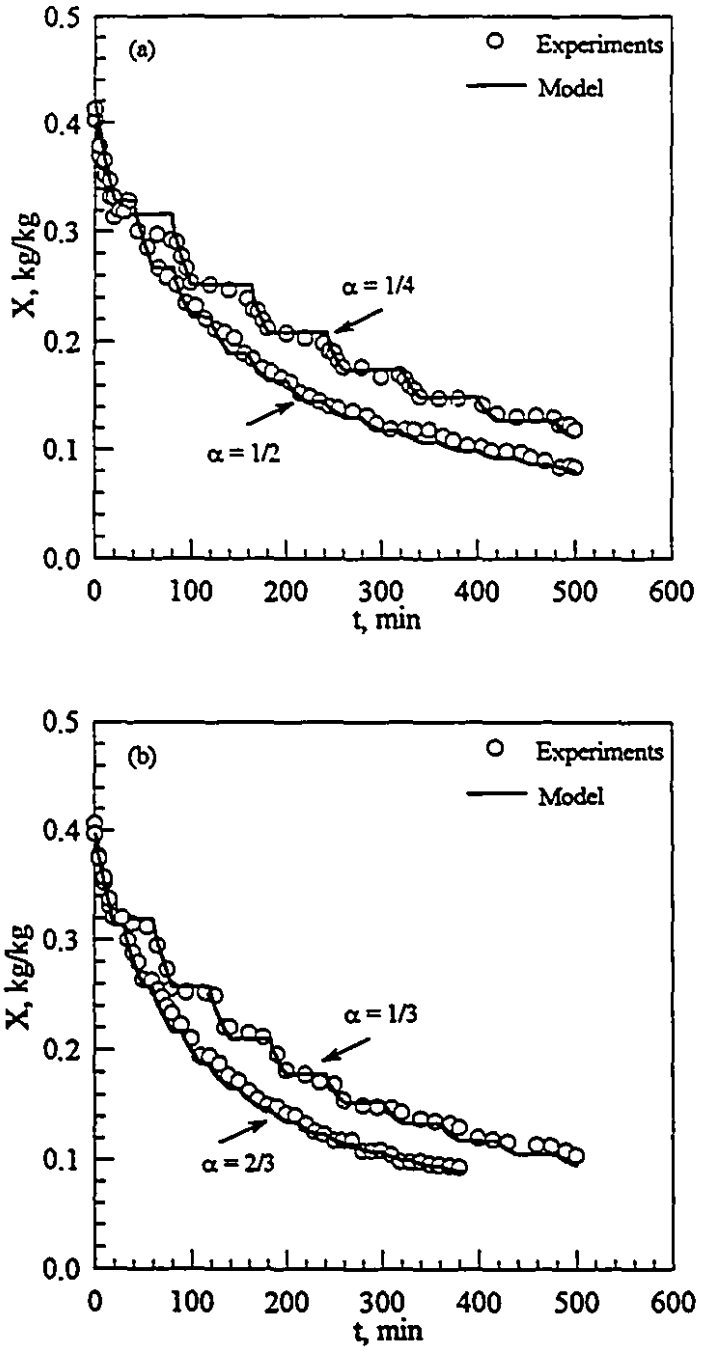

Figure 6.13: Predicted and experimental drying curves for on/off spouting-heating. $D_a = 3$ cm, $N = 4$ rpm, $U = 0.475$ m/s.

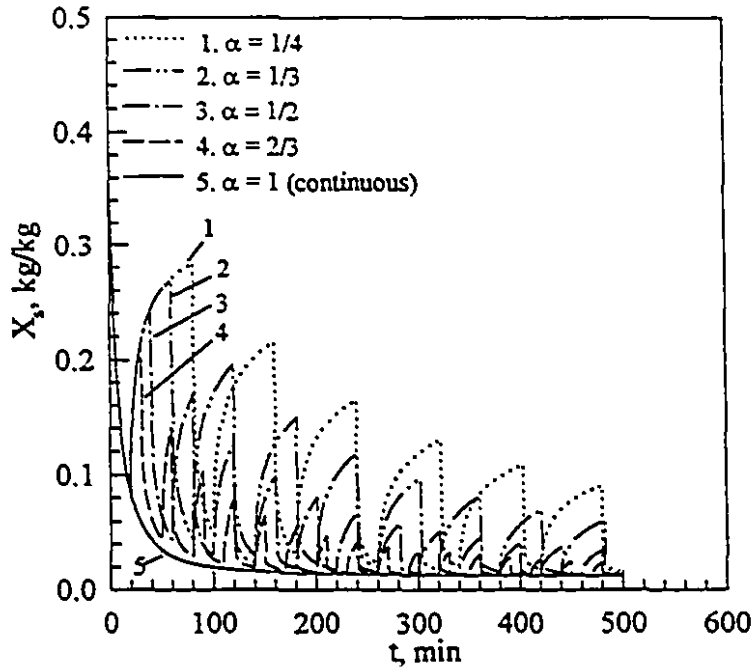

Figure 6.14: Predicted surface moisture content evolution for on/off spouting-heating. D_a = 3 cm, N = 4 rpm, U = 0.475 m/s.

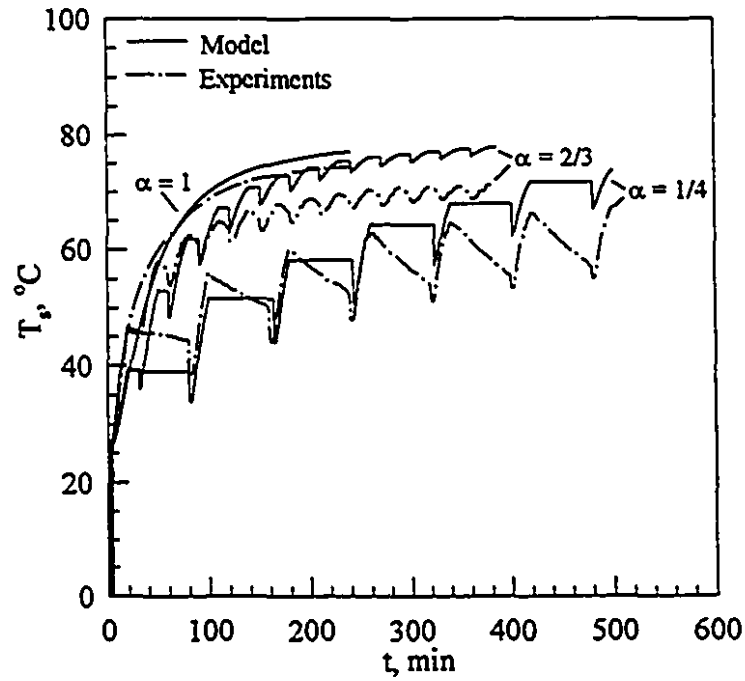

Figure 6.15: Predicted and experimental particle surface temperature evolution for on/off spouting-heating. D_a = 3 cm, N = 4 rpm, U = 0.475 m/s.

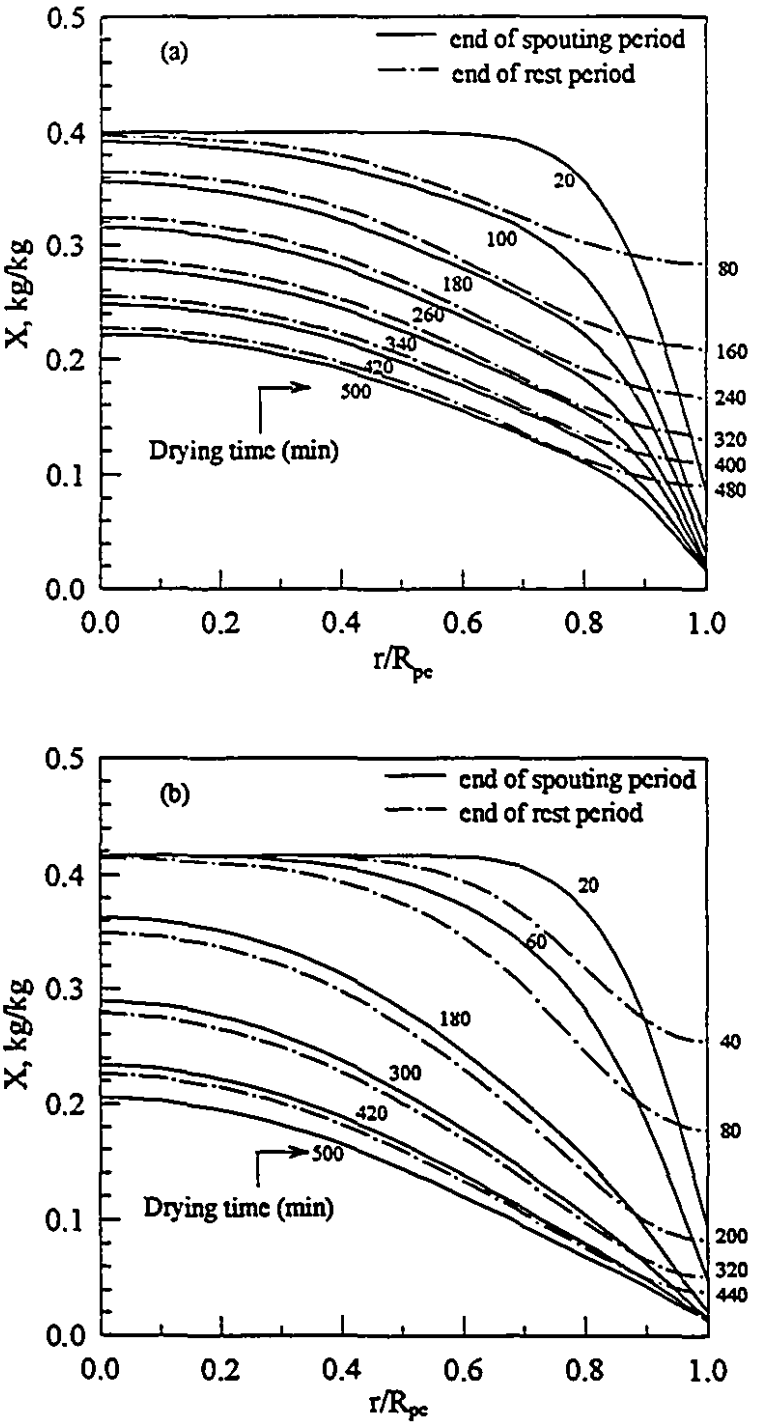

Figure 6.16: Predicted moisture profiles for on/off spouting-heating, (a): α =1/4, (b) α =1/2. D_a = 3 cm, N = 4 rpm, U = 0.475 m/s.

6.4.4 Simulation of Several Spouting-Heating Schemes

Numerical simulations were carried out for the following periodic heating patterns with the spouting air kept continuous and constant:

1. ON/OFF heating with on period fraction, α = 1/4, 1/2, and 3/4, hot air temperature (on period), T_h = 80 °C and cool air temperature (off period), T_c = 40 °C.
2. Sinusoidal heating with mean temperature, T_m = 60 and 80 °C. Both using an amplitude, T_a = 20 °C.
3. Saw tooth heating with hot air temperature, T_h = 80 °C and cool air temperature, T_c = 40 °C.

Yellow dent corn is used as the test material with the same thermophysical and transport properties used in the experimental study. The fixed parameters used in the simulation are listed in the following table.

Table 6.6: Values of Fixed Parameters Used in the Periodic Heating Simulation

Parameter	Value	Unit
τ	60	min.
Y_{gi}	0.040	kg/kg
U	0.5	m/s
T_{po}	20	°C
m_s	12	kg
X_o	0.4	kg/kg
R_{pc}	4.70×10^{-3}	m
A_p	3.89×10^{-4}	m^2
V_p	4.35×10^{-7}	m^3

Figure 6.17 shows the calculated time variations of particle average moisture content using different periodic heating schemes while the continuous spouting air superficial velocity is fixed at 0.5 m/s. A curve representing continuous heating (α = 1) is included for comparison. It can be shown readily that the moisture content curves for on/off heating with α = 1/2, saw tooth, and sinusoidal heating (T_m = 60 °C) coincide. Whilst sinusoidal heating curve (T_m = 80 °C) harmonizes with the continuous heating curve. A likely explanation is that the corresponding schemes have the same cumulative heat flux and thus mass flux at the end of each period.

The other feature of the drying curves is that, except for the sinusoidal heating curve (T_m = 80 °C), periodic heating requires longer drying time as compared to the continuous case. The effect of introducing cooler air (in the on/off heating scheme), in addition to partial drying, is to repeat the initial steep drying curve and thus high drying rate during the following heating period. This due to the favorable moisture supply to the surface of the kernel during the off-heating periods as portrayed in Figure 6.18.

Figures 6.19 presents the corresponding surface temperature profiles. It is demonstrated that sinusoidal heating with a mean inlet air temperature of 80 °C and an amplitude of 20 °C leads to an oscillating surface temperature around the continuous heating curve (T_{gi} = 80 °C). Again, this can be attributed to the fact that both have the same accumulative heat flux at the end of each heating cycle. Hence, little benefit would be achieved using this heating scheme as far as product temperature is concerned. Other heating schemes give rise to successively higher values (peaks) at the end of each period of heating.

Heating schemes including sinusoidal heating with T_m = 60 °C, saw tooth, and on/off heating yield to lower surface temperatures than the continuous one. This might be of interest in the drying of heat sensitive materials, especially those of biological origin (

e.g., agricultural grains in this study). This is because gentle heating using these heating schemes offer flexible control of the surface temperature and hence reduce common product quality problems such as germinability, vigor, fragility, or protein denaturation [43,44].

Typical moisture profiles inside the kernel are shown in Figures 5.20 and 5.21 for different heating schemes. The results shown, indicate steeper profiles and thus less moisture redistribution than the profiles obtained using on/off spouting-heating (Figure 6.16, section 6.4.3). However, the profiles are still flatter than the continuous heating case.

6.5 Closure

A simple particle-based model has been developed and validated by comparison with experimental data for diffusion-controlled drying of corn kernels in a batch RJSB dryer. This model is valid for RJSB dryer operated in the well-mixed rotating spouting flow regime. It does not include surface moisture removal. It is also valid for cases where internal diffusion time scale is order-of-magnitude longer than the period of rotation. The model is fully predictive in the sense that no parameter is fitted using data generated for the RJSB dryer. It is shown that significant energy and quality advantages may accrue from intermittent drying of heat-sensitive particles.

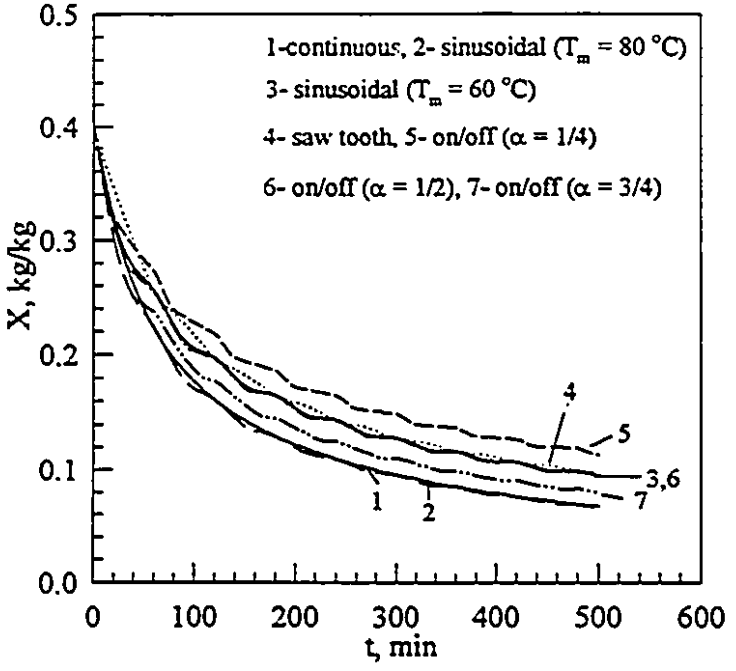

Figure 6.17: Predicted drying curves for different heating schemes.

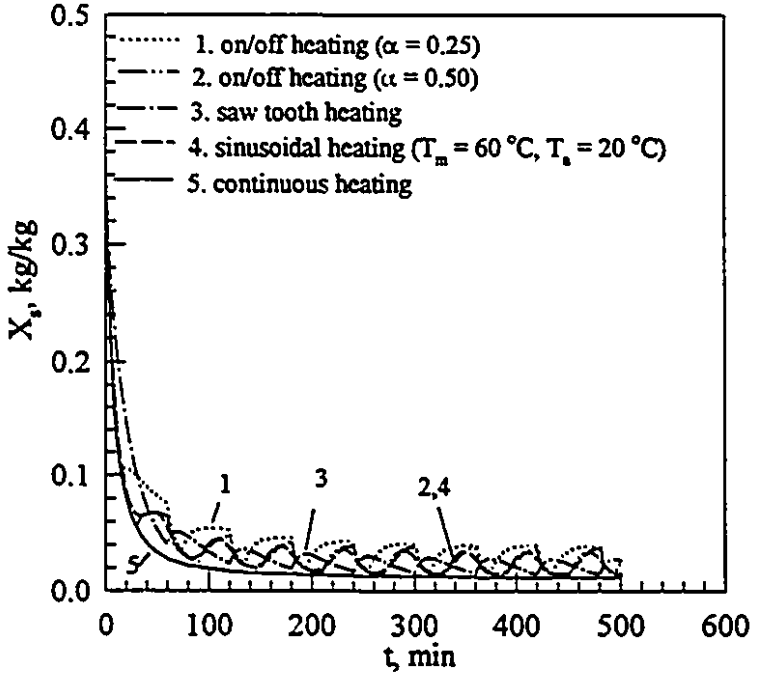

Figure 6.18: Predicted surface moisture content profiles for different heating schemes.

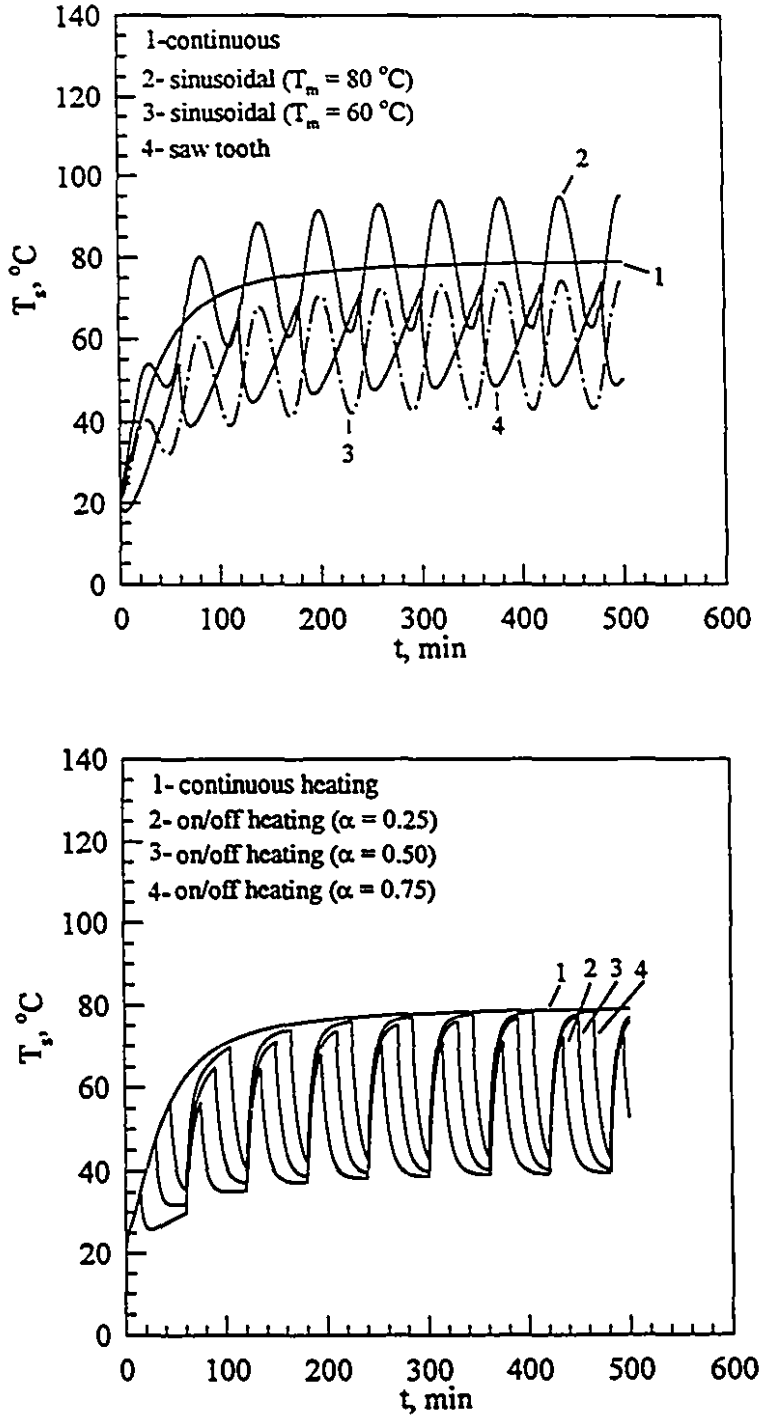

Figure 6.19: Predicted particle surface temperature profiles for different heating schemes.

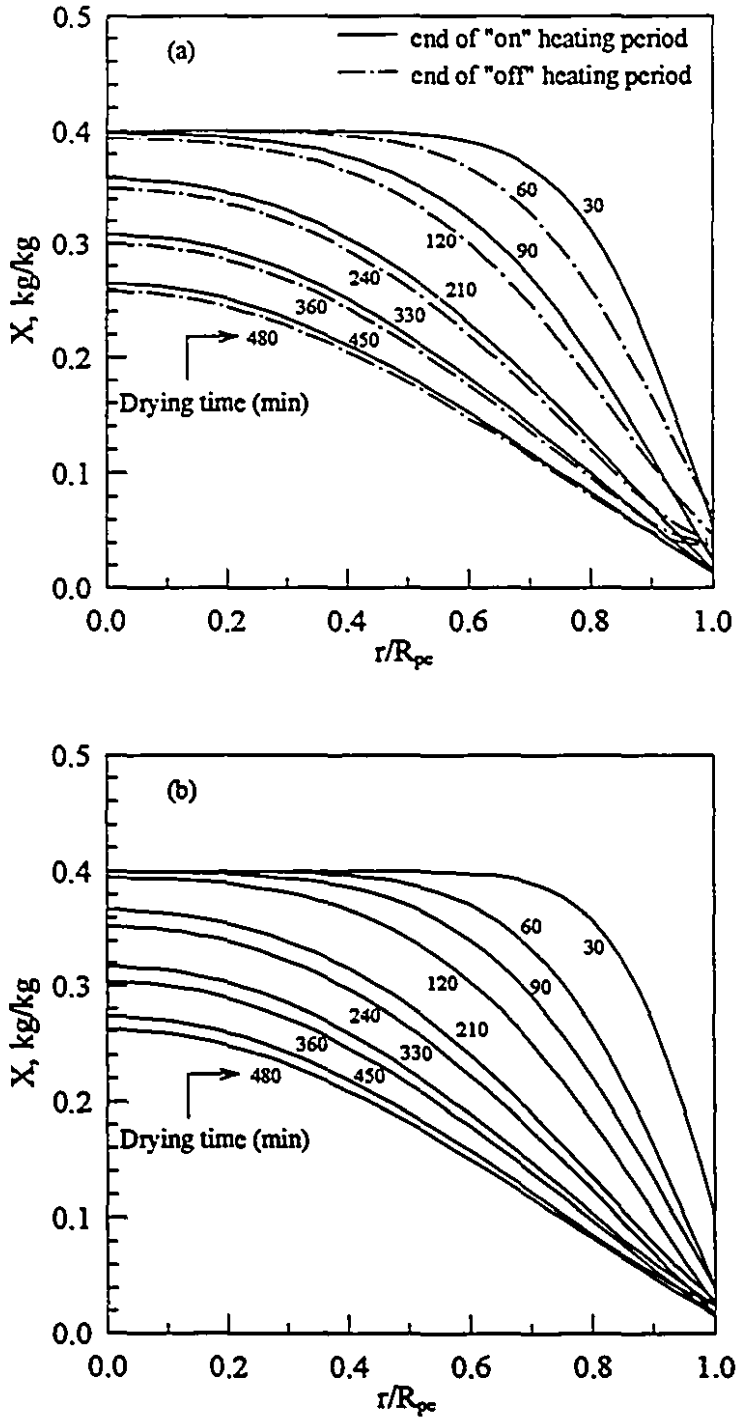

Figure 6.20: Predicted moisture profiles inside the particle.
(a) on/off heating (α =1/2), (b) saw tooth heating

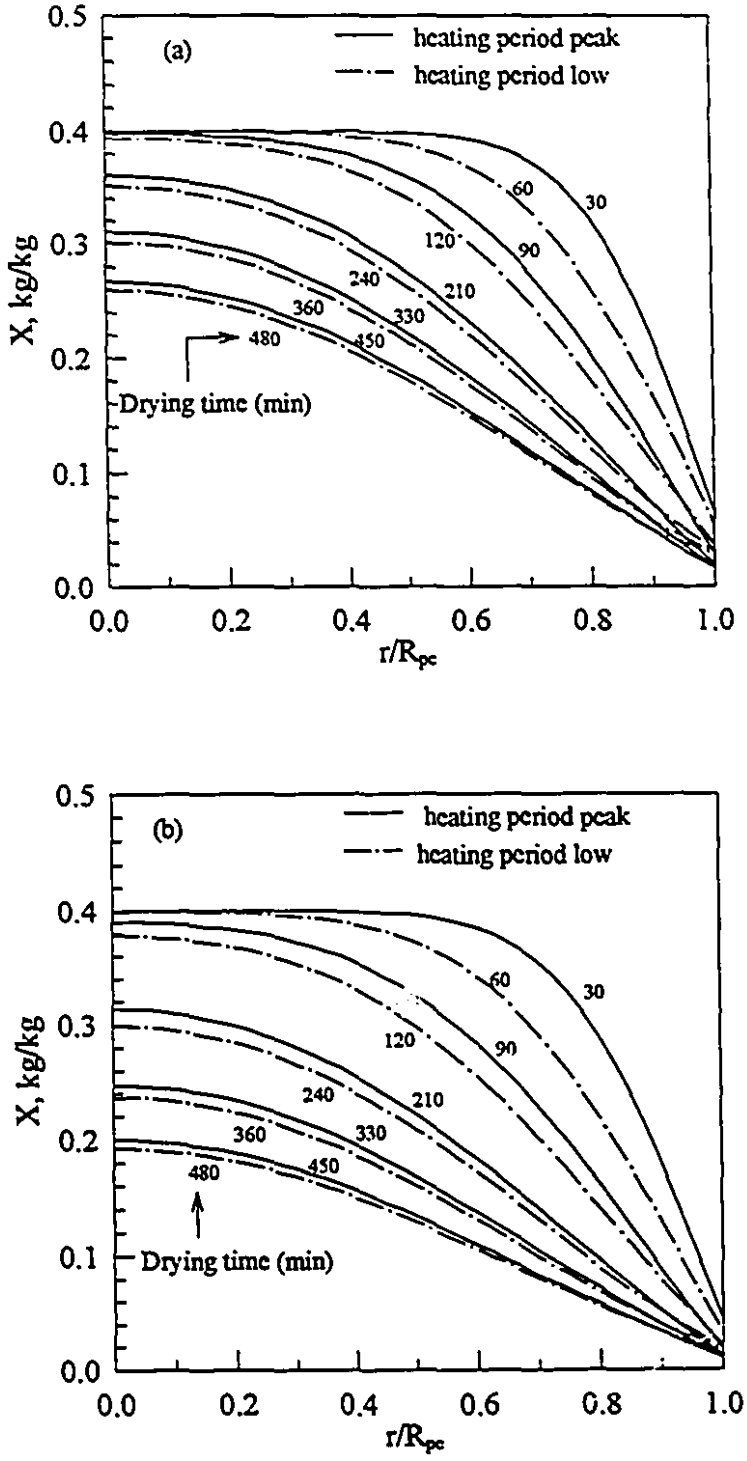

Figure 6.21: Predicted moisture profiles inside the particle.
(a) sinusoidal heating (T_m = 60 °C), (b) sinusoidal heating (T_m = 80 °C).

Nomenclature

Symbols

A_p	surface area of a single particle, m^2
A_s	total surface area of bed particles, m^2
c_{pg}	heat capacity at constant pressure of dry air, J/kg K
c_{ps}	heat capacity at constant pressure of dry solid, J/kg K
c_{pw}	heat capacity at constant pressure of liquid water, J/kg K
c_{pws}	heat capacity at constant pressure of wet solids, J/kg K
d	characteristic particle dimension, m
$\mathcal{D}$	effective moisture diffusivity in solid, m^2/s
$\mathcal{D}_v$	moisture diffusivity of vapor in gas, m^2/s
D_n	nozzle diameter, m
D_p	effective particle diameter, m
D_{pc}	equivalent particle diameter, m
D_{Pgm}	geometric mean particle diameter, m
D_{ps}	smaller particle diameter, m
g	acceleration of gravity, m/s^2
$\bar{h}_p$	overall bed heat transfer coefficient
H	bed height, m
ΔH_{d-v}	local isosteric heat of desorption-vaporization at temperature T, J/kg
$\Delta \bar{H}_{d-v}$	volume average isosteric heat of desorption-vaporization, J/kg
I_{ge}	enthalpy of exit gas, J/kg
I_{gi}	enthalpy of inlet gas, J/kg
I_s	enthalpy of solid material, J/kg
I_v	enthalpy of water vapor, J/kg
I_w	enthalpy of liquid water, J/kg

k_c	mass transfer coefficient
k_g	thermal conductivity of dry air, W/m K
k_{ws}	effective thermal conductivity of wet solids, W/m K
M_g	molar mass of air, kg/mol
M_w	molar mass of water, kg/mol
$\dot{m}_g$	mass flow rate of dry air, kg/s
m_s	mass of dry solid in bed, kg
$\dot{m}_w$	total mass rate of evaporation of water, kg/s
n	number of heating cycles, -
n_p	number of particles in bed, -
n_w	mass flux from a single particle, kg/s m^2
N	distributor rotational speed
P_v	vapor pressure of pure water, Pa
q	heat flux from a single particle, J/s m^2
Q	total heat transfer rate, J/s
r	radial distance from center of sphere, m
R_{pc}	equivalent particle radius, m
R_g	universal gas constant = 8.314 J/mol K
R_v	R_g/M_w = 462 J/kg K
RH	fractional relative humidity, -
t	time, s
T	temperature, °C
T_a	amplitude of inlet air temperature variation, °C
T_{abs}	absolute temperature, K
T_c	hot air temperature, °C
T_h	cool air temperature, °C
T_{ge}	exit gas temperature, °C
T_{gi}	inlet gas temperature, °C

T_m	mean air temperature, °C
$\overline{T}_p$	volume average particle temperature, °C
T_p	initial particle temperature, °C
U	superficial air velocity, m/s
V_p	volume of a single particle, m^3
V_s	total volume of solids in bed, m^3
X	local moisture content (dry basis), kg /kg
$\overline{X}$	volume average moisture content (dry basis), kg /kg
X_e	equilibrium moisture content (dry basis), kg /kg
X_o	initial moisture content (dry basis), kg /kg
X_s	surface moisture content (dry basis), kg /kg
Y_{ge}	exit air absolute humidity, kg water vapor/kg dry air
Y_{gi}	inlet air absolute humidity, kg water vapor/kg dry air

Greek Letters

α	intermittency, -
α_T	thermal diffusivity, m^2/s
φ	particle shape factor, -
μ	viscosity, kg/m s
ρ_g	density of dry gas, kg/m^3
ρ_s	density of dry solids, kg/m^3
λ_o	Enthalpy of vaporization of water at reference temperature, J/kg
τ	period, s
ϕ	sphericity, -

Subscripts and Superscripts

a	amplitude
e	exit, equivalent
g	gas
h	hot
i	inlet
m	mean
n	nozzle
o	initial, reference
p	particle
s	solid
v	vapor
w	water, moisture
ws	wet solid

Dimensionless Groups

Ar — Archimedes number = $\dfrac{D_{pe}^3 \rho_g (\rho_s - \rho_g) g}{\mu_g^2}$

$\overline{Bi}_H$ — Heat transfer Biot number = $\dfrac{\overline{h}_p R_{pe}}{k_{ws}}$

Le — Lewis number = $\dfrac{\alpha_T}{\mathcal{D}}$

Lu — Luikov number = $\dfrac{\mathcal{D}}{\alpha_T}$

Nu — Nusselt number = $\dfrac{h_p D_{pe}}{k_g}$

Pr Prandtl number = $\frac{c_{pg}\mu_g}{k_g}$

Re particle Reynolds number = $\frac{d\,U\rho_g}{\mu_g}$

Sh Sherwood number = $\frac{k_c D_{pe}}{\mathcal{D}_v}$

References

1. H. A. Becker and H. R. Sallans , "Drying wheat in a spouted bed", *Chem. Eng. Sci.*, 13, 97-112 (1960).
2. H. A. Becker and R. A. Isaacson, "Wheat drying in well-stirred-batch and continuous-moving-bed dryers", *Can. J. Chem. Eng.*, 48, 560-567 (1970).
3. G. Brunello, R. E. Peck, and G. Della Nina, "The drying of barley malt in the spouted bed dryer", *Can. J. Chem. Eng.*, 52, 201-205 (1974).
4. K. Viswanathan, M. S. Lyall, K. S. Negi, and B. C. Raychaudhury, "Experimental and theoretical study of batch drying of wheat in spouted beds", *Proc. 4th int. Drying Symp.*, Vol. 2, R. Toei and A. S. Mujumdar (eds.), Kyoto, 552-557 (1984).
5. K. Viswanathan, M. S. Lyall, and S. C. Dhingra, "Dynamic model for batch drying of a well-stirred bed of solids", *Drying'86*, Vol. 1, A. S. Mujumdar (ed.), Hemisphere Publishing Corp., Washington, D.C., 135-141 (1986).
6. K. Viswanathan, "Model for continuous drying of solids in fluidized/spouted beds", *Can. J. Chem. Eng.*, 64, 87-95 (1986).
7. C. A. Zuritz and R. P. Singh, "Simulation of rough rice drying in a spouted-bed", *Drying'82*, A. S. Mujumdar (ed.), McGraw-Hill /Hemisphere, New York, 239-247 (1982).
8. M. L. Passos, A. S. Mujumdar, and V. G. S. Raghavan, "Spouted and spout-fluidized beds for grain drying", *Drying Technology*, 7, 663-696 (1989).

9. A. H. Zahed and N. Epstein, "Batch and continuous spouted bed drying of cereal grains: the thermal equilibrium model", *Can. J. Chem. Eng.*, 70, 945-953 (1992).
10. A. H. Zahed and N. Epstein, "On the diffusion mechanism during spouted bed drying of cereal grains", *Drying Technology*, 11, 401-409 (1993).
11. A. V. Luikov, *Heat and Mass Transfer in Capillary Porous Bodies*, Pergammon Press, Oxford (1966).
12. A. V. Luikov, "Systems of differential equations of heat and mass transfer in capillary porous bodies (review)", *Int. J. Heat Mass Transfer*, 18, 1-14 (1975).
13. M. J. Milketinac, S. Sokhansanj, and Z. Tutek, "Determination of heat and mass transfer coefficients in thin layer drying of grain", *Trans. ASAE*, 35, 1853-1858 (1992).
14. A. Husain, C. S. Chen, J. T. Clayton, and L. F. Whitney, "Simultaneous heat and mass diffusion in biological materials", *J. Agric. Engng Res.*, 18, 343-354 (1973).
15. M. Abid, R. Gibert, and C. Laguerie, "An Experimental and theoretical analysis of the mechanisms of heat and mass transfer during the drying of corn grains in a fluidized bed", *Int. Chem. Eng.*, 4, 632-642 (1990).
16. J. Irudayaraj, K. Haghighi, and R. L. Stroshine, "Finite element analysis of drying with application to cereal grains", *J. Agric. Engng Res.*, 53, 209-229 (1992).
17. A. Kmiec, "Simultaneous heat and mass transfer in spouted beds", *Can. J. Chem. Eng.*, 53, 18-24 (1975).
18. M. Hemati, M. Mourad, D. Steinmetz and C. Laguerie, "Continuous and intermittent drying of maize on a flotation fluidized bed", *Fluidization VII, Engineering Foundation for International Fluidization Conference*, Australia, (1992).
19. J. F. Davidson, M. W. Robson, and F.C. Roesler, "Drying of granular solids subjected to alternating boundary conditions", *Chem. Eng. Sci.*, 24, 815-828 (1969).
20. A. Hallsträm, "Alternating boundary conditions in drying", *Chem. Eng. Sci.*, 41, 2225-2234 (1986).

21. P. Carabin, "Simulation of periodic convective and volumetric heating of finite and semi-infinite slabs", *Drying of Solids*, A.S. Mujumdar (Ed.), Prakashan, New Delhi (1990).
22. S. -T. Chu and A. Hustrulid, "Numerical solution of diffusion equations", *Trans. ASAE*, 11, 705-708 (1968).
23. H. B. Pfost, S. G. Maurer, D. S. Chung, and G. A. Milliken, "Summarizing and reporting equilibrium moisture data for grains", *Paper No. 76-3520 presented at 1976 Winter Meeting of ASAE*, Chicago, December (1996).
24. E. A. Kazarian and C. W. Hall, "Thermal properties of grains", *Trans. ASAE*, 8, 33-37 (1965).
25. D. B. Brooker, F. W. Bakker-Arkema, and C. W. Hall, *Drying and Storage of Grains and Oilseeds*, Van Nostrand Reinhold, New York (1992).
26. Z. Pakowski, Z. Bartczak, C. Strumillo, S. Stenstrom, "Evaluation of equations approximating thermodynamic and transport properties of water, steam and air for use in CAD of drying processes", *Drying technology*, 9, 753-773 (1991).
27. A. S. Mujumdar, *Handbook of Industrial Drying*, 2nd ed., Marcel Dekker, Inc., New York (1995).
28. K. Madsen and R. F. Sincovec, "The numerical method of lines for the solution of non-linear partial differential equations", In: *Computational Methods in Nonlinear Mechanics*, J.T. Oden (Ed.), Texas Inst. for Computational Mechanics, Austin, Tex. (1974).
29. F. Sincovec and N. K. Madsen, "Algorithm 494-PDEONE, solutions of systems of partial differential equations", *ACM Trans. on Math. Software*, 1, 261-263 (1975).
30. Sincovec and N. K. Madsen, "Software for nonlinear partial differential equations", *ACM Trans. on Math. Software*, 1, 232-260 (1975).
31. Hindmarch, "LSODE and LSODI, two new initial value ordinary differential equation solvers", *ACM SIGNUM Newsletter*, 15, 10-11 (1980).
32. W. Gear, *Numerical Initial-Value Problems in Ordinary Differential Equations*, Prentice-Hall, Englewood Cliffs, N.J. (1971).

33. S. Pabis and S. Henderson, "Grain drying theory II. A critical analysis of the drying curve of shelled maize", *J. Agric. Engng Res.*, 6, 272-277 (1961).
34. S. Cobinah, M. Abid, C. Laguerie, and H. Gibert, "Kinetics of whole corn grains drying in a fluidized bed of fine inert particles", *Drying'84*, A.S. Mujumdar (ed.), Hemisphere Publishing Company, 186-192 (1984).
35. S. Ulku and G. Uckan, "Corn Drying of fluidized beds", *Drying'86*, Vol. 2, A.S. Mujumdar (ed.), Hemisphere Publishing Company, 531-536 (1986).
36. K. B. Mathur and P. E. Gishler, "A technique for contacting gases with coarse solid particles", *AIChE J.*, 1, 157-164 (1955).
37. Mathur and N. Epstein, *Spouted Beds*, Academic Press, New York (1974).
38. R. B. Keey, *Drying of Loose and Particulate Materials*, Hemisphere Publishing Corporation, New York (1992).
39. S. Sokhansanj, "Drying induced stresses in food grains - a finite element approach" in *Drying'82*, A. S. Mujumdar (ed.), Hemisphere Publishing Corporation, Washington (1982).
40. J. B. Filho, M. Fortes, V. E. Sweat, and M. R. Okos, "Intermittent drying of soybeans", *Drying'82*, A. S. Mujumdar (ed.), Hemisphere Publishing Corporation, Washington, 220-226 (1982).
41. J. B. Litchfield and M. R. Okos, "Prediction of corn kernel stress and breakage induced by drying, tempering, and cooling", *Trans. ASAE*, 31, 585-594 (1988).
42. D. Zhang and A. S. Mujumdar, "Deformation and stress analysis of porous capillary bodies during intermittent volumetric thermal drying", *Drying Technology*, 10, 421-443 (1992).
43. M. Mourad, M. Hemati, and C. Laguerie, "D ; .ng of corn kernels in a flotation fluidized bed - influence of the operating conditions on product quality", *Drying'92*, A. S. Mujumdar (Ed.), Elsevier, Amsterdam, 1456-1464 (1992).
44. J. Beke, A.S. Mujumdar, "Influence of drying conditions on the fragility of corn kernels", *Drying Technology*, 11, 603-614 (1993).

Chapter 7

Conclusions, Contributions and Recommendations

7.1 Conclusions

This thesis has examined the rotating jet spouted bed (RJSB) as a new gas-solid contacting method. A predictive model was developed for both continuous and intermittent drying of particles in a batch mode.

I. Flow Characteristics

- The RJSB features more efficient air utilization and enhanced particle mixing and circulation as compared with conventional spouted beds.
- Operation of the RJSB is very flexible because of the adjustable rotational speed. The following three distinct flow regimes were identified:
    1. Full rotating spouting (low rpm)
    2. Rotating central spouting-pulsating annulus (moderate rpm)
    3. No spouting with local pulsation; pseudo fluidization (high rpm)
- Adjustment of the rotational speed of the distributor provides a simple means to control particle circulation and turn-over in the bed. The significance of such control is especially important in drying different materials.
- The performance of the RJSB was explored with respect to the spouting mechanism, minimum spouting velocity, steady spouting pressure drop, and peak pressure drop using corn, soybean, and pellets of polyethylene and polystyrene as test particles.

- Empirical correlations were developed for the key flow parameters as functions of bed height, nozzle diameter, distributor rotational speed, bed and particle properties.
- The distributor rotational speed has a major effect on the spouting mechanism and the flow regimes. However, it has only a minor effect on the minimum spouting velocity and pressure drop values within the rotating spouting regime.
- The minimum spouting Reynolds number varies almost linearly with the dimensionless bed height and nozzle diameter and with the square root of the Archimedes number.
- The RJSB has lower peak pressure drop but a comparable steady spouting pressure drop compared with the conventional spouted beds.

II. Continuous Drying

- Yellow dent corn was successfully dried in the RJSB with reproducible drying curves under different operating conditions.
- The batch drying kinetics are comparable with conventional spouted and fluidized beds for slow drying materials where the drying rate is controlled by internal moisture diffusion.
- Drying characteristics of corn in the RJSB indicate that the inlet air temperature is the parameter which most significantly affects the drying rate as well as the quality of the product.
- The distributor rotational speed, air flow rate, bed height, and nozzle diameter have little effect on the drying kinetics of slow-drying materials in the ranges of operating conditions tested.

III. Intermittent Drying

- Intermittent drying of particles in a batch RJSB dryer takes longer than continuous drying if the total process time is considered. However, it takes shorter "net" time if only the effective drying time is considered.
- Energy consumption can be reduced by 20-40 % with intermittent drying.
- Supplying hot air periodically rather than continuously results in a better quality product with no drying-induced stress cracking.

IV. Mathematical Model

- Using published thermophysical properties and an overall bed heat transfer coefficient, the model accurately predicts the experimental results without the need for adjustable parameters..
- Numerical computations based on this model were carried out to study the effects of process parameters on the average particle moisture content, temperature, moisture content and temperature profiles inside the particle, surface temperature and moisture content, and heat and mass fluxes at the surface of the particle.

7.2 Contributions to Knowledge

- A novel fluid-solid contacting device, termed the rotating jet spouted bed (RJSB), is proposed, designed, fabricated and tested.
- Empirical correlations were developed for the minimum spouting velocity, steady spouting pressure drop, and peak pressure drop as functions of design parameters and materials physical properties.
- Drying kinetics of corn were investigated under different operating parameters.

- Intermittent drying of corn in the RJSB was explored in terms of the effective drying time and thermal energy savings.
- A fully predictive mathematical model was developed for batch drying of materials for which internal moisture diffusion controls the drying kinetics.
- A general PC-code was developed based on the model which can be used to simulate the drying of other materials under different conditions. It is a useful design and analysis tool for batch drying in a RJSB with constant or time-varying drying conditions.
- A simulation study was performed to investigate the possible application of different time-dependent spouting and heating schemes in drying of particles with diffusion-controlled drying kinetics.

7.3 Recommendations for Further Research

I. Design

- It is recommended to use separate air supply lines with individual flow controllers for the central and annular nozzles in order to introduce the required amount of air flow in each section and to reduce distributor pressure drop and thus pumping power requirements.
- The dryer may be fitted with a mechanical agitator to enhance mixing of sticky and difficult to spout materials.

II. Aerodynamics

- Experiments using deeper bed heights should be carried out in order to quantify the maximum spoutable bed height.

- Quantitative measurements of solids mixing, segregation, and particle circulation rates are needed.
- Spouting characteristics of polydispersed and particles other than Geldart's D-type should be studied. Also, mixtures of particles should be studies.

III. Continuous Drying

- The local heat and mass transfer coefficients in both active and static regions should be investigated to help understand the actual transfer mechanisms in these zones and to improve the model predictions.
- Drying of other grains as well as other materials (e.g. fertilizers) should be tested in the system.

IV. Time-dependent Spouting and Heating

- Further tests similar to those presented in Chapter 5 should be performed for other levels of inlet air temperature, intermittency, and drying periods. Applying different drying temperatures in each "on" period is another possibility.
- Several other spouting/heating schemes should be verified experimentally including: continuous spouting-on/off heating, continuous spouting-sinusoidal heating and continuous spouting-saw tooth heating.
- A general optimization strategy is needed in order to select the optimum spouting-heating method, intermittency, cycle period, inlet air temperature, and number of units with respect to energy consumption, fixed cost, operating cost, and product quality.

V. Mathematical Modeling

- The batch drying model should be tested for other materials using both continuous and periodic spouting/heating schemes.
- The effect of parameters such as sphericity, shrinkage, inlet air humidity, etc. should be examined.
- Alternative surface boundary conditions should be developed for the tempering periods in order to improve the model predictions.
- The model may be extended to predict the performance of a multi-stage drying system.
- Combining the drying model with a fundamental aerodynamics model would provide useful information about the combined flow, heat and mass transfer mechanisms in this complex cyclic system.
- Since the model does give good agreement with experiment, it should provide a reliable basis for predicting the performance, and for the design, optimization and scale up of the system for other operating parameters, materials and production capacities.

Appendix

Dimensional Analysis

The Backingham π theorem states that the functional relationship among q quantities or variables whose units may be given in terms of u fundamental units or dimensions may be written as (q-u) independent dimensionless groups, often called π groups. The fundemental units or dimensions that are involved in the aerodynamic parameters of the rotating spouted bed are mass, M, lenght or size, L, and time, t. The units of the applicable variables (q) in terms of these fundamental units (u) are listed in Table A.1.

For U_{ms1} and U_{ms2}, the number of dimensionless groups or π's is q-u=7. Thus:

$$\pi_1 = f(\pi_2, \pi_3, \pi_4, \pi_5, \pi_6, \pi_7) \qquad (A.1)$$

If D_p, ρ_g, and μ_g, are selected to be the repeated parameters, then the seven dimensionless groups can be written as:

$$\pi_1 = D_p^{c1} \rho_g^{c2} \mu_g^{c3} U_{ms} \qquad (A.2)$$

similar equations can be written for other groups.

Table A.1: The significant variables for the dimensional analysis of U_{ms} and ΔP.

Variable	Fundamental Dimension	U_{mso}	U_{ms1}	U_{ms2}	ΔP_M	ΔP_s
U	LT^{-1}	+	+	+	-	-
ρ_g	ML^{-3}	+	+	+	+	+
μ_g	$ML^{-1}T^{-1}$	+	+	+	+	+
D_p	L	+	+	+	+	+
$g(\rho_p-\rho_g)$	$ML^{-2}T^{-2}$	+	+	+	+	+
U_t	LT^{-1}	+	+	+	-	-
$(1-\varepsilon)$	-	-	-	-	+	+
H	L	+	+	+	+	+
D_c	L	+	+	+	+	+
D_n	L	+	+	+	+	+
$V_{\theta 1}$	LT^{-1}	-	+	-	-	-
$V_{\theta 2}$	LT^{-1}	-	-	+	-	-
ΔP	$ML^{-1}T^{-2}$	-	-	-	+	+

+: included, -: not included

Using dimensional analysis, the resulting π groups are as follows:

$$\pi_1 = \frac{\rho_g D_p U_{ms1}}{\mu_g} = Re_{ms1} \qquad (A.3)$$

$$\pi_2 = \frac{H}{D_p} \qquad (A.4)$$

$$\pi_3 = \frac{D_c}{D_p} \qquad (A.5)$$

$$\pi_4 = \frac{D_N}{D_p} \tag{A.6}$$

$$\pi_5 = \frac{\rho_g D_p^3 g(\rho_p - \rho_g)}{\mu_g^2} = Ar \tag{A.7}$$

$$\pi_6 = \frac{\rho_g D_p U_t}{\mu_g} \tag{A.8}$$

$$\pi_7 = \frac{\rho_g D_p V_{\theta 1}}{\mu_g} \tag{A.9}$$

Equation A.1 can reduced to the following form:

$$\pi_1 = f\left(\frac{\pi_2}{\pi_3}, \frac{\pi_4}{\pi_3}, \pi_5, \frac{\pi_7}{\pi_6}\right) \tag{A.10}$$

or

$$Re_{ms1} = f\left(\frac{H}{D_c}, \frac{D_n}{D_c}, Ar, \frac{V_{\theta 1}}{U_t}\right) \tag{A.11}$$

Using the same procedure, the following equations can be written:

$$Re_{ms2} = f\left(\frac{H}{D_c}, \frac{D_n}{D_c}, Ar, \frac{V_{\theta 2}}{U_t}\right) \tag{A.12}$$

$$Re_{ms0} = f\left(\frac{H}{D_c}, \frac{D_n}{D_c}, Ar\right) \tag{A.13}$$

$$\frac{\Delta P_M}{(1-\varepsilon)(\rho_p - \rho_g)gH} = \frac{\Delta P_M}{\rho_b g H} = f\left(\frac{H}{D_c}, \frac{D_N}{D_c}\right) \tag{A.14}$$

$$\frac{\Delta P_s}{(1-\varepsilon)(\rho_p - \rho_g)gH} = \frac{\Delta P_s}{\rho_b g H} = f\left(\frac{H}{D_c}, \frac{D_N}{D_c}\right) \tag{A.15}$$